THE EFFECT OF HEAT TRANSFER ON BOUNDARY LAYER STABILITY

Thesis submitted for the Degree of Ph.D.

by

Andrew D. Grant, B.Sc.

Department of Mechanical Engineering
The University of Glasgow

May 1973

SUMMARY

During transient running of an axial flow compressor, considerable temperature differences are set up between the metal surfaces and the adjacent airstream. It was suggested that these temperature differences might have an adverse effect upon the aerodynamic performance of the compressor, and increase the likelihood of stall. Rolls-Royce Ltd. expressed interest in this hypothesis, and offered to sponsor a three-year programme of investigation.

The essential study was considered to be that of turbulent separation of boundary layers from heated surfaces, but an initial experimental investigation of laminar transition was carried out for low-speed flow over a flat plate. This indicated that the transition point is generally advanced by wall heating, and confirmed the results of other authors. The turbulent separation measurements were made on the inner wall of a curved duct, again at low air velocities. Advancement of the separation point in response to wall heating was observed, but dependence on flow velocity was evident. Attempts were made to relate separation point movement to a single parameter, but these were unsuccessful.

The curved duct results were compared with predictions from an integral-type boundary layer calculation program, which had been developed by staff at Rolls-Royce. This, after modification by the author, gave acceptable results for the majority of the experimental data. The predictions were then extended to cover flow over compressor blades.

It was concluded that premature separation of the boundary layer

in a compressor is most likely to occur on the aerofoil suction surfaces, although separation from the drum is a further possibility. On the aerofoils, separation point movements as a result of thermal transients are likely to be small (less than 5% of the chord). However, a small departure from design conditions is likely to produce a larger one further downstream. Thus it was considered that the aerodynamic consequences of heat transfer from the blading can be a major factor in reducing compressor stall margins during transient running.

ACKNOWLEDGEMENT

I should like to express my thanks to the following for their help and co-operation: to Professor R.S. Silver; to Rolls-Royce Ltd. for sponsorship of the majority of the project, and especially to Dr. J.H. Perry and Mr. B.A. Ntim for their assistance in its early stages; to Dr. N.R.L. Maccallum for his constant help and advice; to Mr. A. Ritchie, who played a major part in the construction and development of the apparatus; and to numerous colleagues at the University for their encouragement and support.

CONTENTS

Page

SUMMARY

Acknowledgement

CHAPTER 1 INTRODUCTION

1.1 The Problem 1
1.2 The Rolls-Royce Contract 2
1.3 Blading Aerodynamics 4
1.4 Literature Survey 6

CHAPTER 2 FLAT PLATE EXPERIMENTS - THE EFFECT OF PLATE HEATING ON TRANSITION

2.1 The Wind Tunnel 16
2.2 The Flat Plate 16
2.3 Instrumentation 17
2.4 Early Testing and Development 18
2.5 Main Test Programme 20
2.6 Discussion

2.6.1 Laminar velocity profiles 23
2.6.2 Plate spacers 24
2.6.3 Pressure gradient effects 24
2.6.4 Static pressure variation 25
2.6.5 Manometer accuracy 25
2.6.6 Buoyancy effects 25
2.6.7 Transition point fixing 26
2.6.8 Effect of heat transfer on transition 26
2.6.9 Nearness to laminar separation 28

2.7 Conculsions

CHAPTER 3 CURVED PLATE EXPERIMENTS - THE EFFECT OF PLATE HEATING ON TURBULENT SEPARATION

3.1 The Curved Duct 30
3.2 Instrumentation 31
3.3 Early Testing and Development

3.3.1 The thermocouple probe 32
3.3.2 Duct entry conditions 32
3.3.3 Static pressure measurements 33
3.3.4 Separation point location 34
3.3.5 First measurements with plate heating 35

Page

3.4 Main Test Programme

3.4.1 Co-ordinates 36
3.4.2 Laminar separation 37
3.4.3 Turbulent separation 37
3.4.4 Velocity profiles, and derived quantities 39
3.4.5 Temperature profiles, and derived quantities 40
3.4.6 Flow visualisation 41

CHAPTER 4 CURVED PLATE - DISCUSSION OF EXPERIMENTAL RESULTS

4.1 Duct Geometry 43
4.2 Entry Conditions 44
4.3 Static Pressure Measurement 45
4.4 Separation Point Location 47
4.5 Velocity + Temperature Profiles 48
4.6 The Parameters δ^*, θ and H 51
4.7 Skin Friction 52
4.8 Heat Transfer and Stanton Numbers 54
4.9 Effects of Flow Velocity and Wall Temperature on Separation 59
4.10 Radial Acceleration Parameters 63

CHAPTER 5 PREDICTION PROGRAM Q195 - DESCRIPTION

5.1 Reasons for Adoption 66
5.2 General Description 68
5.3 The Equations in Detail 69

CHAPTER 6 PREDICTION PROGRAM Q195 - TESTING AND DEVELOPMENT

6.1 Computing Facilities 74
6.2 Schubauer and Klebanoff's Data 74
6.3 The Author's Data - Modifications for Duct Flow 77
6.4 The Author's Data - Modifications for Entrainment Theory 79
6.5 The Author's Data with Heat Transfer - Predictions from Modified Q195

6.5.1 Adiabatic conditions 82
6.5.2 Wall temperature 425 K 83
6.5.3 Separation points for u_{in} = 24 ft/s 84
6.5.4 Separation points at other inlet velocities 85
6.5.5 Discussion of results 86

Page

6.6 Further Predictions using Schubauer and Klebanoff's Data 90
6.7 Investigations of the Parameter K_r 91
6.8 Aerofoil Predictions 92

CHAPTER 7 PREDICTION PROGRAM Q195 - DISCUSSION

7.1 Momentum Integral Equation 97
7.2 Entrainment Theory and Skin Friction 98
7.3 Stanton Number 99
7.4 Future Developments 100

CHAPTER 8 FINAL DISCUSSION AND CONCLUSIONS

8.1 Comparison with Published Work 102
8.2 The Author's Results for the Curved Duct 103
8.3 Flow in Compressor Blading during Thermal Transients 103
8.4 The Transition Point 106
8.5 The Turbulent Layer - Flow Relaminarisation 107
8.6 The Turbulent Layer - Separation 108
8.7 Conclusions 110
8.8 Future Work 112

APPENDIX A - The Effects of Free-Stream Turbulence 113

APPENDIX B - The Effects of Body Forces 121

APPENDIX C - Corrections for Thermocouple Probe 129

NOMENCLATURE i

BIBLIOGRAPHY I iii

BIBLIOGRAPHY II vi

LIST OF FIGURES x

CHAPTER 1

INTRODUCTION

The work described in this thesis is quite general in nature, and it is hoped that it will be of assistance in many aerodynamic studies. However, the research was embarked upon with a specific industrial problem in mind, and financial support was provided by the company concerned.

1.1 The Problem

For several years, there has been co-operation between Glasgow University Engineering department and the Scottish branches of Rolls-Royce Ltd. In June 1968, Rolls-Royce contacted the University to discuss a failure occurring with certain jet engines on test, during what they term the "hot re-slam" procedure. This consists of a long period of running at maximum continuous thrust, during which time all temperatures within the engine attain a steady value. The fuel supply is then reduced, to cut engine revolutions to those at ground idling conditions, at which point the throttle is opened again to return the engine to maximum thrust. The cycle is completed in about 20 seconds.

In certain tests, however, the engines failed to respond to the increase in fuel supply. Rotational speeds remained constant or even fell, while a rapid rise in turbine exit temperature indicated a reduction in the air/fuel ratio. The engines showed no signs of recovering from this condition, and the fuel supply had to be cut off to avoid permanent damage. An important parameter was found to be the

time spent at ground idling speed before acceleration was attempted; if this was more than a few seconds, engine response was normal. Fortunately, Rolls-Royce had no evidence of problems of this nature occurring in flight, although certain circumstances, for example a baulked landing, make in-flight difficulties conceivable. Interest in the phenomenon is not confined to Rolls-Royce; for example, Warne (36) has described its adverse effect on permissible overfuel margins.

It was agreed that the engine failure was the result of stalling in the compressor, probably in the high-pressure stages. This caused the reduced airflow and affected the air/fuel ratio. It was then suggested by Dr. Maccallum of the University (11) that the stall might be the result of transient thermal effects on the internal aerodynamics of the compressor. For a very rapid "re-slam", the metal components, and notably the blades, would be at a relatively higher temperature than the air flowing through at low engine revolutions; a less rapid cycle would give the blades more time to cool. This theory accounted for the importance of cycle time as a controlling factor, but rested on the hypothesis that the airflow was sufficiently disturbed by the hot blades for compressor stall to result. However, it could be argued that a small change in flow pattern at one compressor stage would disturb entry conditions for the next stage, and deterioration would then be rapid.

1.2 The Rolls-Royce Contract

It was clear that knowledge of boundary layer behaviour over

heated surfaces was required before further progress could be made. On compressor blading, the boundary layer is predominantly turbulent, and an investigation of turbulent separation was considered essential. In September 1968, an approach was made to Rolls-Royce in Derby, who expressed considerable interest and agreed to provide full financial support for a research programme. Three areas of study were agreed upon:-

(a) experimental investigations of laminar transition on a flat plate, with heating; this would not be an exhaustive study, but would be included partly to develop instrumentation and experimental techniques.

(b) detailed experimental investigations of turbulent separation, probably in a curved duct of constant radius, with a heated inner wall. In addition to the separation measurements, velocity and temperature profiles would be produced, and skin friction and Stanton Number distributions calculated. Measurements on the outer wall, which were likely to prove troublesome, were provisionally included.

(c) development of a theory, using computational techniques, to extend the results of (b) to prediction of aerofoil performance during temperature transients.

Experimental measurements on aerofoils were not contemplated, as only unacceptably large blades would provide boundary layers of suitable thickness for investigation.

A three-year research contract, covering the years 1969-71, was

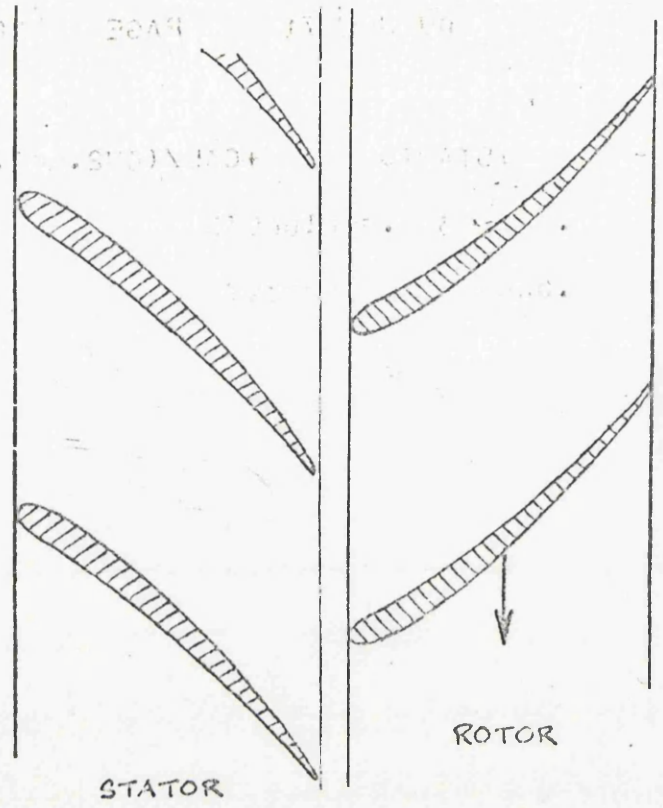

Figure 1: Axial-flow compressor blading.

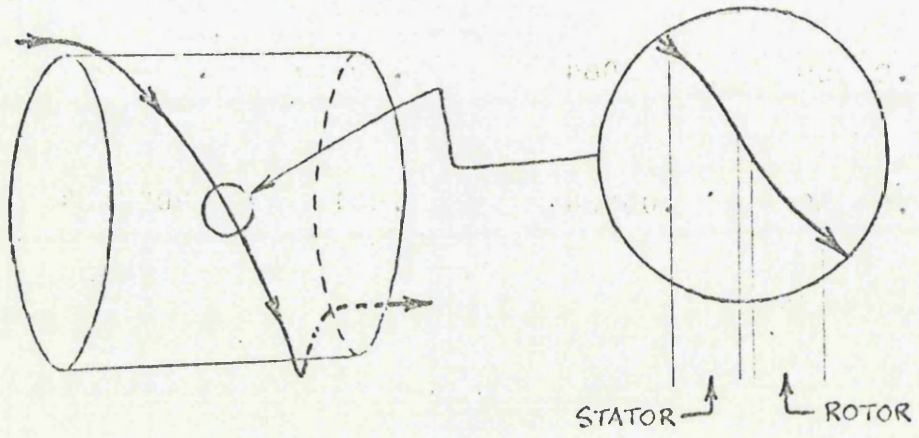

Figure 2: Flow around the compressor drum.

drawn up and signed in July, 1969.

Blading Aerodynamics

It is not proposed to give details of the operating principles of an axial-flow compressor; these are available from other sources, e.g. Horlock (7) and Howell (8). The aerodynamic conditions in the flow through the blading, however, will be discussed, as these are fundamental to the problem to be investigated. An axial-flow compressor operates by drawing air through a number of blade rows, the blades being shaped to form a series of divergent passageways, (Figure 1). These blade rows are alternately fixed stators or moving rotors, and each pair of rows is termed a stage of the compressor.

On its way through the blading the air follows a helical path about the axis of the annulus, and so experiences a centripetal acceleration towards this axis. Also, the curved blades impart a further acceleration, approximately at right-angles to the direction of flow, with no radial component (see Figure 2). The direction is reversed at each blade row, and so this acceleration may be regarded as an alternating one. Compared with gravity, these accelerations are very severe; typical values are 8,000g and 80,000g respectively. However, such is the velocity of the air through the compressor that they have effect for a very short time, typically 5×10^{-3} seconds and 0.3×10^{-3} seconds. The acceleration towards the engine axis is relatively steady, and applies throughout the time a given air particle is within the compressor; that due to the blading, being reversed at each row, can only have effect for the time required to pass over one blade row.

The influence of these accelerations on aerodynamic behaviour may be considerable. As soon as temperature differentials between metal components and air are set up, air density changes are produced, and the action of centripetal fields in these conditions may be most disruptive. But the duration of the acceleration is a factor in determining the extent to which density and pressure gradients are set up in the airstream.

Another significant factor is likely to be the turbulence in the main body of the airstream. The flow within a compressor is, of course, highly complex; the scale of turbulence is initially large, but decreases towards the high-pressure stages. Intensity of turbulence has been measured experimentally, and as expected increases with distance from the inlet; typical values may be around 5%. In the author's experiments, the effect of heat transfer was the main consideration; a separate investigation of turbulence effects was not attempted. However, certain relevant contributions on this topic by other authors are reviewed in the following section, and a general discussion on turbulence, including the likely effects of performing the author's experiments in a highly turbulent environment, is given in Appendix A.

The review of literature overleaf completes Chapter 1, and the following chapter describes the experimental work on the flat plate. The curved duct experiments are dealt with in Chapters 3 and 4, while Chapters 5, 6 and 7 describe the prediction method, its development and testing. Finally, Chapter 8 attempts to estimate the effect of heat transfer to the boundary layer on the transient performance of turbojet engines.

Three appendices follow the main text. The first two attempt to relate the author's experimental data to the flow conditions in compressor blading, by considering respectively the effects of freestream turbulence and of buoyancy and other forces normal to the direction of flow. The third appendix

contains a calculation of temperature corrections for the author's thermocouple probe.

1.4 Literature Survey

Introduction

The work described in this thesis is a study of the effects of heat transfer on laminar transition and on turbulent separation of the boundary layer. The former effect is reasonably well documented, especially for supersonic flows; references to the latter are extremely rare. The literature on surface curvature and buoyancy effects was also of interest, as these subjects were relevant both to the author's experimental work and to flow over compressor blading; a serious lack of reliable experimental data was noted. Further topics examined were reverse transition, especially under the action of body forces, and the effect of free-stream turbulence on boundary layer development; study of the latter was necessary in order to relate the author's results to conditions within an axial-flow compressor. Here again, the literature is incomplete in certain respects.

The publications reviewed below have been grouped under the headings of transition, separation, curvature, buoyancy, reverse transition and free-stream turbulence.

Laminar Transition

The phenomenon of boundary layer transition is now reasonably well understood. Instability in the laminar layer begins with the amplification of small disturbances to the flow. However, the observed transition point is always some distance downstream from the calculated origin of instability, and so an empirical approach involving a parameter based on boundary layer thickness and pressure gradient is generally used to predict transition.

Heat transfer effects in subsonic flows are the main concern of the present author, but a related problem is that of supersonic flows, where the reported experimental work is extensive. Typical papers are those of Jack and Diaconis (9) and Czarnecki and Sinclair (2), who measured transition on bodies of revolution which could be heated or cooled relative to the airstream. In these and many other such experiments on aerodynamic models, curvature effects (both axial and transverse) might have had some influence on the data obtained. A flat plate experiment, again in supersonic flow, was performed by Higgins and Pappas (6); the plate was mounted horizontally, and boundary layer measurements were taken on the upper surface.

The only extensive investigation in subsonic flow appears to be that of Liepmann and Fila (10), using a vertical plate at a free-stream velocity of 200 ft/s; some three-dimensional effects were apparent when the plate was heated, but appeared to be intermittent in nature. An unusual feature was the repetition of the experiment at a higher free-stream turbulence level, using a grid at entry to the working section.

All the above experiments agree that wall heating caused an upstream movement of the transition point, while cooling of the wall was found to delay transition, and could be used to eliminate it in certain circumstances. A temperature ratio T_{wall}/T_{∞} of 1.4 was found to reduce the transition Reynolds number to approximately half its adiabatic value, the exact reduction depending on buoyancy and curvature effects; this is discussed in more detail in Section 2.6.8. Liepmann and Fila observed that the effect of wall heating was increased at a higher turbulence level.

Separation

The topic most relevant to the present study is the effect of heat transfer on separation of the turbulent boundary layer in subsonic flow, but the literature reveals that no detailed investigations of this have been made. The situation is rather different for supersonic flow, where a number of contributions have appeared. The majority of these are adiabatic studies involving shock-wave boundary layer interactions, compression corners or sudden steps to promote separation, but considerable effort has also been made to obtain heat transfer coefficients in regions of reversed flow. More recent experiments on subsonic separation from bodies with continuous surfaces have led to the realisation that detachment of the boundary layer is in this case a regional phenomenon, with attached and separated flow occuring alternately in this separating region. Reviews of the literature on separation of the boundary layer have been published by Chilcott (47) and more recently by Elfstrom (49).

General Investigations

Typical of the majority of experimental work are the early papers of Gadd, Cope and Attridge (54) and Bogdonoff and Kepler (41), who measured velocity profiles and heat transfer coefficients around a series of forward and backward facing steps in supersonic flow. In a more recent experiment, Chui and Kline (48) observed separation from one wall of a suddenly - diverging channel, and measured boundary layer profiles well beyond the separation point, in this case for subsonic flow. Chapman, Kuehn and Larson (46) compared subsonic and supersonic separation data, using a range of models with steps, compression corners and concave compression

surfaces. It was found that Reynolds number effects were considerable in supersonic flow, but that they could be ignored for $M = 0.4$ to $M = 1.0$.

The papers of Sandborn (70), von Doenhoff and Tetervin (3), Stratford (33) and Schubauer and Klebanoff (28) all describe how adverse pressure gradients have been employed to produce separating or near-separating boundary layers on continuous surfaces in subsonic flow. The data presented are helpful in describing the development of the turbulent boundary layer and the variation in its characteristic parameters as it nears the point of separation. The Schubauer and Klebanoff experiment is particularly well documented, and their data have been used extensively in the development of prediction methods.

Curvature Effects

The effects of curvature on supersonic separation were studied by Gadd (53), who employed a model with a convex trailing edge which fell away from the airstream. A laminar boundary layer was found to separate much more rapidly than a turbulent one. In this experiment, however, the effect of surface curvature was likely to be minor compared with that of the adverse pressure gradient created by the model shape.

Curved surfaces were also employed by Sandborn and Liu (71), in a recent detailed study of turbulent separation in subsonic flow. In this case, however, the purpose of the experiment was a thorough examination of the separating region. Forward and reversed pitot tubes, a pair of hot wires (one in the wake of the other) and flow visualisation techniques were all used to explore the region; all suggested slightly different "separation points", as a result of the unsteadiness of the flow. Downstream, where

reversed flow was continuous, it was found that the velocity profiles were similar to those for laminar boundary layers after separation.

Heat Transfer Effects

The effects of a change in wall temperature on separating flows have not been widely studied. In an early experiment by Gadd (52), a flat plate was used along with a compression surface, which brought about separation of the boundary layer. The plate could be heated or cooled over a moderate temperature range. With a turbulent boundary layer on the plate, Gadd found that the upstream effect of the compression surface could be increased by raising the plate temperature, but the effect was a small one. Measurements of boundary layer data were not extensive, and the experiment was restricted to supersonic flow. More recently, Back, Massier and Cuffel (40) studied the effect of pre-cooling the flow in a subsonic convergent nozzle. A short separation bubble was noted at entry to the convergent section in adiabatic flow; however, wall cooling was not applied at this point, but some distance upstream. Thus no significant changes in the separation behaviour were observed. Direct wall cooling was investigated by Lynes, Nielsen and Goodwin (61), on a compression corner model in hypersonic flow. Here, the cooling was applied to the wall at the separation region. For a laminar boundary layer, the distance between separation and reattachment points progressively reduced as the wall temperature was lowered, the implication being that it might be possible, at a very high rate of heat transfer, to eliminate separation entirely. Unfortunately, the investigation did not cover turbulent boundary layers, nor were the effects of wall heating studied.

Curvature

The earliest experiments involving surface curvature were those of Schmidbauer (27) and Wilcken (37), who employed ducts of rectangular cross-section and constant radius of curvature. Some attempt was made to isolate the effects of the curvature of the inner and outer duct walls on the boundary layers. However, attempts to achieve zero streamwise pressure gradient were unsuccessful, and considerable changes in static pressure were noted at entry to the curved ducts in all tests; this was partly a consequence of the small radii of curvature of the ducts.

More recently, Patel (16) and So (29) have performed similar experiments on apparatus of a somewhat larger scale. Detailed measurements near the inner wall disclosed a considerable curvature influence on the turbulent boundary layer, and Patel revised the momentum integral equation to allow for constant-radius streamline curvature.

Curvature effects on complete duct flows have been studied by Eskinazi and Yeh (50) and Mori, Uchida and Ukon (63). The former measured a developing flow in a very narrow curved duct of constant radius, with particular attention to the turbulence structure. The latter investigation was restricted to laminar flow, but included an analytical model, in which the duct cross-section was divided into a wall region and a core region: in the wall region, secondary flows were a major factor.

It is generally accepted that the detailed flow pattern near a concave surface is three-dimensional in nature, at least in laminar conditions. Patel (17) studied a turbulent boundary layer on the outer wall of a curved duct, using banks of yaw-meter probes, and disclosed a regular pattern of secondary

flows within the boundary layer. This suggested the presence of an underlying series of streamwise vortices, similar to those in concave-surface laminar layers. Vortex flows were also studied by Persen (68) who analysed a swirling stream entering a pipe. Discrepancies with experimental data were found, notably in heat transfer coefficients, which had been calculated from a universal temperature profile assumption. Persen suggested that further rotational flow within the wall layer in the pipe might be responsible, but had no method of checking this experimentally. Increased rates of heat transfer from concave surfaces, compared with flat ones, have also been measured by Thomann (34) in supersonic flow.

The incorporation of streamline curvature effects into boundary layer prediction methods is not far advanced, no doubt partly as a result of the lack of suitable experimental data. Bradshaw (42) has drawn a formal analogy between buoyancy and curvature influences in turbulent flow, and concluded that the latter are considerable if δ/R exceeds $\frac{1}{300}$. Boundary layer predictions, using the analogy to determine an effective mixing length dependent on surface curvature, were made by the method of Bradshaw, Ferriss and Atwell (44) for certain experimental data; considerable improvement was noted over the "flat plate" prediction. Rastogi and Whitelaw (69) have recently developed a version of the Spalding and Patankar (32) method for radii of curvature of the same order as δ, intended primarily for calculation of turbine blading boundary layers. Again, a mixing length theory was used; evaluation of the method was limited by lack of experimental data, but it appeared promising.

Buoyancy

In this present study, buoyancy effects in isolation are not of interest; it is only when they are combined with general fluid motion that they are of relevance, and this review has been limited accordingly. Again, the literature is not extensive.

The early work of Richardson (23) established a parameter for stability in stratified flows, after observation of atmospheric boundary layers, and give a qualitative picture of the growth and decay of turbulence brought about by density gradients. Detailed analyses of boundary layer behaviour are confined to laminar flow; Sparrow and Minkowycz (75) have studied flow over a heated floor, predicting an increase in local skin friction over the adiabatic case, for zero stream-wise pressure gradient. Gunness and Gebhart (56) analysed wedge flows for a variety of wedge angles in both horizontal and vertical configurations. Acrivos (38) has produced a general analysis of combined free and forced convection, again for laminar boundary layers.

Experimental work has been contributed by Mori and Uchida (62), on combined free and forced convection effects between parallel plates, and by Nicholl (66) on turbulent boundary layer behaviour in stably and unstably stratified flow conditions; most notable here were the observed effects of stabilising forces in encouraging reverse transition. A detailed discussion of buoyancy and other body forces is included in Appendix B.

Re-laminarisation

The subject of reverse transition has been covered by a number of papers, typical of which are those of Narayanan and Ramjee (65) and Back, Cuffel and Massier (39). These authors measured quantities within

accelerated boundary layers; reverse transition was found to be dependent on the value of a parameter based on streamwise pressure or velocity gradient. The influence of body forces even in adiabatic flow was demonstrated by Eskinazi and Yeh (50) in their curved channel experiment, where significant turbulent decay was noted in the region of the inner wall.

A fuller account of certain of the above papers, along with a general discussion of reverse transition, is presented in Appendix B.

Free-Stream Turbulence

The effect of free-stream turbulence on the development of boundary layers has been examined in a number of papers. Experimental data have been provided by Smith and Kuethe (74) on laminar boundary layers, and by Buyuktur, Kestin and Maeder (45), Junkhan and Serovy (58), Kearney et al (59) and Talmor and Weber (77) for both laminar and turbulent layers; Kestin (60) has contributed a general discussion on the topic. There is a general agreement among these authors that the influence of turbulence on the turbulent layer is at most very slight, but that some effect on the laminar layer may occur, especially in the presence of streamwise pressure gradients. In contradiction to this, a measurable effect on the turbulent layer has been claimed by Evans (51) from his measurements on an aerofoil in a cascade. Theoretical treatments are rare: Kearney et al (59) employed a prediction method incorporating the turbulent kinetic energy equation and found good agreement with experiment, in that effects on the turbulent boundary layer were negligible up to the experimental maximum intensity of 4%. The theoretical work of Morsy and Silver (64), at present incomplete, may well throw further light on the subject.

A more detailed discussion on free-stream turbulence effects, and an appraisal of the experimental data, is contained in Appendix A.

Conclusions

In this review, an attempt has been made to describe the present state of knowledge of boundary layer behaviour under a variety of influences. Arrival at firm conclusions has generally been prevented by the incompleteness of the literature, and in particular by a serious lack of experimental data. Exceptions to this are the studies of supersonic transition and separation, from which it may be possible to obtain at least a qualitative picture of the equivalent behaviour of subsonic flows. Certain other relevant topics, notably the influence of streamline curvature, are beginning to receive more attention, and future progress may be rapid

It must be emphasised that the effect of wall heating on turbulent separation has undergone no previous detailed examination, and that no direct comparison may be drawn between the data presented in this thesis and those from earlier experiments.

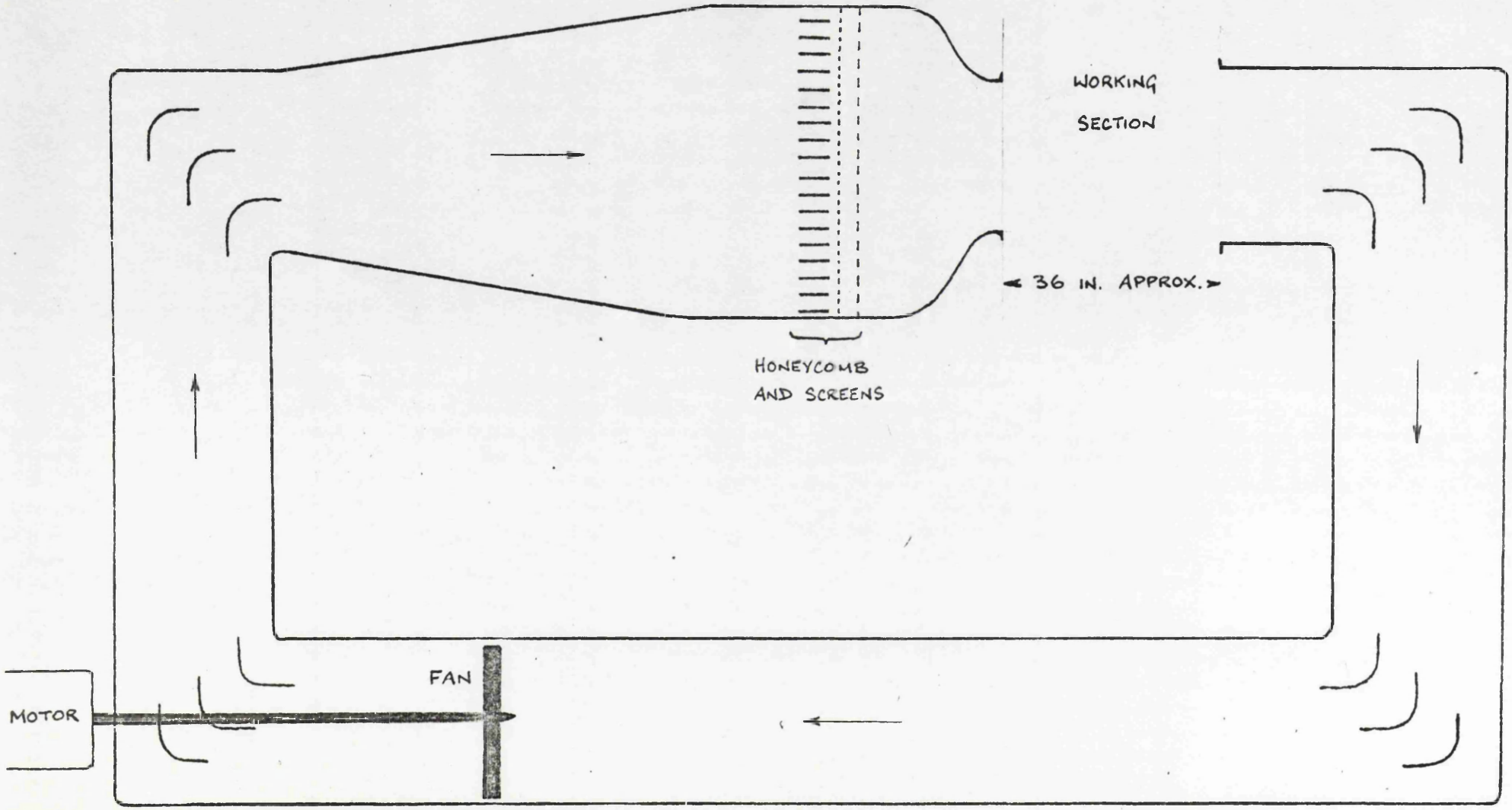

Figure 3: Plan view of the wind tunnel.

CHAPTER 2

FLAT PLATE EXPERIMENTS - THE EFFECT OF PLATE HEATING ON TRANSITION

An experimental study of boundary layer transition on a flat plate, and the effect of plate heating on movement of the transition point, began the research programme. The amount of time to be devoted to this study was of necessity limited, so the measurements taken were not extensive; nevertheless, it was hoped that comparisons could be drawn with other published work. As mentioned in Chapter 1, the value of these tests lay partly in the development of instrumentation and experimental techniques, for use in the more extensive measurements in the curved duct (see Chapters 3 and 4).

2.1 The Wind Tunnel

A low-speed, recirculatory wind tunnel was used, with an open working section, the layout of which is shown in Figure 3. This was powered by a D.C. electric motor, initially operating off a 440-V supply, giving airspeeds of up to 120 ft/s. Later, this supply was removed (see Section 2.4) in favour of the normal 250-V A.C. mains, with full-wave rectification. The contraction ratio of the tunnel was approximately 6:1, giving a 16 inch diameter jet across the working section, the length of which was limited to 36 in.

2.2 The Flat Plate

A plate of high thermal capacity was thought desirable, to minimise temperature fluctuations. Accordingly a 0.5 in. copper plate was used, measuring 26 in. x 6 in. Its leading edge was chamfered and the

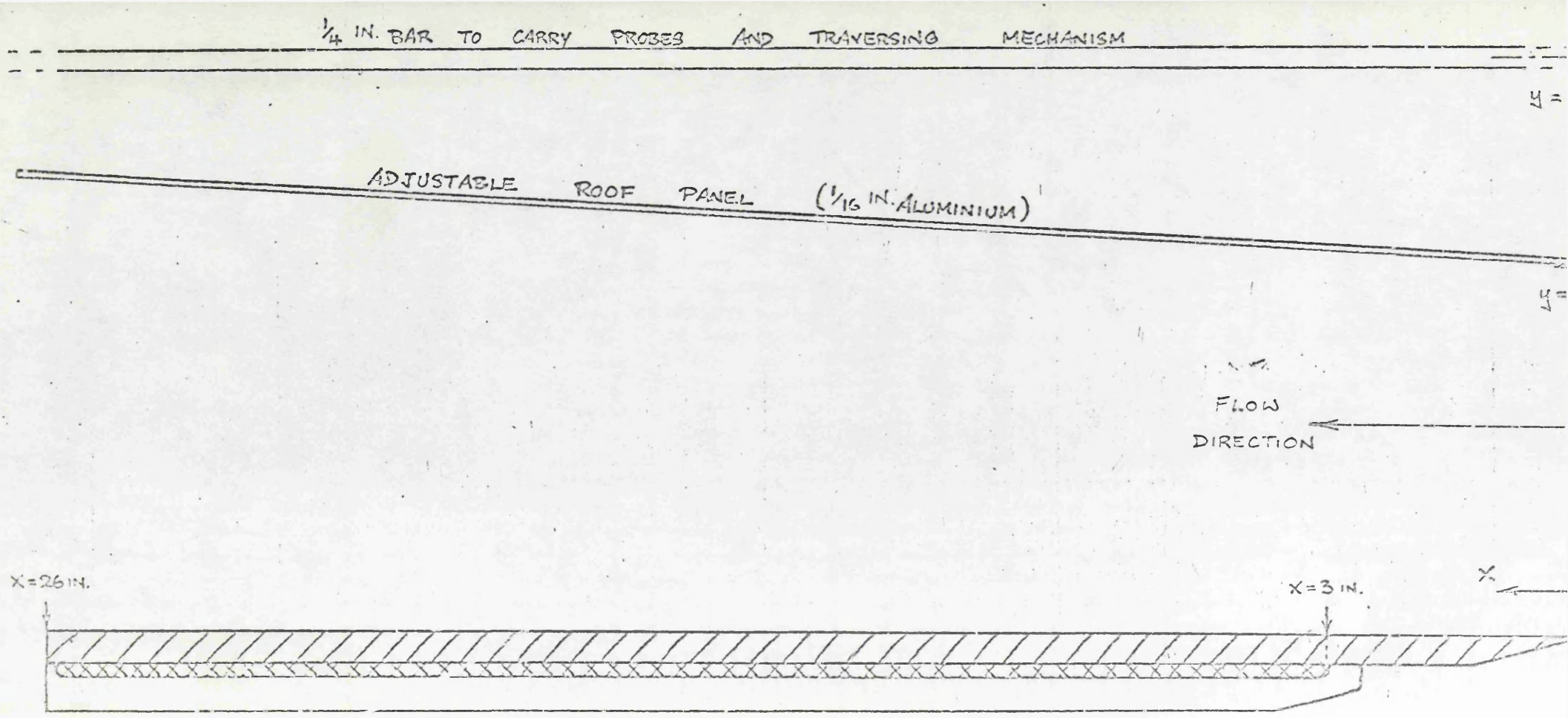

Figure 4: The flat plate.

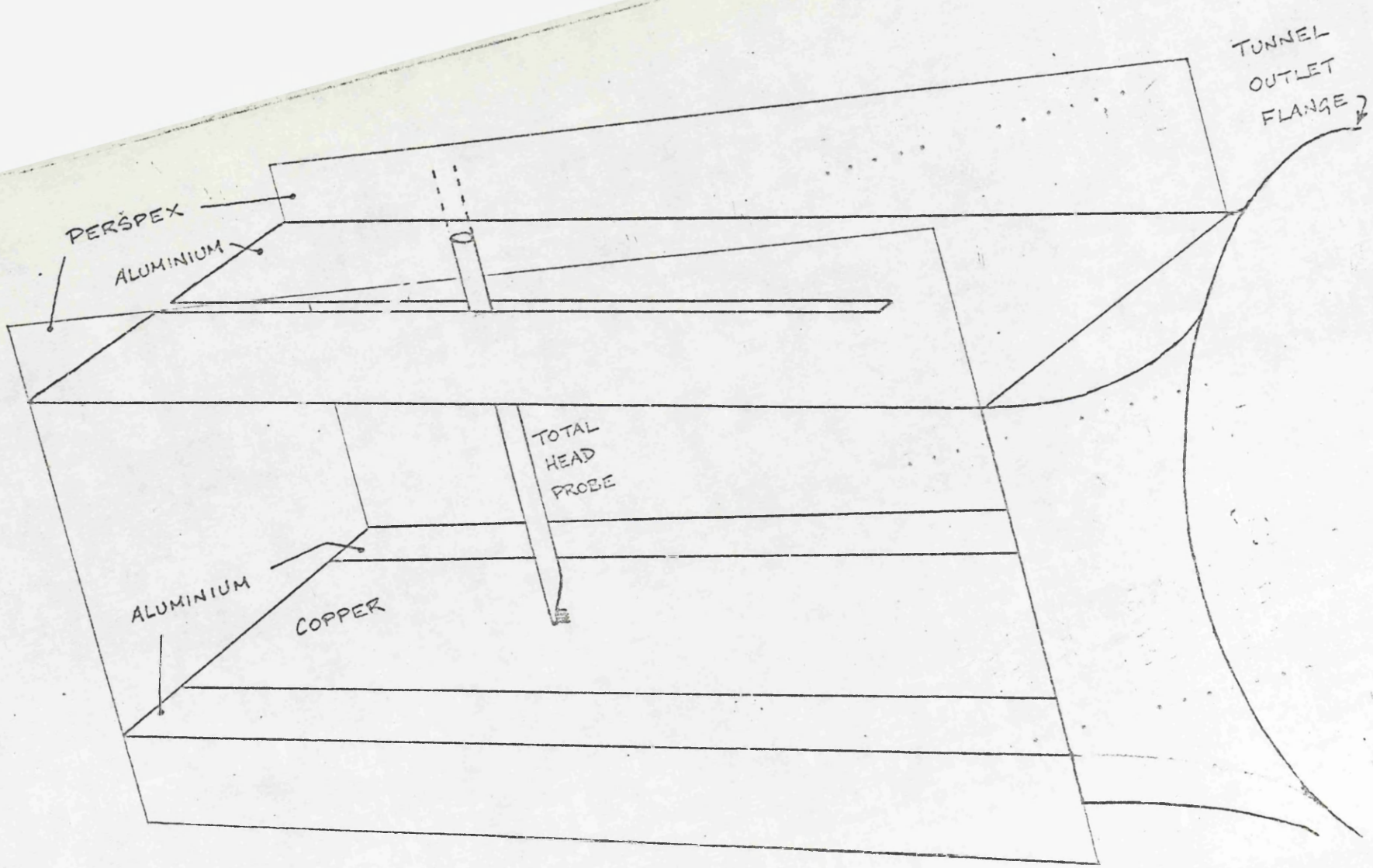

Figure 5: The flat plate installed.

surface highly polished. Static pressure tappings and thermocouple locations were drilled, and the positions of these are given in Figure 4. It was decided to build up a duct, with the copper plate acting as the floor (a vertical alignment was considered, but it was feared that buoyancy effects might cause three-dimensional flow). Perspex walls and an aluminium roof, which was adjustable to vary the streamwise pressure gradient, completed the duct. Before installation, the copper plate was fitted with 2 in. spacers in thin aluminium along its sides, to protect the perspex walls from excessive heat. The roof was adjusted so that the duct cross-section was about 10 in. square at entry. This was joined to the circular exit of the tunnel by curved aluminium panels on three sides, the floor being kept open to allow a laminar boundary layer to form on the copper plate. The complete installation is shown in Figure 5.

Plate heating was performed by a 500 W Isopad element, measuring 24 in. x 6 in., directly under the copper, insulated beneath by a sheet of Sindanyo (see Figure 4). The regulator employed a variable on/off cycle, the thermal inertia of the copper ensuring that no measurable cyclic temperature fluctuations reached the upper surface of the plate. Such fluctuations as did exist must therefore have been below $\pm$ 0.1 deg C at all times (see Section 2.3).

2.3 Instrumentation

Provision was made for up to four pitot-static tubes to be inserted through the duct roof, to monitor the mainstream flow. A total-head probe (see Figure 6), was constructed, using four hypodermic-

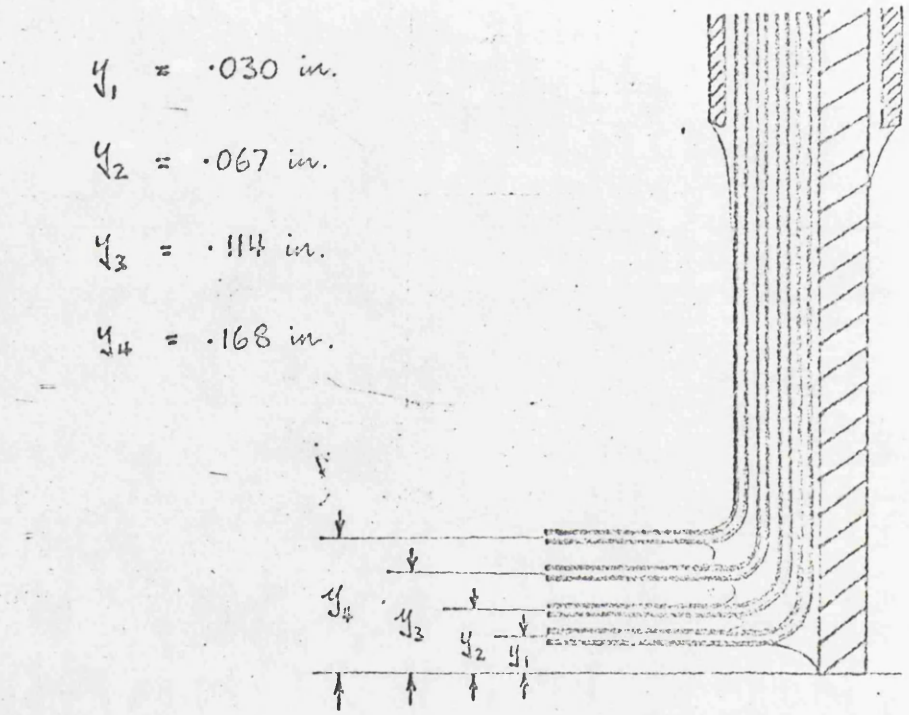

Figure 6: The total head probe.

needle tubes of 0.023 in. outer diameter and 0.010 in. bore, to measure the total head pressure and hence the velocity distribution within the boundary layer. This probe was carried on traversing gear and inserted through the roof of the duct. The design incorporated a pedestal which made contact with the plate surface when the probe was in position. Spacers could be fitted below this pedestal to extend the range of the probe.

Pressure leads from pitot-static and total-head probes, and from the static pressure tappings in the plate itself, were connected to a multi-tube manometer. This had a scale of 24 in. and incorporated a tilting mechanism which permitted any attitude between horizontal and vertical. The manometer fluid was hexane (specific gravity 0.68). With this instrument, pressures were measurable to within 0.001 in. of water.

Plate temperature was measured by iron-constantan thermocouples inserted into drillings in the copper, so that the hot junctions lay along the plate's centre-line. These were connected through a multi-position switch to a potentiometer, giving accuracy of measurement to within 0.1 deg C.

2.4 Early Testing and Development

During early testing of the flat plate assembly, it became clear that the speed stability of the tunnel motor, particularly at low air speeds, was quite unsatisfactory. The 440-volt supply was disconnected, and a diode circuit built to provide full-wave rectification

of the normal A.C. mains. This supply gave much improved performance, and speed fluctuations were held well below 1% throughout the working range. Inevitably the reduced supply voltage cut the maximum available airspeed; this was found to be 60 ft/s.

A check on turbulent intensity in the duct, made with a single hot wire outside the boundary layer, showed this to be below 0.1% throughout the speed range. This was judged to be satisfactory, and no modifications were made to the tunnel screen system. A series of exploratory tests were then made, at zero pressure gradient to determine the nature of the boundary layer on the copper plate.

It was found at first that for all airspeeds, this boundary layer was turbulent throughout. Alteration of the plate angle of attack, which was possible within a generous range, had no effect. After further tests, a region of relatively high-pressure air was found to exist immediately below the plate leading edge. This was diverting the airstream, giving a very large effective angle of attack, which could not be countered by plate movement. Separation from the upper surface was promoted at the leading edge, with turbulent reattachment taking place some distance downstream. The cause of the problem was excessive blockage from the plate mounting, obstructing the airflow below the plate. A new design of support reduced the blockage and allowed a laminar boundary layer to form on the upper surface.

Total-head pressure showed no measurable variation either along or across the mainstream, so only a single pitot tube was required outside the boundary layer. To minimise interference, this was

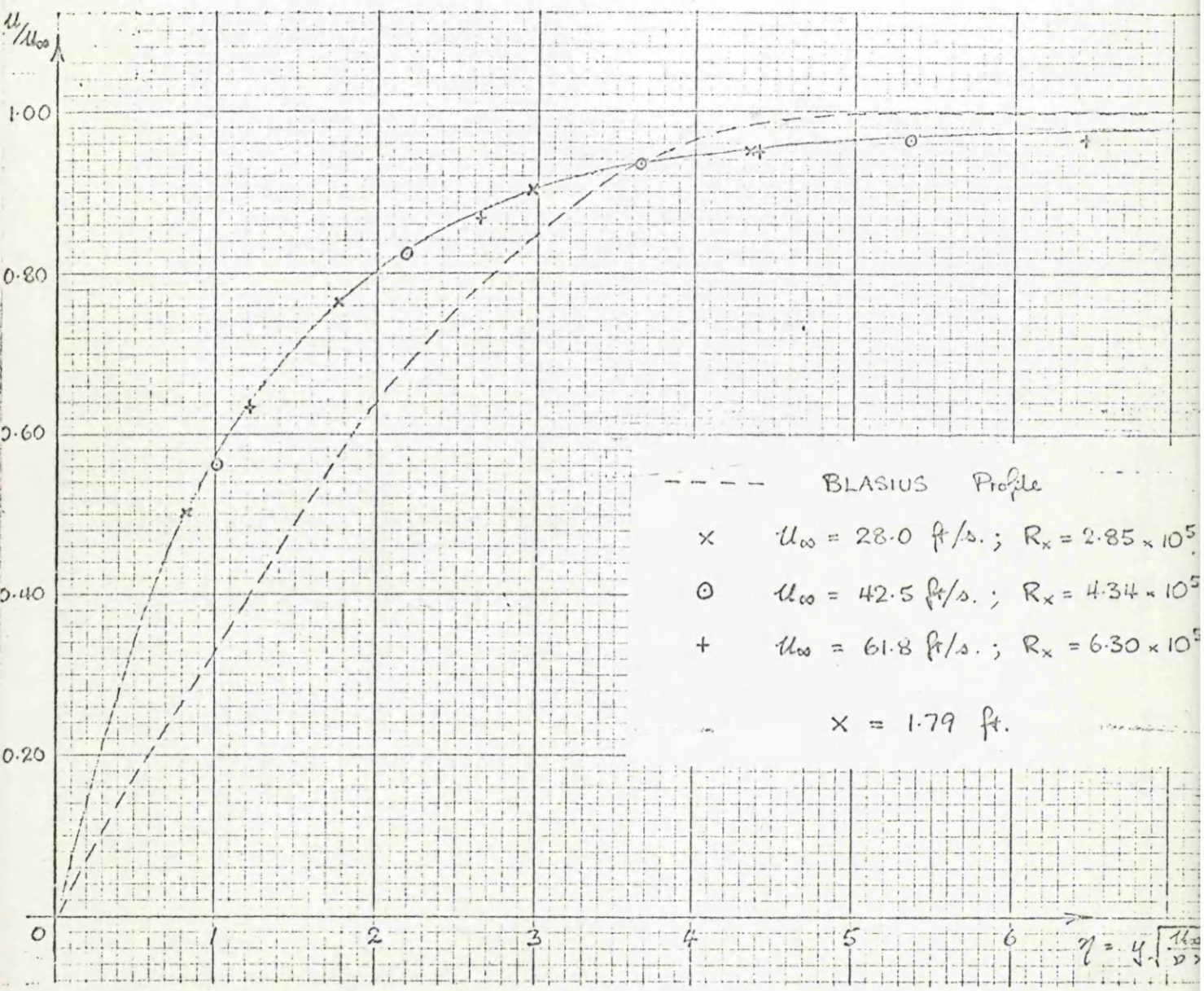

Figure 7: Laminar velocity profiles at zero streamwise pressure gradient.

positioned just upstream of the duct exit.

The restricted tunnel working section, with its limitations on the possible length of the flat plate, did not make for ideal conditions. Low airspeeds were essential to produce a boundary layer of generous thickness, but the resulting low Reynolds numbers suggested that laminar transition at zero streamwise pressure gradient would not occur.

2.5 Main Test Programme

The nature of this boundary layer at several flow speeds, under adiabatic conditions at zero streamwise pressure gradient, was then investigated. The velocity profiles obtained were plotted in the form $\frac{u}{u_\infty}$ against η, where

$$\eta = y\sqrt{\frac{u_\infty}{\nu x}} ,$$

and are shown in Figure 7 along with the Blasius laminar profile. It will be seen that there is considerable disparity between the two profiles. Variations of underside blockage and plate angle of attack failed to reduce this disparity. It was nevertheless concluded for various reasons (see Section 2.6), that the experimental boundary layer was laminar. The reduced speed range of the tunnel precluded the attainment of critical Reynolds numbers within the length of the plate. Tests on the effect of heating at this (zero) pressure gradient were inconclusive, as the heater output was too low to give rise to any marked change in velocity profile.

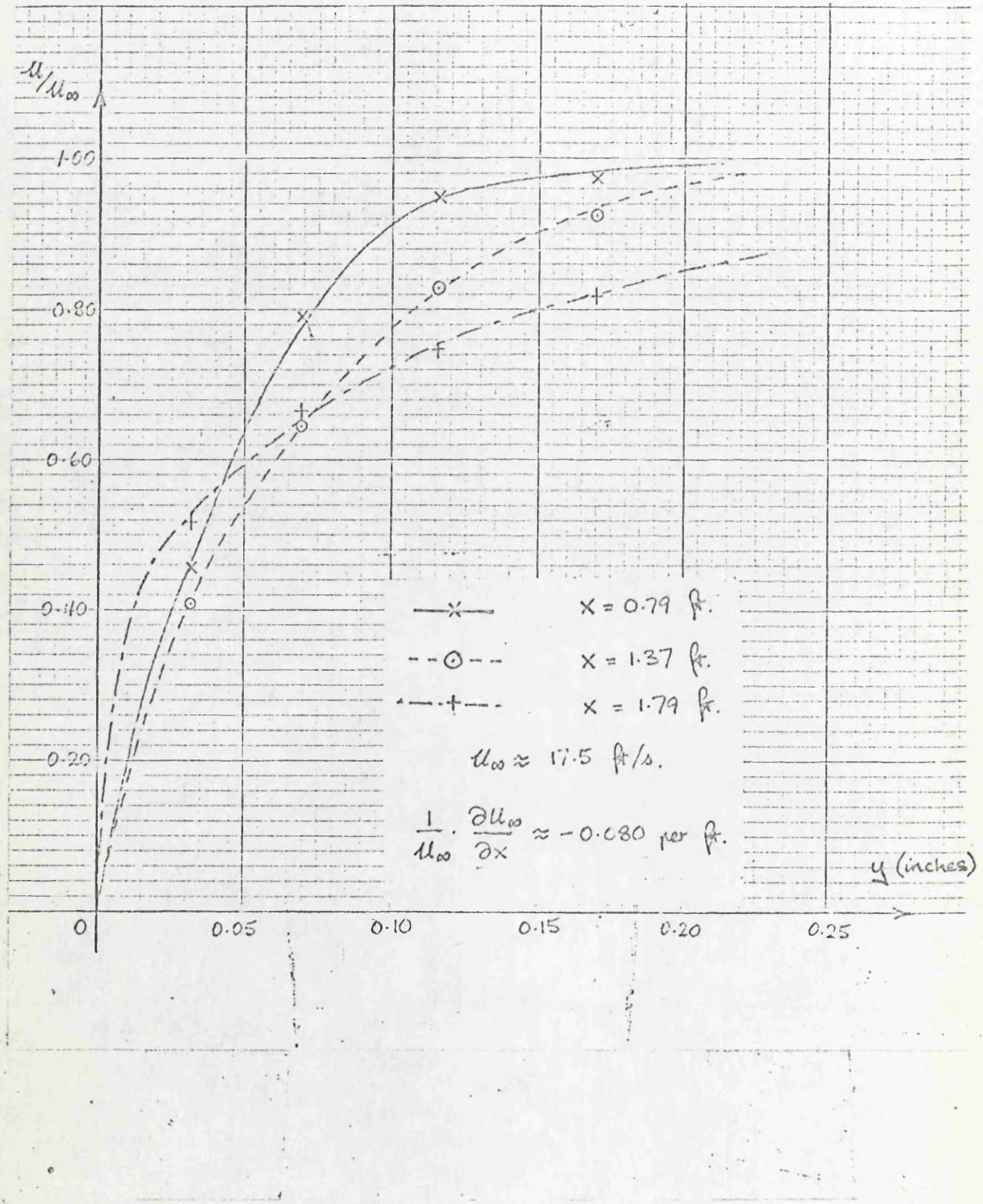

Figure 8: Laminar, transition and turbulent velocity profiles.

It was clearly necessary to introduce an adverse pressure gradient if laminar transition were to be observed at all. Further, the first tube of the pitot probe (i.e. that nearest the plate surface) was still reading around 60% of the mainstream velocity near the trailing edge (see Figure 7), and so a thicker boundary layer was most desirable. The next series of tests was performed at an adverse static pressure gradient, and corresponding adverse velocity gradient, given by

$$\frac{1}{u_\infty} \cdot \frac{\partial u_\infty}{\partial x} \doteq -0.080 \text{ per foot},$$

with a mean value of u_∞ around 17.5 ft/s. Profile measurements showed that transition took place well within the traverse zone on the plate.

The transition point was fixed in the following manner. The four branch pitot probe was traversed from its most forward position, and laminar, transition and turbulent velocity profiles were recorded in turn (see Figure 8). Particular attention was paid to the reading P_{o1} of the tube nearest to the plate surface, and to the dynamic pressure ratio at this point,

$$\frac{P_{o1} - P}{P_{o\infty} - P}$$

where P is the local static pressure, assumed to be independent of y. In the laminar region, as the layer thickens, this pressure ratio falls steadily, because y_1 is constant and successive profiles are geometrically similar. At transition (see Figure 8), the ratio shows a sudden rise, reaching a maximum and falling again when

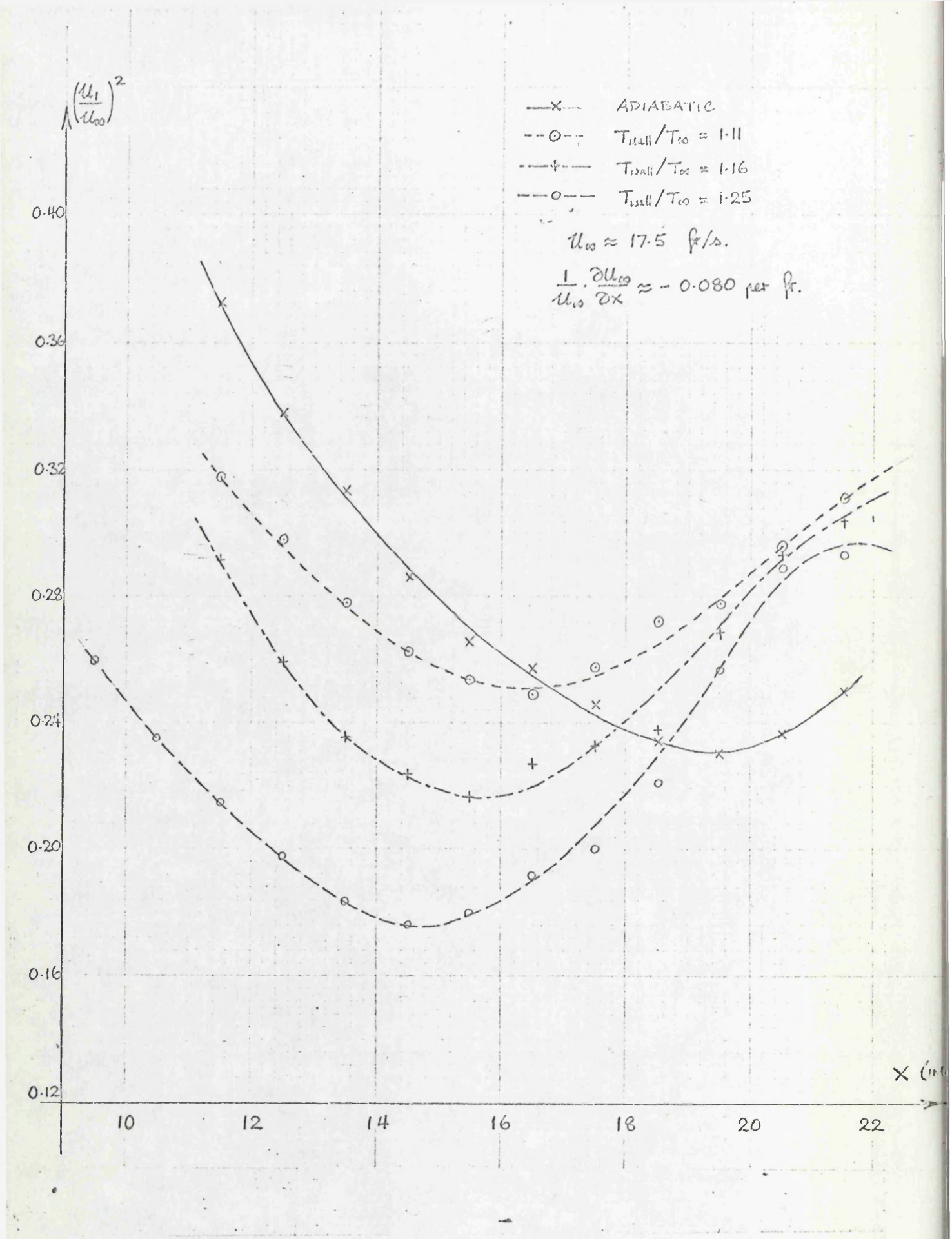

Figure 11: Dynamic pressure ratio distributions for four plate temperatures.

TABLE 1.

INSTRUMENT	TOTAL-HEAD PROBE				STATIC TAPPING	PROBE P_∞	NONE (AMBIENT PRESSURE)
MANO. TUBE NO.	1	2.	3	4	9	15	20
ZERO READINGS	10·67	10·68	10·47	10·55	10·31	10·54	10·66
TEST READINGS	10·49	10·22	9·83	9·69	10·53	9·14	10·70
Δl = (ZERO) - (TEST)	0·18	0·46	0·64	0·86	-0·22	1·40	-0·04
CORRECTED Δl_c	0·22	0·50	0·68	0·90	-0·18	1·44	—
$L = \Delta l_c - (\Delta l_c)_9$	0·40	0·68	0·86	1·08		1·62	
$\frac{L}{L_{15}} = \frac{L}{L_\infty}$	0·247	0·420	0·531	0·667		1·00	
$\sqrt{\frac{L}{L_{15}}}$	0·497	0·648	0·729	0·816		1·00	
PROBE POSN.* y =	0·030	0·067	0·114	0·168		(∞)	inches
AIR TEMP.**	304	300	297	295		290	K
P_∞ / P_{local}	1·05	1·035	1·025	1·020		1·000	
$\sqrt{P_\infty / \rho_{local}}$	1·025	1·020	1·015	1·010		1·000	
$\sqrt{\frac{L}{L_{15}} \cdot \frac{P_\infty}{P_{local}}} = \frac{u}{u_\infty}$	0·510	0·661	0·740	0·824		1·000	

This last entry gives the true, temperature-corrected values for plotting the velocity profile. The readings were taken at a point 1.79 ft from the plate leading edge, for values $u_\infty = 11.5$ ft/s., $T_{wall} = 35$ K.

* A correction of 0.002 in. is to be added here to allow for the effects of wall proximity - this is included in all graphs.

** Assuming that the thermal and velocity boundary layers are of similar thickness.

turbulence is fully established. The positions of the minimum and maximum values were taken as the start and end of transition respectively.

Traverses were produced, for adiabatic flow and for three heat input rates to the plate. Plate temperatures were checked regularly, and found to be satisfactorily constant with time. A considerably reduced temperature near the leading edge was noted and accepted as inevitable with a single heater circuit; fortunately the traverse zone was not greatly affected. The resulting curves of dynamic pressure ratio against x are given in Figure 11; it will be seen that the end of transition has not generally been reached, but that the start of transition is evident in all cases. The Reynolds number for each start of transition was calculated, and plotted as a ratio of the adiabatic value against the temperature ratio T_{wall}/T_{∞} in Figure 12. Two curves are shown, for values of ν calculated at ambient and wall temperatures.

Throughout these tests, extreme care was found to be necessary when reading the manometer. Because of the low airspeeds involved and the small corresponding pressure differences, the manometer was tilted to $1^{o}30'$ from the horizontal to increase sensitivity; even so, measuring accuracy within 0.01 in. was necessary in many cases. Table 1 shows the recording of a transition velocity profile in typical conditions, showing the calculations and corrections needed to obtain the true velocity distribution. Manometer response to the boundary layer pitot probe was inevitably quite slow: intervals between readings of at least ten minutes were required.

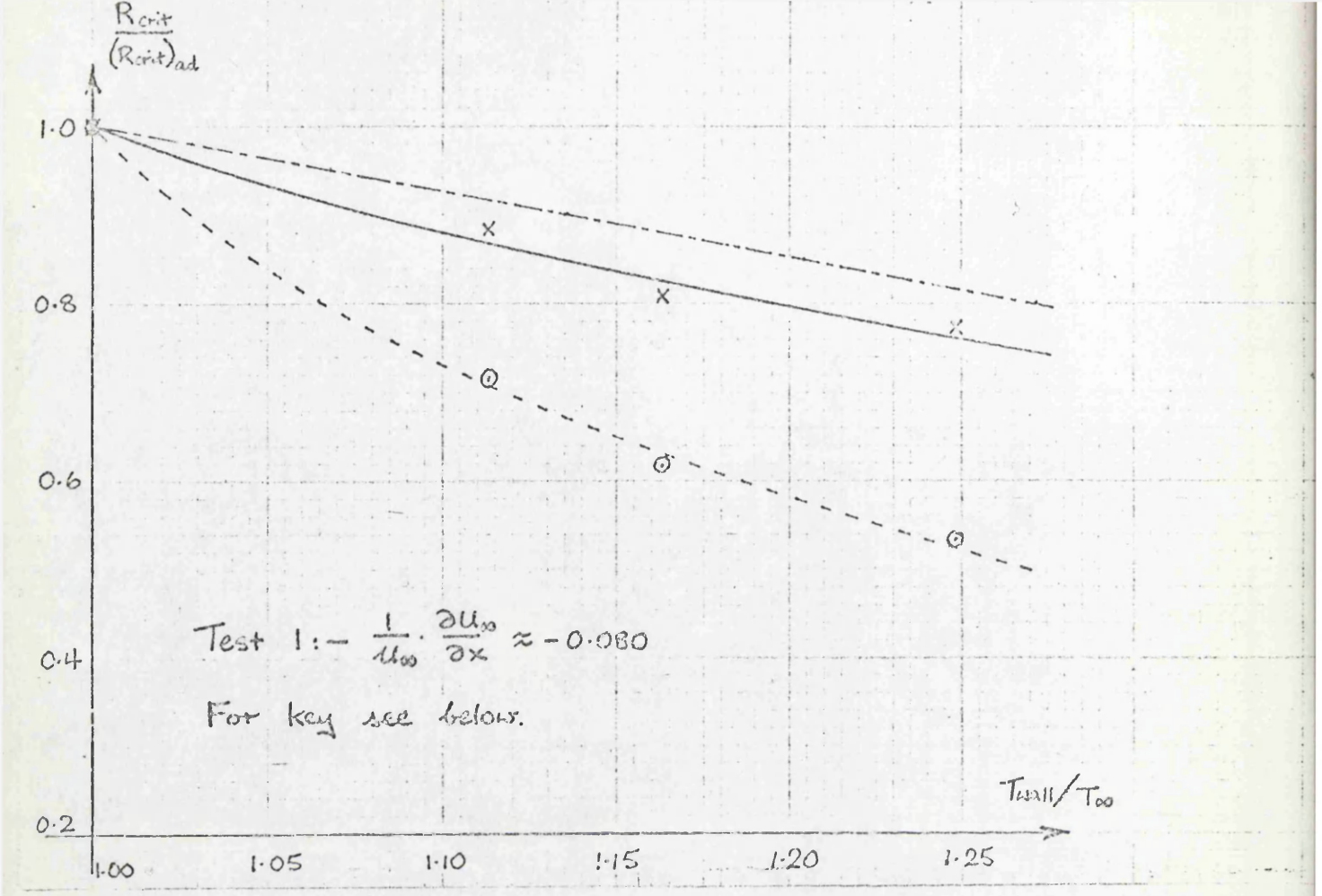

Figure 12: The effect of heating on transition - Test 1.

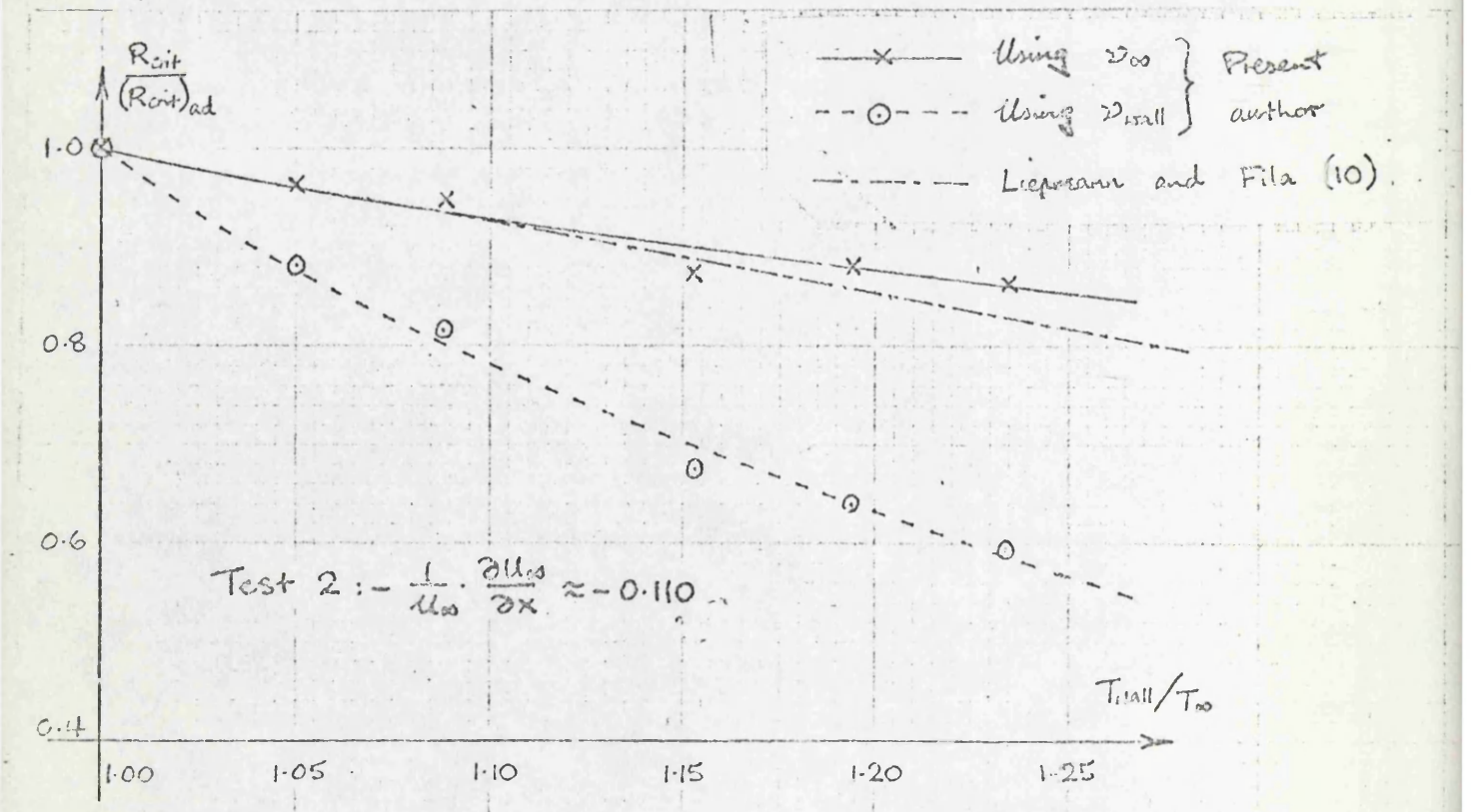

Figure 13: The effect of heating on transition - Test 2.

A second set of traverses to supplement those described above, was then obtained. It was originally intended that these be taken at a higher airspeed, to reduce the difficulties with the manometer, but the boundary layers then became too thin to give clear evidence of transition. Consequently, airspeed was reduced to around 12 ft/s., and a more severe adverse pressure gradient, with

$$\frac{1}{u_\infty} \cdot \frac{\partial u_\infty}{\partial x} \doteq -0.110 \text{ per foot},$$

was set up. In this case, six traverses of dynamic pressure ratio were produced, in an identical manner to the previous set. Curves of critical Reynolds number ratio against T_{wall}/T_∞ were again produced, and are shown in Figure 13.

2.6 Discussion

2.6.1 Laminar velocity profiles.

The behaviour of the flat plate boundary layer under zero streamwise pressure gradient is worthy of comment. As may be seen from Figure 7, comparison with Blasius would seem to indicate that the measured profile is in the transition region. Yet this cannot be the case: the profile shows remarkable stability, and persists in geometrically similar form along the full length of the plate. Under adverse pressure gradients, the profile behaves in an identical fashion, until a rapid change to a typical turbulent profile takes place. Hot wire investigation, using a probe too large for accurate boundary layer work, confirms a satisfactorily low level of turbulence in the layer upstream of this rapid change of profile. So it was accepted that despite its untypical velocity distribution, the boundary layer

at zero pressure gradient was laminar throughout.

The explanation for this phenomenon is open to conjecture. Plate angle of attack was not responsible. Mention has already been made of the short working section of the tunnel and the restrictions this imposed, one of which was a rapid change in duct cross-section upstream of the plate leading edge. It is suggested that these far-from-ideal entry conditions were responsible. The fact that other workers, with greater freedom in this area, have had no trouble in obtaining Blasius laminar profiles, lends weight to this suggestion.

2.6.2 Plate spacers.

The copper plate was fitted with aluminium spacers to protect the perspex walls of the duct, as described earlier. In practice, the plate temperature never approached a value high enough to threaten perspex, and the spacers could have been omitted without damage.

2.6.3 Pressure gradient effects

No quantitative study was made of the effects to streamwise pressure gradient. That its effect on transition is considerable is evident from a study of the test results; a reduction in critical Reynolds number by a factor of at least 7 has been produced by an adverse pressure gradient alone (Figures 7 and 13.) Only the effect of heating at a given duct geometry was investigated in detail. Of course, application of heat to a boundary layer may alter considerably the streamwise gradient due to thickening of the layer. Here, however, the change was quite small, so the pressure gradient was almost constant.

Compensation may be made by adjusting the duct geometry until the pressure distribution returns to its adiabatic form. This was not attempted in these experiments, since fixed-geometry results were felt to have more relevance to flow in rotary machines.

2.6.4 Static pressure variation.

The assumption was made that static pressure was uniform across the duct, for a given value of x. This was verified by comparing the distributions given by plate static tappings and mainstream pitot-static tubes.

2.6.5 Manometer accuracy.

Accuracy in manometer reading was an essential factor, as has already been mentioned. The adopted angle of $1^{\circ}30'$ from the horizontal for the manometer tubes was fixed after testing at a 1° angle disclosed a lack of repeatability in the readings. This was unfortunate, as more sensitivity would have been appreciated. Even so, repeatble accuracy of pressure measurement to within 0.0005 in. of water was possible at the adopted angle. For tests at airspeeds above 30 ft/s, the angle of tilt was increased to a suitable value.

2.6.6 Buoyancy effects.

The location of the copper plate on the floor of the duct inevitably gave rise to buoyancy effects when heated. One method of eliminating these is to mount the plate vertically, as one of the walls of the duct; this approach was used by Liepmann and Fila (10). However, there is a possibility that air density changes near the heated surface will set up an upward velocity component, and the flow

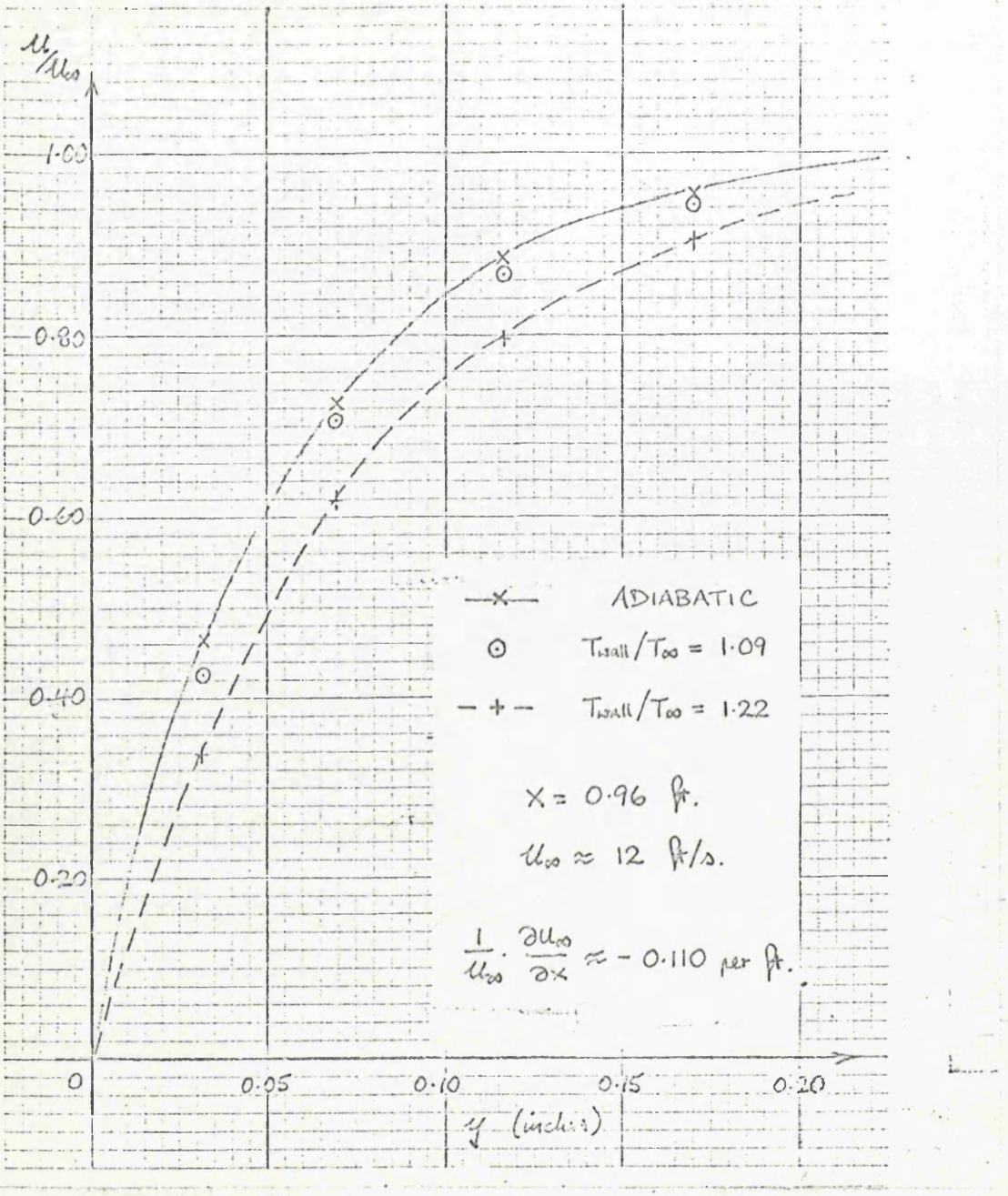

Figure 9: The effect of heating on the laminar boundary layer.

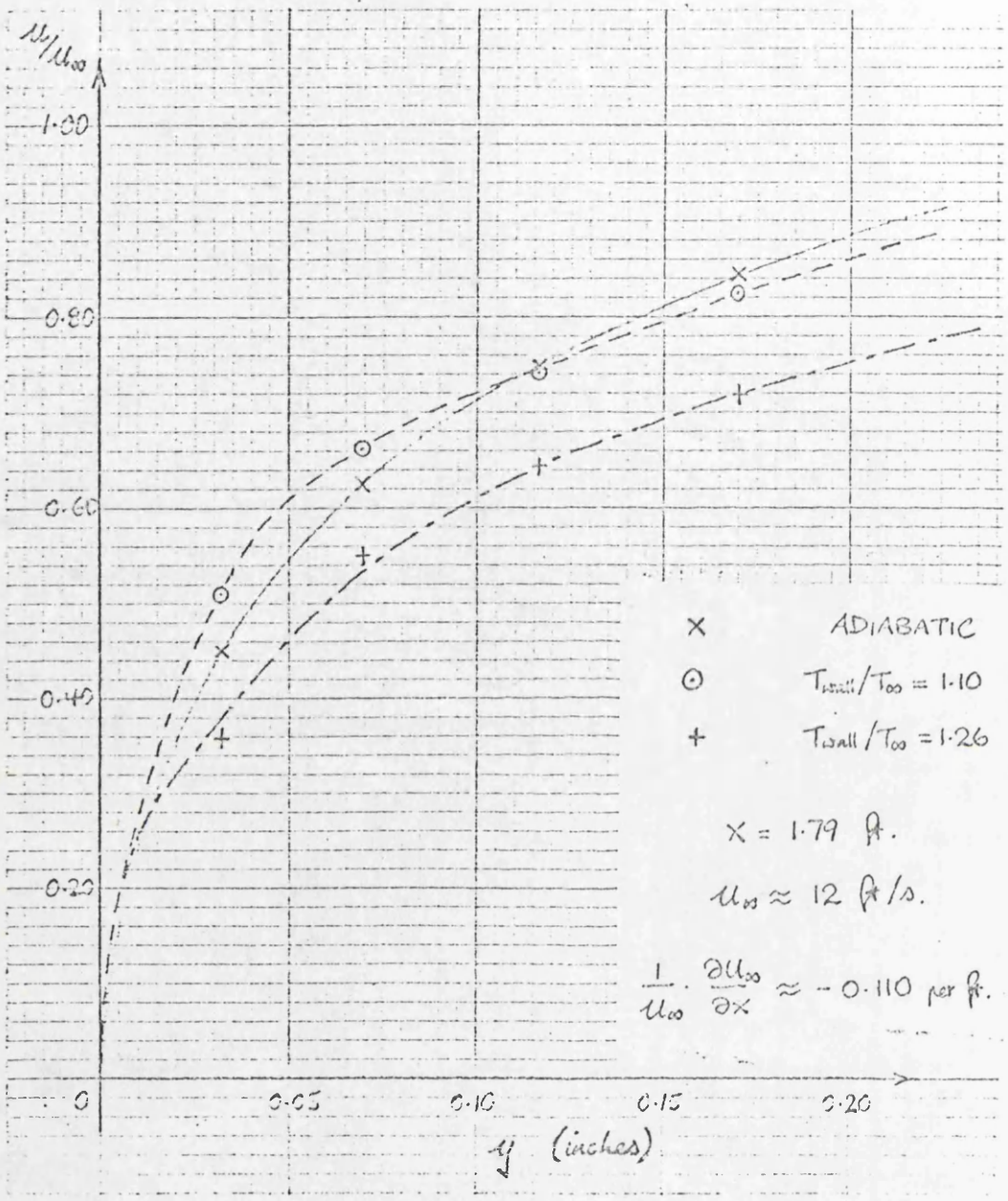

Figure 10: The effect of heating on the transition boundary layer

becomes three-dimensional. Liepmann and Fila experienced some difficulty in obtaining regular velocity profiles on their plate, and it is suggested that this may have been the cause. It was felt that with airspeeds an order of magnitude below those used by Liepmann and Fila, use of a vertical plate was to be avoided.

No attempt was made to evaluate experimentally the effects of buoyancy from the horizontal plate. Although it was appreciated that these effects were likely to be considerable in this experiment, it was considered that in the overall picture of flow over compressor blading, gravitational buoyancy would be insignificant. A fuller discussion of buoyancy effects, both gravitational and centripetal, is given in Appendix B.

2.6.7 Transition point fixing.

The method for locating the point of transition from laminar to turbulent flow in the boundary layer has already been described; it is a well-established one (24). It is to be expected that other methods, for example, using hot wires, might give slightly different results. However, for comparative tests, such as in this experiment, the absolute position of the transition point is of secondary importance to its movement, an accurate picture of which was given by the method used.

2.6.8 Effect of heat transfer on transition.

In general, heat transfer to the boundary layer has a similar effect to that of an adverse pressure gradient. Thus a laminar layer in sufficiently stable conditions will merely be thickened (Figure 9) while a transition velocity profile will become fully turbulent as in Figure 10. Most important to this investigation, transition takes

place at a lower Reynolds number than before.

A study of Figures 12 and 13 shows a good agreement between the two tests. Critical Reynolds number falls almost linearly with rising values of T_{wall}/T_{∞}, with a tendency towards levelling-off in the upper ranges. Thickening of the boundary layer under heating is beginning to reduce the magnitude of the adverse pressure gradient, though only to a small degree.

Published experimental work on heated flat plates is fairly common, but investigations of transition in such cases are comparatively rare. Generally these are supersonic tests, and investigate wall cooling effects as well as heating. Jack and Diaconis (9) and Czarnecki and Sinclair (2) experimented on bodies of revolution, while Higgins and Pappas (6) used a horizontal flat plat with zero pressure gradient, the tests being made at Mach numbers between 1.6 and 3.2. The only comparable subsonic results are those of Liepmann and Fila (10) on a vertical flat plate at zero pressure gradient with a flow velocity of 200 ft/s. The severe adverse pressure gradients used in the author's experiments prevented exact comparisons with the above work. However, the results of Liepmann and Fila are included in Figures 12 and 13 to give some guidance.

From these Figures, it will be seen that for $(T_{wall} - T_{\infty}) = 80$ deg.C giving $T_{wall}/T_{\infty} = 1.27$, critical Reynolds number at v_{∞} falls by 33% and 19% from its adiabatic value, for the two tests. For the same temperature ratio, Liepmann and Fila quote 22%: the authors of (9),(2) and (6) quote about 30%, 40% and 40% respectively. Comparison of the flat plate results is further complicated by the fact that Liepmann

and Fila avoided buoyancy effects; Higgins and Pappas and the author did not.

Comparing conditions for the author's two tests in some detail, it is seen that the transition boundary layer is considerably thicker for the second test, at all heat inputs; what is more, it thickens much more rapidly under heating. This, it is suggested, brings about diminution of the adverse pressure gradient much more rapidly, reducing the apparent effect of heating.

Thus the results of the first test more closely approach the constant pressure gradient case for which a reduction in critical Reynolds number of about 40% might be expected. This figure is similar to that recorded by Higgins and Pappas (6) at zero pressure gradient. It may be that the effect is independent of Mach number and pressure gradient, provided the latter is held constant.

2.6.9 Nearness to laminar separation

From Figure 11, it is apparent that increasing heat inputs depress the minimum critical pressure ratio, at the start of transition. Presumably under suitable conditions, this process may continue until the ratio becomes zero and laminar separation occurs. Schlichting (25) reporting on the work of Pohlhausen, quotes a dimensionless parameter for laminar boundary layer stability,

$$\Lambda = \frac{\delta^2}{\nu} \cdot \frac{du_\infty}{dx}$$

with $\Lambda <- 12$ for separation to occur. Calculations based on the above experiments give $\Lambda = -10$ in the most extreme case, indicating

that a little extra heating capacity might produce laminar separation.

2.7 Conclusions

It may be concluded that heat transfer into the boundary layer on a flat plate produces the following effects:

(1) Thickening of the boundary layer.

(2) Movement of the transition point towards the leading edge, i.e. a reduction in the critical Reynolds number.

These are both, qualitatively at least, independent of pressure gradient. In a fixed-geometry duct, boundary layer thickening has a favourable effect on streamwise pressure gradient, and this restricts movement of the transition point. This effect may well merit further investigation.

Such comparison as can be made with published work is quite favourable.

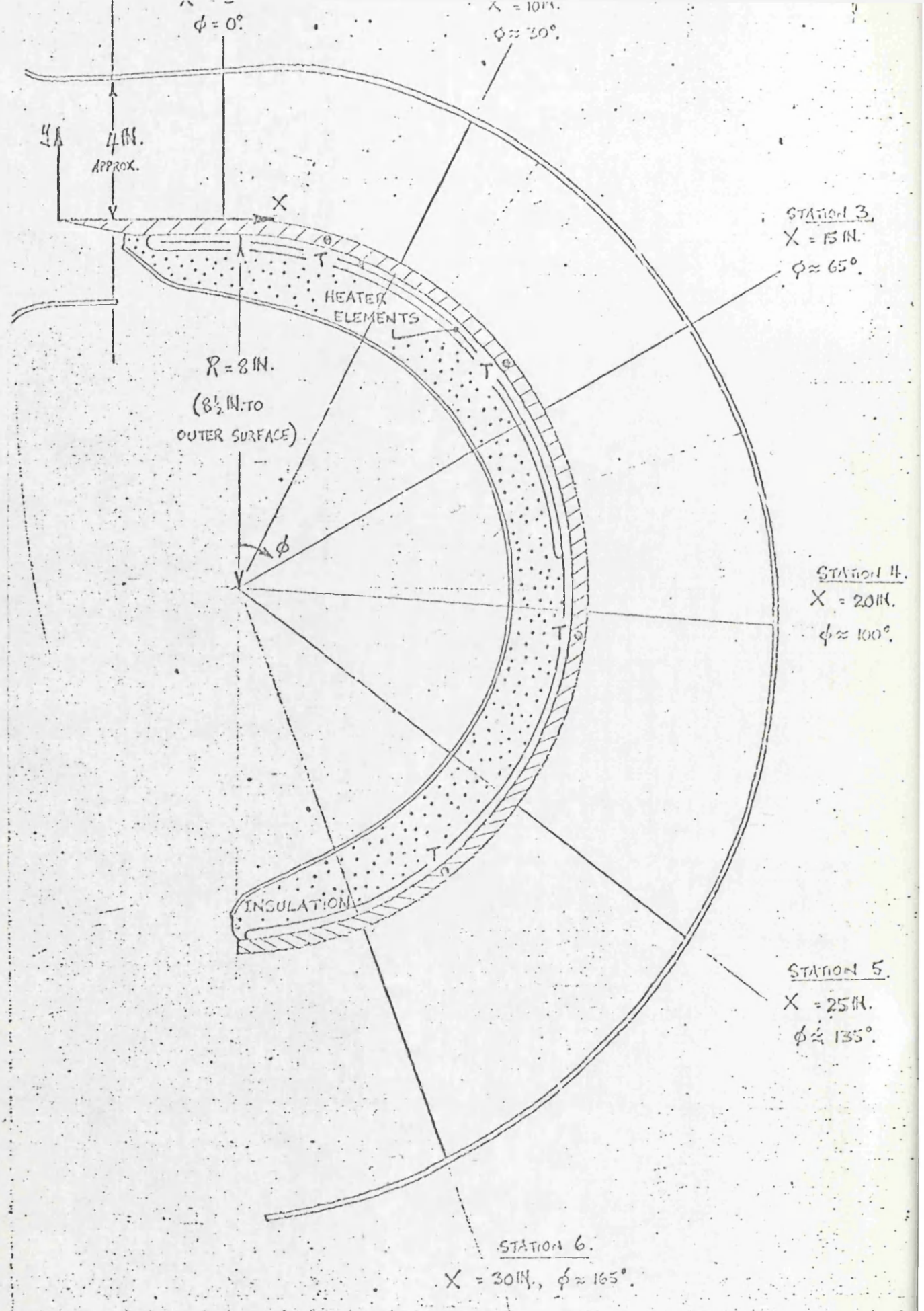

Figure 14: The curved duct.

CHAPTER 3

CURVED PLATE EXPERIMENTS - THE EFFECT OF PLATE HEATING ON TURBULENT SEPARATION

3.1 The Curved Duct

At this point the flat plate work was concluded, and the plate and ducting removed from the tunnel. A second copper plate, measuring 32 in. x 6 in. x 0.5 in. was formed on an 8 in. roller, so that its outer surface had a constant radius of curvature of 8.5 in., apart from a 6 in. length at the leading edge which was kept straight. The length of the plate was such that it curved through approximately 180°. Its outer surface was used as the inner wall of a curved duct of rectangular cross-section, with an adjustable curved outer wall in aluminium, the remaining walls being of flat perspex sheeting. However, the design differed from the flat plate duct in that the perspex sheets lay in the horizontal plane when fitted, i.e. the copper plate was curved about a vertical axis. The reasons for this arrangement are discussed in Section 4.1.

The leading edge of the plate was again bevelled to penetrate the airstream. Static pressure tappings and thermocouple locations were drilled in identical manner to those in the flat plate, all leads emerging through the perspex "roof" as no spacers were fitted in this design. Thermal insulation was provided by asbestos rope cemented to the top and bottom edges of the plate, and separating it from the perspex. A plan view of the duct is shown in Figure 14. A static pressure tapping was located on the plate centre-line, for each of the six measuring stations. Thermocouple locations are indicated by the letter T in the Figure, the hot junctions when inserted lying

roughly on the plate centre-line.

The plate heating system was improved by the addition of a second 500-W element, with separate control apparatus. The two 24 in. elements were placed end-to-end and folded, to give a strip some 30 in. long of double thickness for most of the length. This strip was attached to the inner surface of the curved plate, with the doubled section at the leading edge, (see Figure 14). Glass wool insulation covered the elements, and was compressed by a curved aluminium plate, which served to hold the assembly in position.

3.2 Instrumentation

The instrumentation used on the flat plate was supplemented by two items. Firstly, it was anticipated that static pressures would vary radially across the duct, so a small static probe was constructed to measure these. Stainless steel tubing, of outer diameter 0.05 in. was used to form a probe of conventional design (15) with four 0.015 in. pressure tappings.

Secondly an investigation of thermal boundary layers was to be carried out. The probe used was of similar deisgn to the pitot probe (Figure 6), but with sheathed thermocouples in place of the hypodermic tubes. The four thermocouples were of a commercially-available type, with stainless steel sheaths 0.020 in. in diameter. The hot junctions, insulated as they were within their sheaths, were given no further shielding. The leads were carried away in a copper tube, as with the pitot probe, and this was sealed with Araldite. A change in the pedestal design was made to reduce conduction errors; the pedestal was now divorced from the tube for the first 2 in.

of its length, at which point it was attached by a screwed bracket for ease of adjustment. The thermocouples were connected through a switchbox to a potentiometer, this being the same instrument as was used to measure the copper plate temperatures.

3.3 Early Testing and Development

3.3.1 The thermocouple probe.

Performance of the thermocouple probe was checked on the flat plate apparatus just prior to its dismantling. At the same time an analysis of heat transfer, and the drawing up of a heat balance for the probe, indicated that temperature-difference errors were within 5% at all times, even for a thermocouple very close to the plate surface (see Appendix C). Temperature profiles obtained (without corrections) were of regular shape, and matched closely the corresponding velocity profiles. Also, it was possible to detect transition by traversing the probe in the same manner as the pitot probe, although great care was necessary.

3.3.2 Duct entry conditions

Initially, it was intended that a laminar boundary layer develop on the leading section of the curved plate, with transition and finally turbulent separation occurring further downstream. A series of exploratory tests was begun to see if this was possible to achieve. Considerable difficulty was experienced in producing a laminar layer at all, until the entry conditions to the duct were improved, by positioning a gradually convergent straight duct upstream of the plate leading edge. Nevertheless, it was found impossible to promote laminar transition on the curved surface, application of

adverse pressure gradients causing immediate separation of the boundary layer. A flat plate several feet in length, located upstream of the curved duct, was clearly necessary to achieve natural transition at these low Reynolds numbers, but lack of space prevented any such arrangement.

It was thus decided to trip the boundary layer at the plate leading edge, and induce separation at a suitable point downstream. A simple means of doing this was found to be by increasing the angle of attack of the plate. (It was possible to move the entire curved duct assembly relative to the wind tunnel, so that the selected duct geometrical configuration was not disturbed). A change in angle of less than 2° was sufficient, and an advantage of the method was its reversibility; a return to laminar flow could be made simply, if and when desired.

Measurements were now made of flow conditions near the inner wall of the duct, with the adjustable outer wall set to give an adverse streamwise pressure gradient. The boundary layer near the leading edge was found to be rather thick, the result of laminar separation and turbulent reattachment, and further adjustments to angle of attack gave some improvement.

3.3.3 Static pressure measurements.

Traverses in a radial direction with the static-pressure probe indicated that radial equilibrium conditions obtained in the mainstream over most of the curved duct. However, static pressures recorded by the wall tappings did not line up with the distributions recorded by the probe, the discrepancies in some cases being as high

as 20% of the mainstream dynamic pressure. These wall tappings were plain holes, of 0.030 in. diameter, drilled normal to the surface. Careful surface polishing in the vicinity of the holes reduced the discrepancies, and slight countersinking gave some further improvement, but the difference in readings was still considerable. At this point, a check for three-dimensional flow was made with yaw-meters, and various other static probes were used in radial traverses. However, no measurable three-dimensional velocities were found, and static pressure distributions agreed throughout with those recorded by the first probe. The former result was surprising, as it was to be expected that some circulatory velocity components would arise in a duct of such extreme curvature; it is suggested that the streamwise length of the duct was insufficient for these components to attain significant strength.

As a result of these observations, it was decided to ignore the readings of the wall static tappings, in favour of those from the traversing probe; the latter were recorded across the greater part of the boundary layer, and the wall value could be estimated with acceptable accuracy. A more detailed discussion of static pressure measurement follows in Section 4.3.

3.3.4 Separation point location.

An attempt was then made to locate the point of turbulent separation at a mainstream velocity around 25 ft/s. The four-tube pitot probe was traversed downstream, with its first tube touching the surface of the curved plate. Local static pressures, obtained from probe traverses, were combined with the first tube readings, to

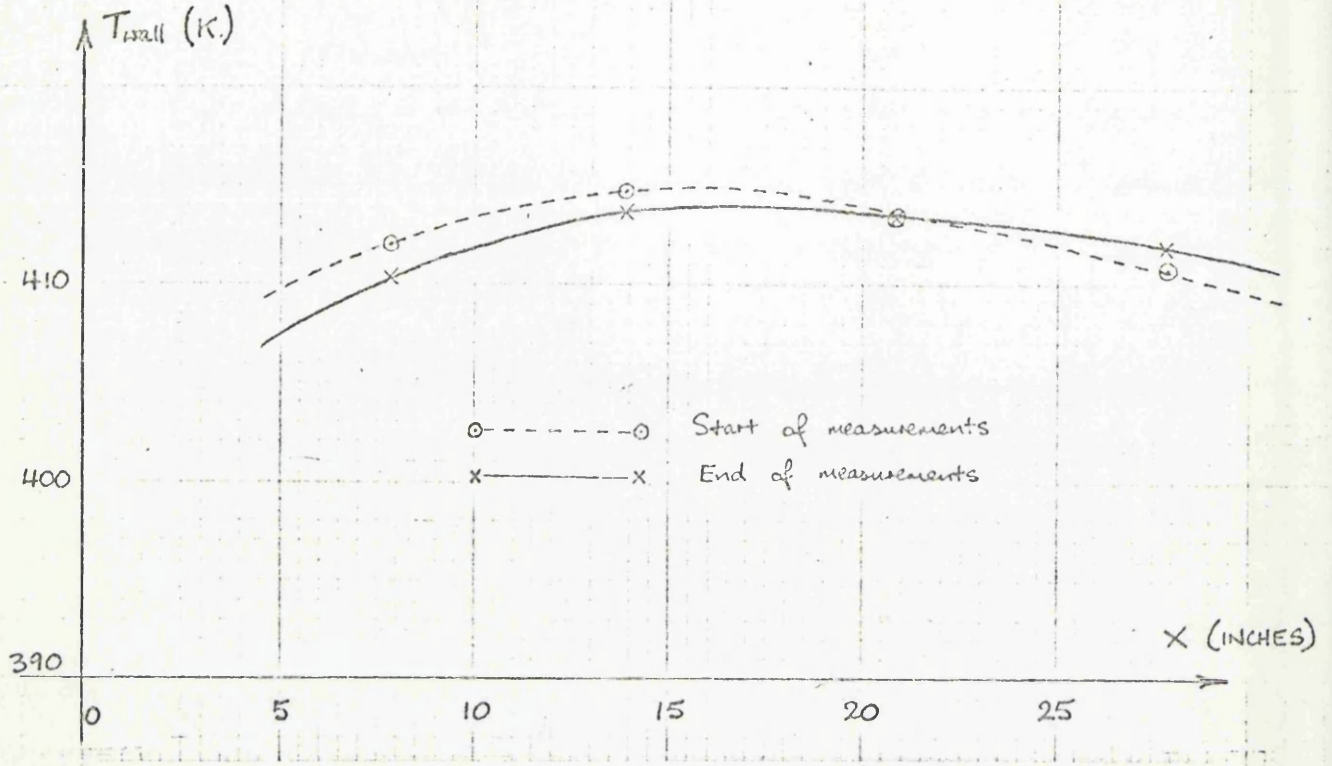

Figure 15: Typical temperature distributions for the curved plate.

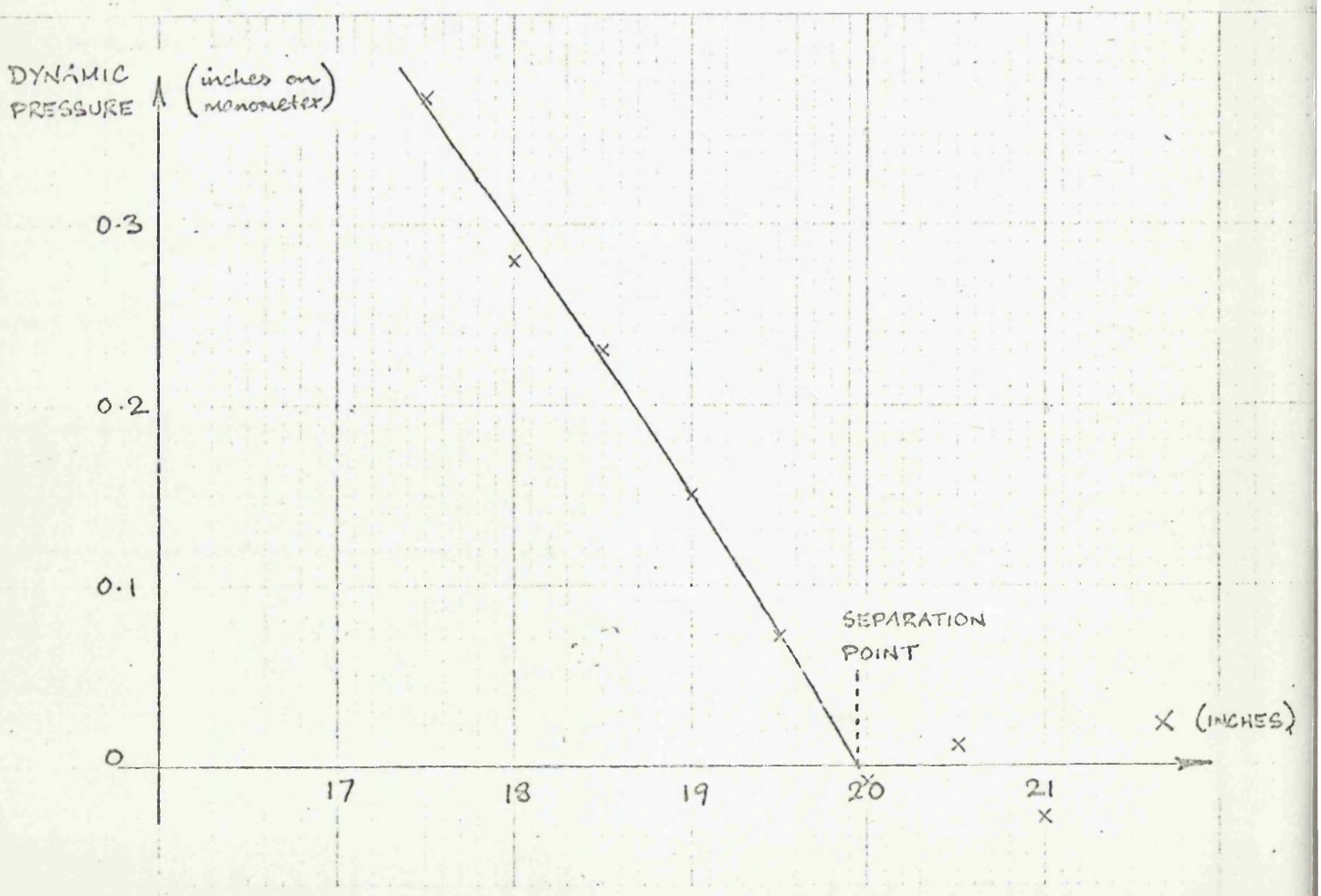

Figure 16: Location of the separation point: typical dynamic pressure plot.

give a dynamic pressure distribution in the streamwise direction, at a small fixed distance from the wall. This distribution was approximately linear, falling as the distance from the leading edge increased. On reaching a value near to zero, however, the readings showed considerable scatter which was maintained downstream of this point, with a mean value near to zero. Even the highest of these dynamic pressures was very small in absolute terms, being around 0.01 in. of water, and great care was necessary to keep scatter within acceptable limits. Also, considerable time was required for manometer response to the pitot probe.

With the object of taking measurements even nearer the plate surface, and at the possible expense of accuracy in that even smaller dynamic pressureswere recorded, a flattened first tube was installed in the pitot probe, allowing pressures 0.008 in. from the wall to be measured. This proved to be a success, in that scatter was much reduced, especially near zero dynamic pressure. The distribution was now clearly discontinuous, falling almost linearly to zero; and then remaining at zero as downstream direction increased (see Figure 16). The point at which zero pressure was reached (extrapolated from positive values) was taken to be the separation point.

3.3.5 First experiments with plate heating .

With an adiabatic separation point measured at about 17 in. from the leading edge, several tests with plate heating were conducted, and the movement of the separation point noted; inlet flow velocity was held constant. A small quantity of heat moved the separation point about one inch downstream, after which it advanced with increasing

wall temperature. This initial downstream movement was unexpected, and a careful examination of flow conditions was performed, especially for the adiabatic case. Here it was found that the adverse pressure gradient was not as steady as might be desired. The adiabatic distribution of static pressure showed a steep increase in the region around the separation point, with relatively mild gradients on either side. Heat transfer to the boundary layer appeared to even out this distribution, so that attached flow was preserved for some distance downstream. This could not be regarded as a representative case, and a revised duct geoemtry giving a smoother adverse pressure gradient was required. It was thought that a gentler overall gradient, causing separation further downstream, was also desirable.

As with the transition point, the position of separation was extremely sensitive to pressure gradient. A small alteration to the duct geoemtry sufficed to give separation a little over 20 in. from the leading edge of the plate, for adiabatic flow at a mainstream velocity of 25 ft/s. This geometry was to remain unaltered throughout the remainder of the test programme.

3.4 Main Test Programme.

3.4.1 Co-ordinates.

The co-ordinate system used is shown in Figure 14. The symbol x is used for the distance along the plate surface in the streamwise direction, measured from the leading edge; y is the distance normal to the plate surface at any point. Thus the separation point was set just downstream of the point x = 20 in., for the mainstream velocity

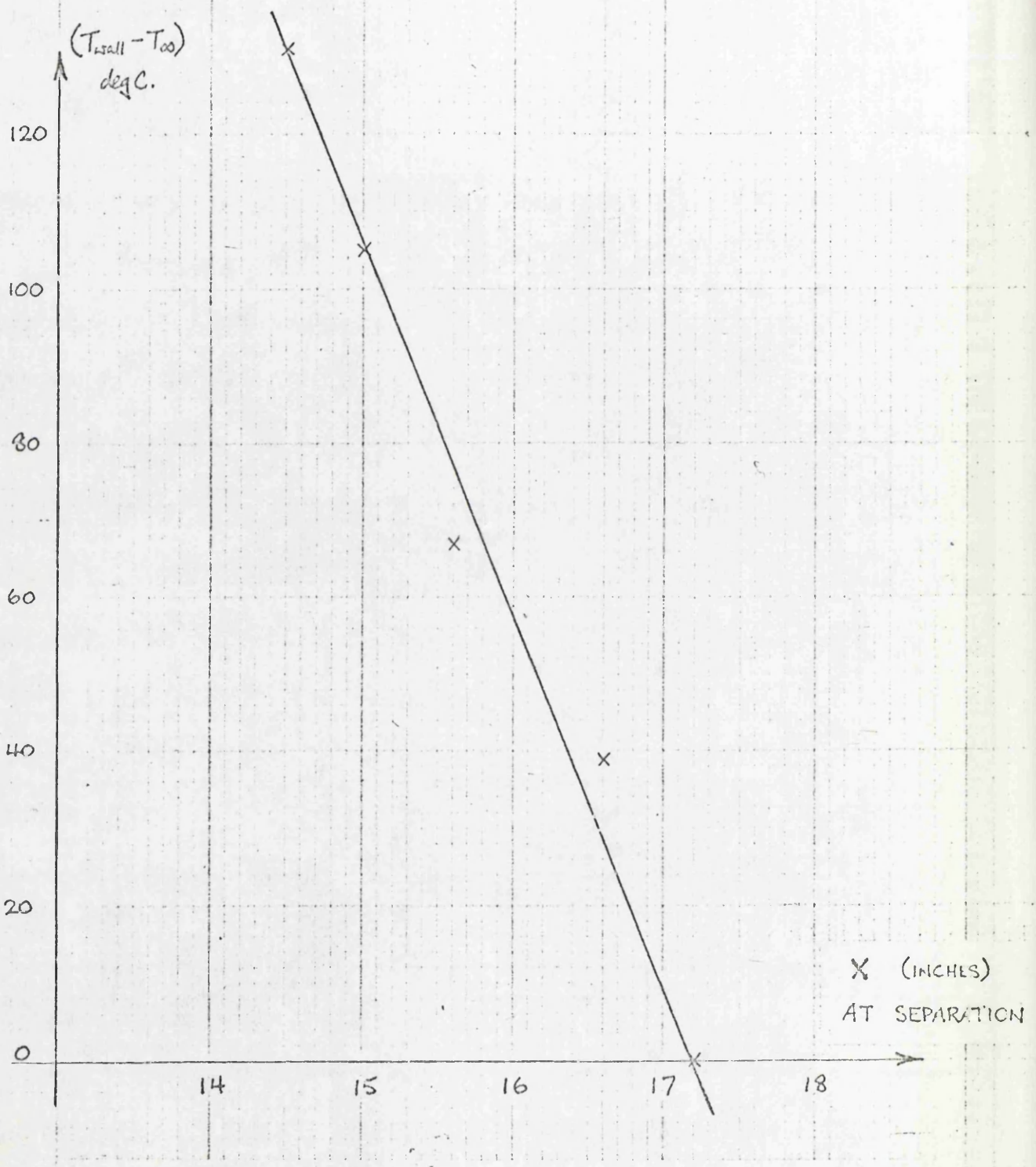

Figure 17: The effect of heating on laminar separation.

quoted.

3.4.2 Laminar separation.

A preliminary series of tests was made concerning laminar separation. With the same duct geometry and velocity, it was found that the laminar layer separated earlier, at about x = 17 in. The effect of plate heating was now examined. The two-channel heater ensured an acceptably even temperature distribution (see Figure 15 for typical examples), and separation points for plate temperatures up to 150°C were measured, using the method described in the previous section. At T_{wall} = 150°C, i.e. T_{wall}/T_{∞} = 1.45, a little heating capacity remained, but it was feared that higher temperatures would damage the perspex.

It was observed that plate heating advanced the separation point quite considerably for the laminar boundary layer, the highest wall temperature reducing the separation value of x by about 16%. The results are illustrated in Figure 17.

3.4.3 Turbulent separation.

The plate angle of attack was returned to its former value, with a turbulent boundary layer formed once more. A check showed that the adiabatic separation point had returned to its former position.

It was noted that this position was almost unaffected by Reynolds number effects up to the maximum available airspeed (65 ft/s). However, there was a speed, around 20 ft/s., below which the flow pattern was disturbed, by the inner and outer boundary layers meeting near the duct exit.

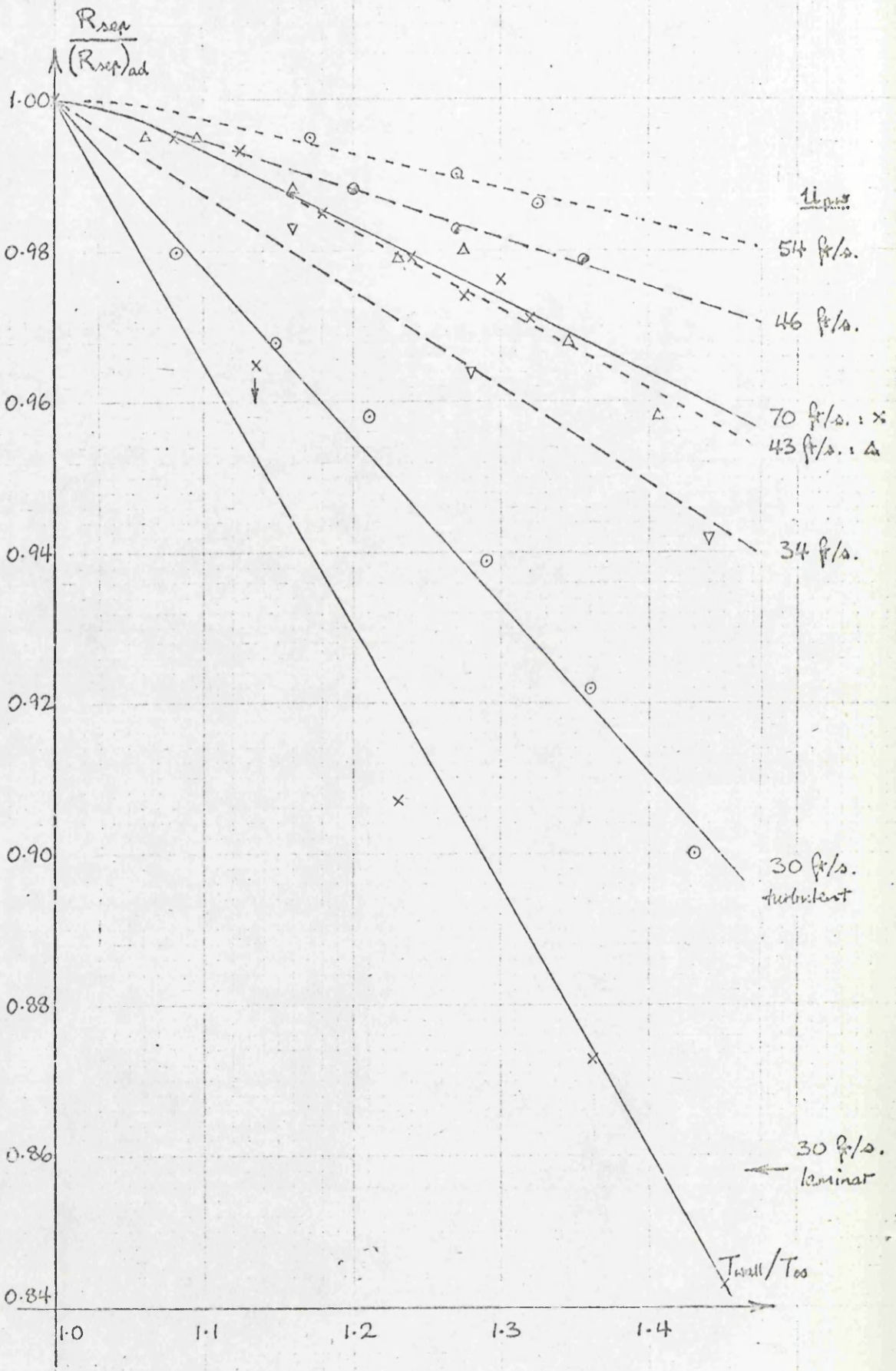

Figure 18: The effect of heating on boundary layer separation.

Two separate objectives were now fixed for this experimental work: the first was separation point measurement, over the full usable speed range (25 to 65 ft/s) and plate temperature range. The second was the recording of velocity and temperature profiles for a wide range of values of x, from which dependent distributions of skin friction, displacement and momentum thickness, and heat transfer coefficient could be derived. One difficulty which arose here was the choice of a representative mainstream velocity, since in a curved duct velocity varies continuously with y, even in the mainstream. It was decided to adopt Patel's (16) potential flow velocity at the wall, u_{pw}, as a scaling factor.

Thus the separation point measurements were carried out for u_{pw} values from a little below 30 ft/s to a little above 70 ft/s; at the higher flow speeds the plate temperature range was limited by heater output. The method used was again as previously described. For each flow speed, the separation point Reynolds number,

$$R_{sep} = \frac{x_{sep}\, u_{pw}}{\nu_\infty},$$

under heating was divided by the adiabatic R_{sep}, and graphs of percentage change drawn (Figure 18). It will be seen that flow velocity, while hardly affecting the adiabatic separation point, may have considerable effect when heat is applied. In general, the higher the flow speed, the smaller the effect of a given plate temperature ratio, T_{wall}/T_∞. However, there appears to be some reversal of this trend in the highest speed ranges. These results, and further investigations of them, are discussed in the later section (4.9). For any given flow velocity, however, two conclusions could

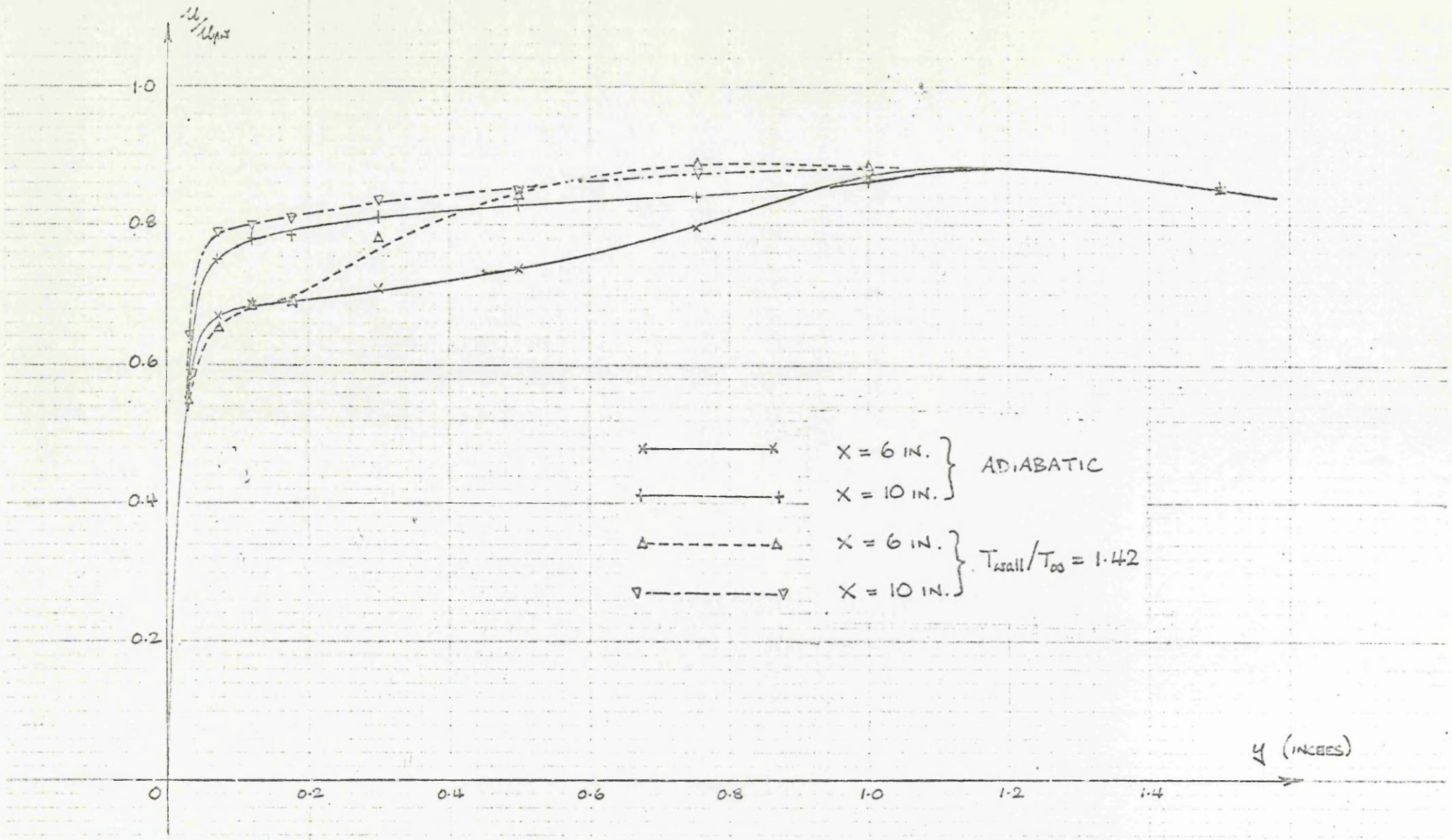

Figure 19: Velocity profiles at x = 6 in. and 10 in.

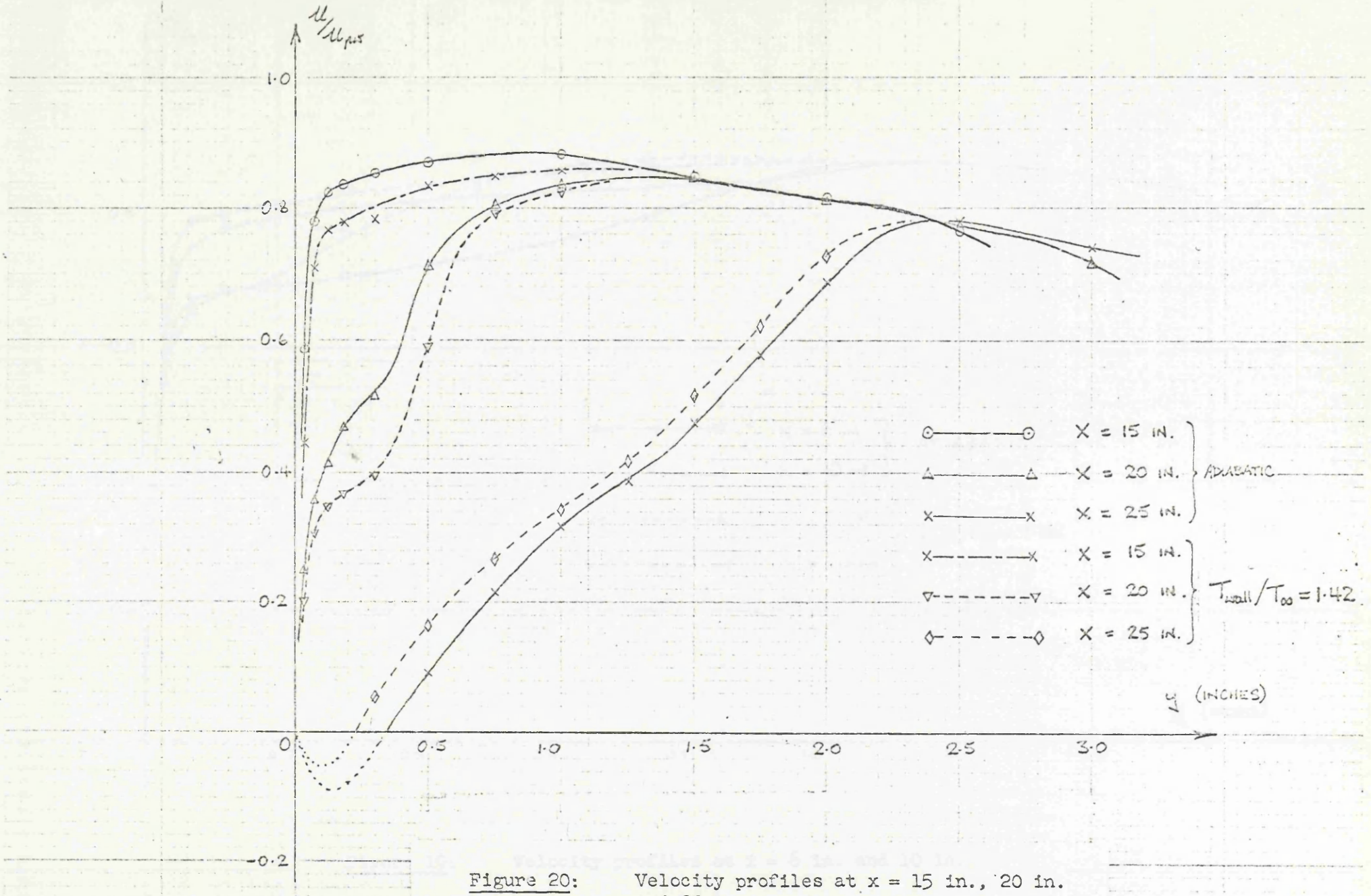

Figure 20: Velocity profiles at x = 15 in., 20 in. and 25 in.

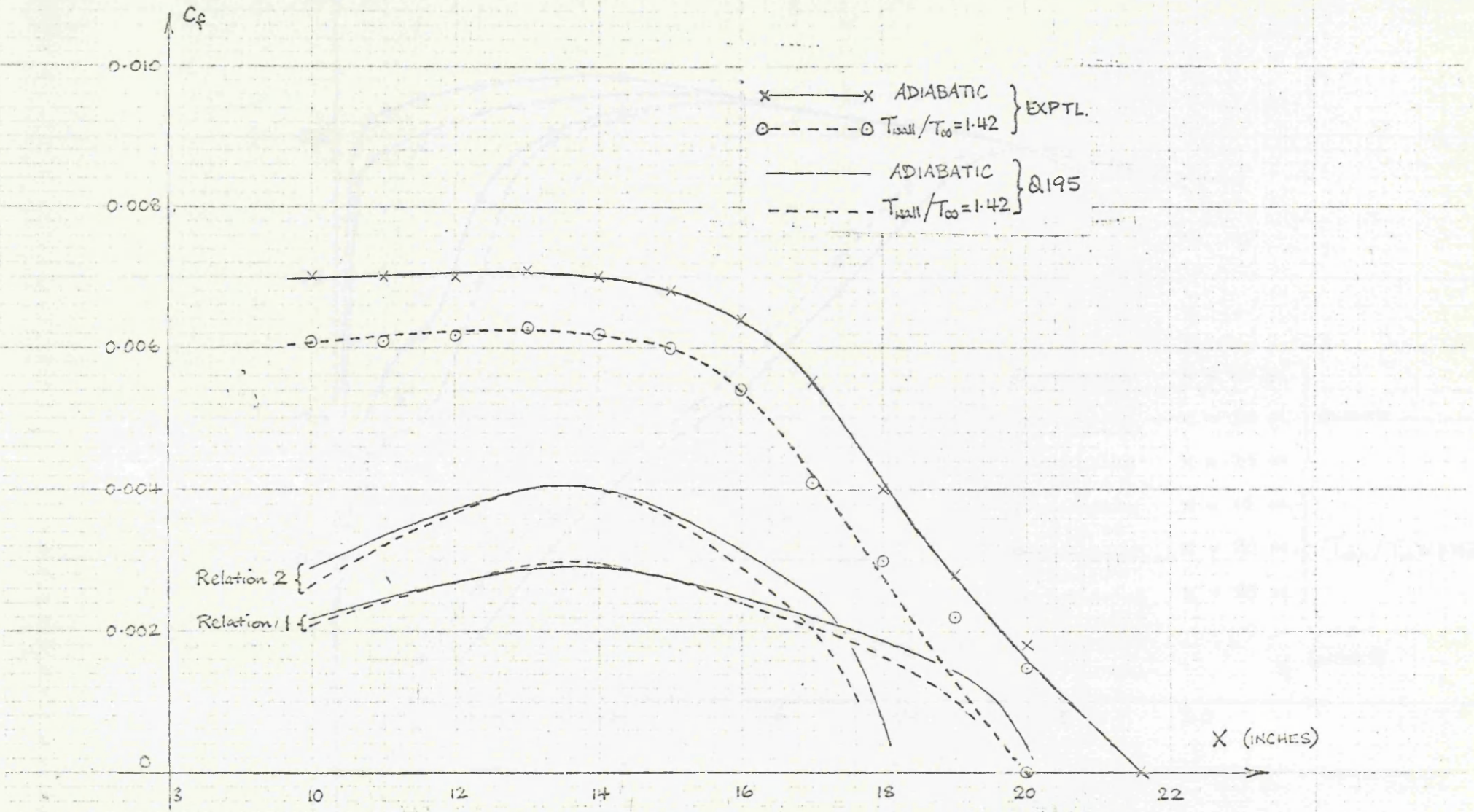

Figure 21: Skin friction coefficients.

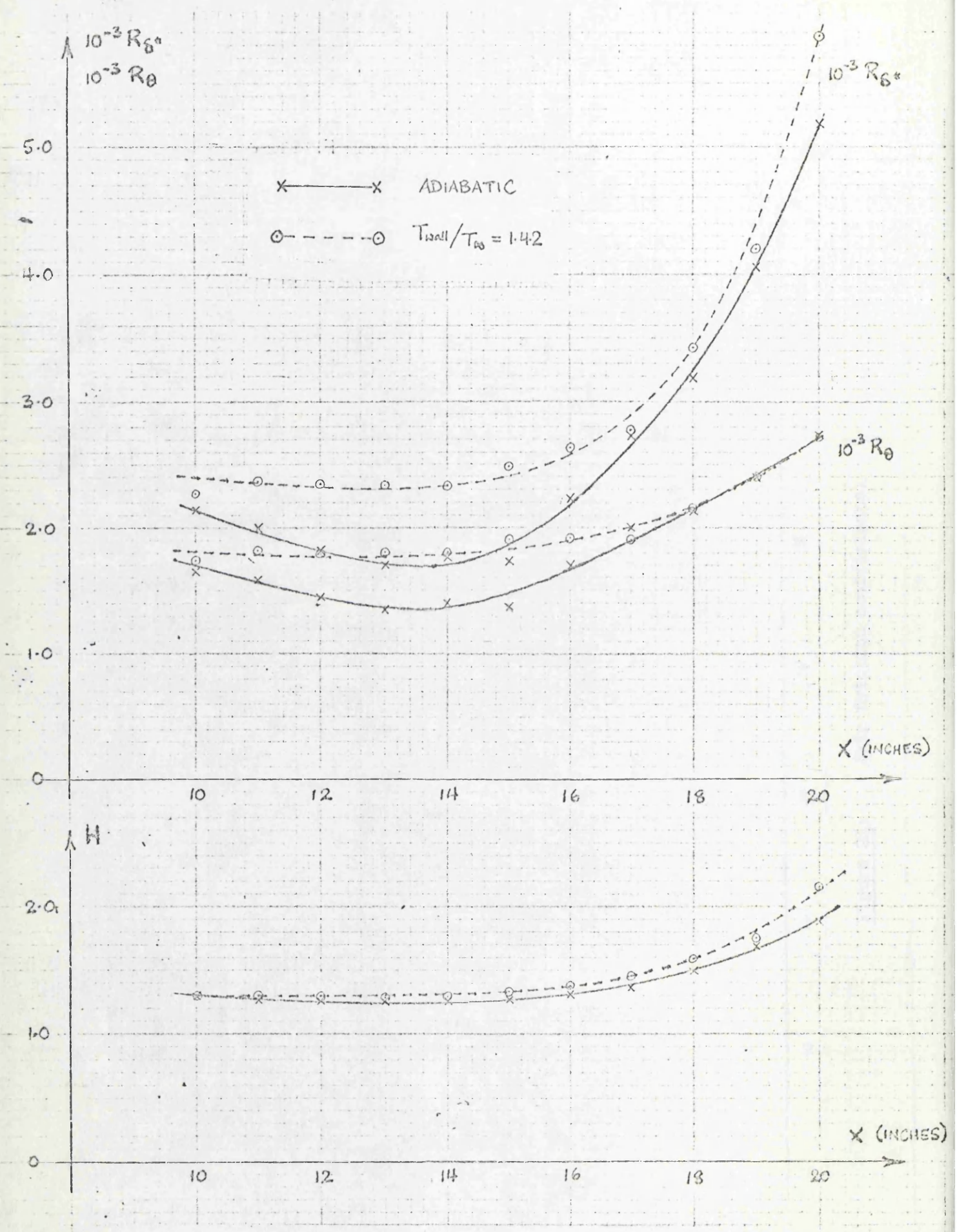

Figure 22: Distributions of R_{δ^*}, R_θ and H

be drawn: plate heating advanced the separation point, and the degree of advancement increased linearly with plate temperature, over the range measured.

3.4.4 Velocity profiles, and derived quantities.

Adiabatic velocity profiles were measured across the duct at values of x of 6 in., 10 in., 15 in., 20 in. and 25 in., up to y = 3 in. No investigation of the boundary layer on the outer curved wall was attempted. Profiles for u_{pw} values of 30 and 70 ft/s. were taken, but found to be indistinguishable; the same was true for profiles at intermediate speeds. Accordingly, only those at 30 ft/s are included, and further experimental investigations were limited to this value of u_{pw}. In all cases, the four-tube pitot probe was used to measure the flow distribution near the wall; a small proprietary pitot tube was used further away from the wall and in the mainstream. Static pressure distribution was measured with the probe described earlier. At the same flow velocity corresponding profiles were measured with the plate heated to approximately 145°C., i.e. for $T_{wall}/T_{\infty} = 1.42$. These are included for comparison (Figures 19 and 20) and are discussed in a later section.

In addition to these, velocity profiles within the boundary layer were measured at 1 in. intervals from x = 10 in. to x = 20 in., for adiabatic conditions and for $T_{wall}/T_{\infty} = 1.42$. From these, local skin friction coefficients were calculated using a Clauser chart (1), and are illustrated in Figure 21. Also, local values of δ^* and θ, the displacement and momentum thicknesses, were derived, from which

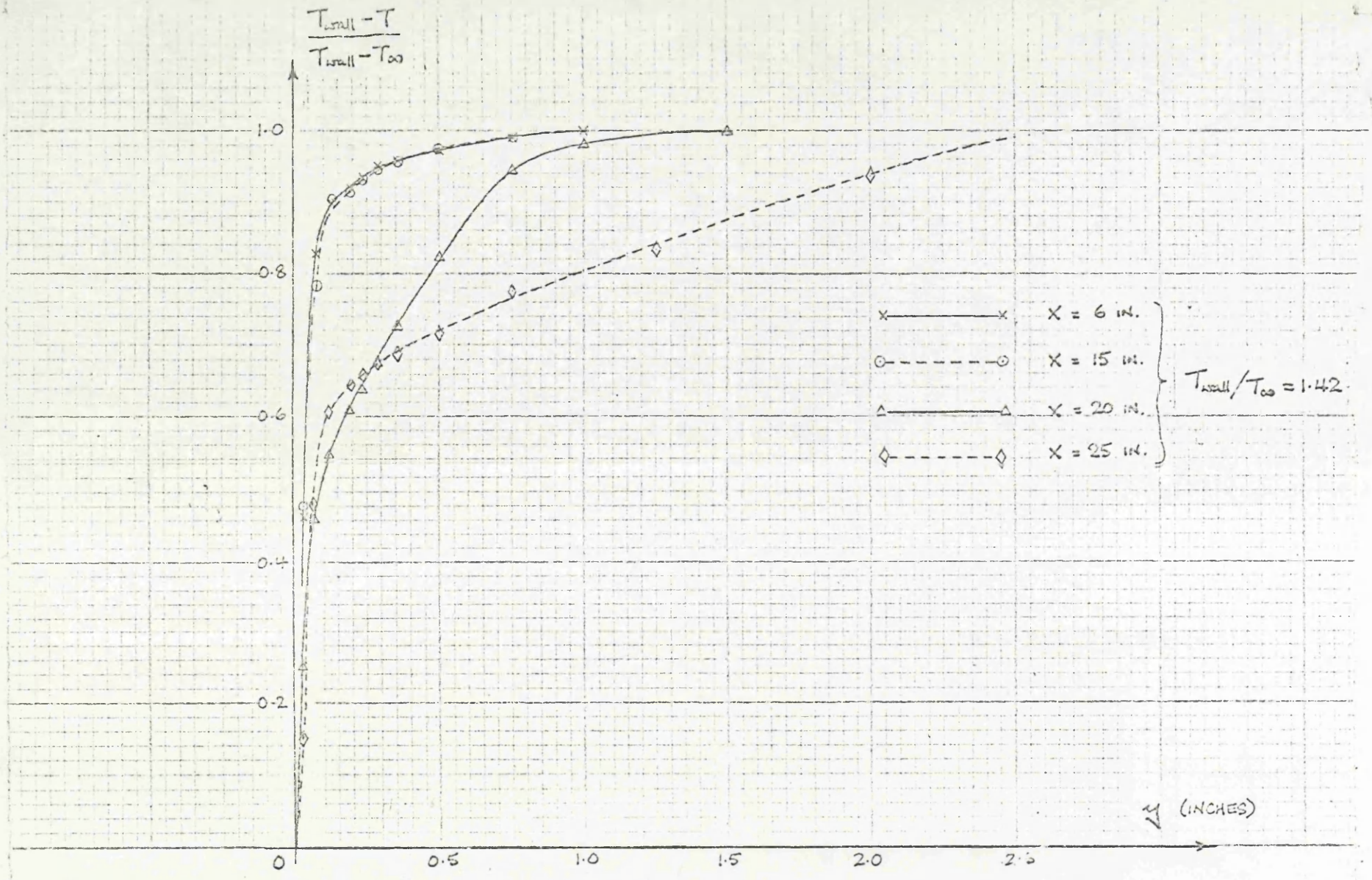

Figure 23: Temperature profiles.

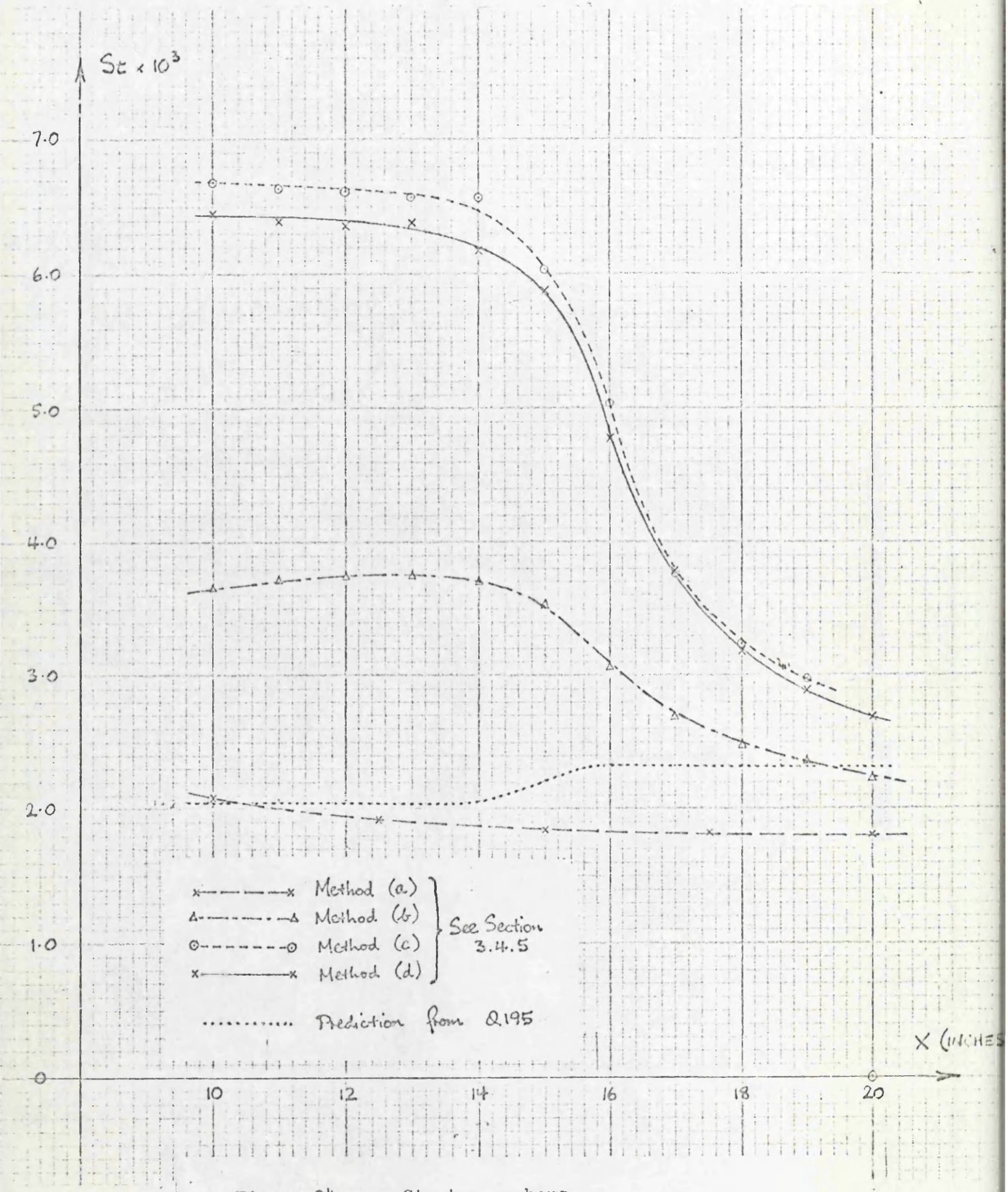

Figure 24: Stanton numbers.

the dependent Reynolds numbers, R_{δ^*} and R_θ, and the shape factor $H = \delta^*/\theta$ were calculated; these are shown in Figure 22.

3.4.5 Temperature profiles, and derived quantities.

Temperature profiles corresponding to these velocity profiles were measured with the four-thermocouple probe, traversed outwards through the boundary layer. Some difficulty was experienced in measuring these; the thermocouples appeared to be responding to very low-frequency eddies in the turbulent flow, making a mean value difficult to estimate. A large capacitor across the potentiometer input terminals reduced the fluctuations, but did not eliminate them. The profiles are shown in Figure 23; that at x = 10 in. has been excluded for clarity.

Further profiles were again measured at 1 in. intervals from x = 10 in., to x = 20 in. Local Stanton numbers were calculated from these by various methods:

(a) a simple Reynolds analogy, taking no account of streamwise pressure gradient.

(b) by graphical estimation of temperature gradient at the wall.

(c) by the method of Reynolds, Kays and Kline (22).

(d) by a simpler method developed by the author and using a Clauser chart.

The Stanton number distributions given by these four methods are shown in Figure 24, again discussed in a later section.

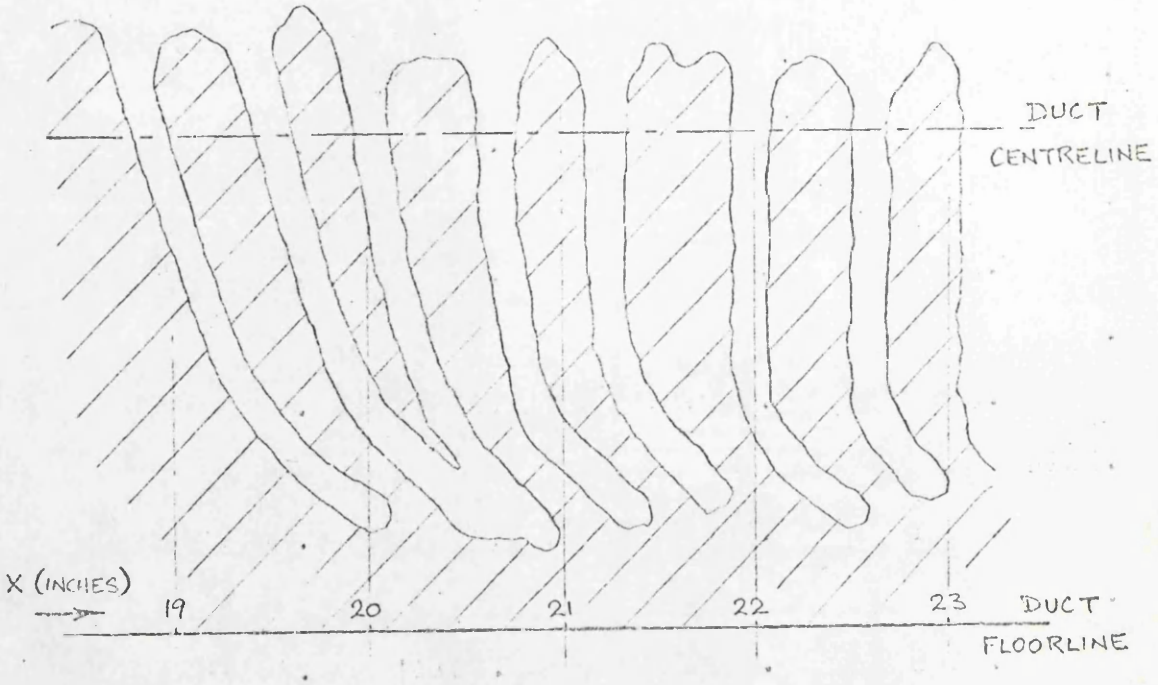

Figure 25: Flow visualisation: titanium dioxide run pattern.

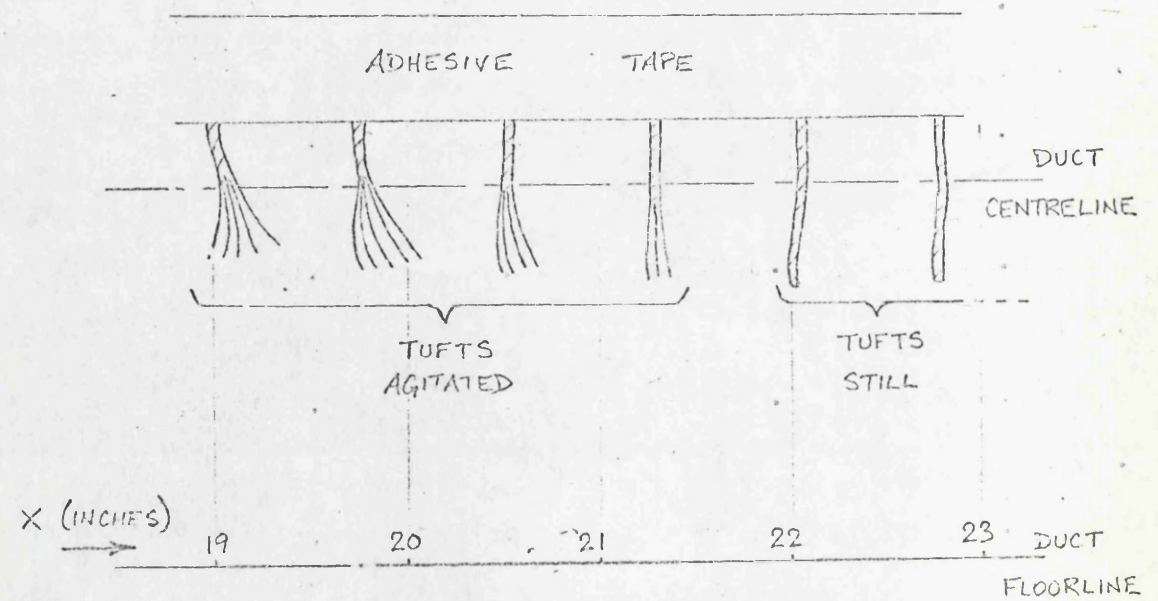

Figure 26: Flow visualisation: tuft behaviour

3.4.6 Flow visualisation.

In view of the problems encountered in static pressure measurement, the use of an independent method for location of the separation point was considered desirable. Flow visualisation was attempted by painting the curved surface with a suspension of titanium dioxide in linseed oil, in a broad strip extending from x = 18 in. to x = 25 in. This was of limited success, as a mixture thin enough to be influenced by the airflow developed runs on the vertical surface. More useful was the somewhat unothodox technique of painting a strip some distance above the duct centre-line, and observing the movement of the runs as they travelled down to the floor. Runs occurring upstream of x = 21 in. had a pronounced downstream component; at greater values of x they generally fell vertically, but occasional runs showed local evidence of small upstream velocities. An illustration of a typical run pattern is given in Figure 25. Closer scrutiny of individual runs disclosed a tendency towards fluid build-up at the downstream edge, upstream of x = 21 in., which disappeared thereafter. Evidence of three-dimensional flow near the duct floor was given by the run behaviour in this region; all runs (regardless of x) displayed a considerable downstream velocity component. This is also illustrated in Figure 25.

A further investigation was carried out using small nylon tufts, taped to the plate surface so as to hang vertically along its centre-line. This arrangement is illustrated in Figure 26. Care was taken to ensure that all tufts hung free of the wall before the wind tunnel was switched on. Subsequent observations agreed with those from the

titanium dioxide run patterns. Upstream of x = 21 in., the tufts were deflected downstream, and experienced some agitation; the remaining tufts were not noticeably disturbed, although still hanging free of the plate surface.

All the flow visualisation tests were conducted at the maximum available flow speed, i.e. about 60 ft/s.

CHAPTER 4

CURVED PLATE - DISCUSSION OF EXPERIMENTAL RESULTS

4.1 Duct Geometry

Most experimenters with curved ducts have preferred fairly gentle radii of curvature, and duct heights several times greater than the radial width. These features assist in minimising the three-dimensional flow which is an inevitable consequence of prolonged streamline curvature. The author, however, found it desirable for the reasons given below to use a duct of comparatively extreme curvature and of a height only slightly greater than the radial width.

It has been mentioned in Section 1.3 that the centripetal accelerations in an axial-flow compressor are very severe. In order to estimate their effect on the boundary layer, similar conditions in the curved duct were clearly required. However, it was found that the compressor accelerations could not be attained experimentally; a compromise between reasonable duct length and high centripetal acceleration gave the adopted configuration.

The height of the duct, at a little over 6 in., was also influenced by the need for high accelerations. Given that the duct width could not be reduced without causing the boundary layers on the inner and outer curved walls to meet, the height-to-width ratio could only be increased by additional duct height. The resulting increase in cross-sectional area would bring an inevitable drop in maximum airspeed, and reduce the available centripetal field. Space limitations in the tunnel working section were a further restriction.

In practice (see Section 3.3.3), no difficulty was experienced

with three-dimensional effects, the short duct length up to separation no doubt being a contributory factor.

The location of the copper plate, with its axis of curvature vertical, was chosen purely for convenience. With the plate heated, air passing over it experienced a vertical buoyancy force; on a flat plate this might have caused three-dimensional flow in the boundary layer. However, in this case the force was swamped by the far greater radial buoyancy due to the streamline curvature, and no difficulties arose.

4.2 Entry Conditions

It has already been described (Section 3.3.2) how it proved impossible to produce laminar transition followed by turbulent separation with the same duct configuration. The adoption of a fully turbulent boundary layer permitted investigation of the separation point movement alone, without complications due to shifting of the transition point. However, this was only valid if the tripping mechanism was consistent throughout the range of conditions applied.

An examination of Figure 19 shows that this was not strictly the case; wall heating appeared to assist reattachment of the leading edge separation bubble (see profiles at x = 6 in). However, by x = 10in. the discrepancy was greatly reduced, and disappeared completely at x = 12 in., under the stabilising action of a favourable pressure gradient. From this point onwards, any changes brought about by wall heating were taken as unconnected with entry conditions.

It is accepted that the above is a less than ideal state of affairs. Other forms of boundary layer tripping would be likely to produce

similar effects, and the only satisfactory solution to the problem would be to employ a flat adiabatic plate upstream, on which the boundary layer may be tripped or experience natural transition. As mentioned earlier, space restrictions forbade this. However, it is considered that the discrepancies at entry are eliminated sufficiently rapidly downstream to allow valid comparisons of the positions of separation.

4.3 Static Pressure Measurement

The difficulties encountered with static pressure measurement have already been described (see Section 3.3.3). As a result, a choice had to be made between accepting the values recorded by the wall tappings, or accepting the readings from the several varieties of static probe used in the freestream and boundary layer. The latter were taken as accurate for a combination of reasons, which will now be discussed in detail.

1. All types of static pressure probe gave consistent readings at all points in the freestream and boundary layer, except very close to the wall where interference might be expected to occur.
2. In the freestream, the static pressure profile in the y-direction (as recorded by the probes) was an exact fit with the distribution predicted from radial equilibrium conditions, from around x = 10 in. downstream. This again is what would be expected as the flow becomes established over the curved surface.

3. In the boundary layer, the static pressure distribution may again be predicted from radial equilibrium considerations, up to the wall where $\partial P / \partial y = 0$. The probe readings followed the predictions, up to a point approximately 0.1 in. from the wall, when readings were terminated.

The wall static pressure extrapolated from these readings was greatly removed from the wall tapping value, at all points on the curved surface.

4. Mass flow continuity was examined for the duct, using velocities calculated from the two sets of static pressures. Lack of information about the boundary layer on the outer curved wall prevented any firm conclusions being drawn, but indications were that acceptance of wall tapping readings would contravene mass flow continuity in the duct.

5. Measurement of the separation point position was performed (as described earlier) by plotting local dynamic pressures near the wall. These clearly are influenced by the static pressure chosen; use of wall tapping values indicate a separation point around x = 16 in., as opposed to x = 21.6 in. from probe values, for adiabatic conditions.

For this reason, among others, the two flow visualisation tests were carried out (see Section 3.4.6).

These provided further evidence in favour of using probe static pressure values throughout.

No explanation for the poor performance of the wall tappings can yet be put forward. Other workers with curved ducts appear to have had no difficulties in this area.

4.4 Separation Point Location

The method of separation point fixing has been described in Section 3.3.4. This method is considered accurate, although a slight downstream extrapolation is necessary. The design of the duct was such that all measuring probes approached the inner wall from the freestream. Thus a probe located in the separated region of the boundary layer would have its leads carried away through the outer, forward-flowing layer. The expected disruption of the flow pattern, as a result of this, meant that measurements within the separated region could not be accepted with any confidence, and none were attempted. However, velocity profiles at x = 25 in. were measured in the outer regions of the boundary layer (see Figure 20).

The presence of three-dimensional flow in the duct to any great extent might be expected to upset the separation behaviour of the boundary layer, causing it to separate at widely varying values of x, depending on local position relative to the duct centreline. In fact, separation appeared to be delayed locally (see flow visualisation results, Section 3.4.6), but only within 1.25 in. of the floor and ceiling of the duct. Between these points (i.e. for about 60% of the duct height), separation occurred at a uniform value of x. Probe

readings in addition to flow visualisation tests, established the existence of this region of uniformity.

4.5 Velocity and Temperature Profiles.

In addition to the velocity profiles measured near the entrance to the curved duct, and discussed above, full velocity distributions extending into the mainstream were measured across planes 15 in., 20 in. and 25 in. from the plate leading edge. These are illustrated in Figure 20, using Patel's (16) u_{pw} as a scaling factor, and having a value around 30 ft/s for the curves shown. It will be seen that a considerable velocity gradient (with respect to y) existed even in the mainstream; this was similar for all curves, and indicated the presence of full radial equilibrium conditions at the planes considered.

At x = 15 in. both adiabatic and heated profiles appeared to be of regular shape for a turbulent boundary layer. Further downstream, at x = 20 in. the profile of the boundary layer showed a point of inflexion, similar to that observed by Stratford (33) and Schubauer and Klebanoff (28); this was particularly noticeable in the heated case, for which this profile coincided with the measured separation point. The accuracy of the measurements at x = 25 in., well downstream of the separation point in both cases, is inevitably open to question. Without doubt, the boundary layer thickness increased rapidly after separation. Comparison of adiabatic and heated velocity distributions suggested that wall heating reduced the amount of reversed flow at this point, indicating that a further increase in wall temperature might bring about re-attachment of the

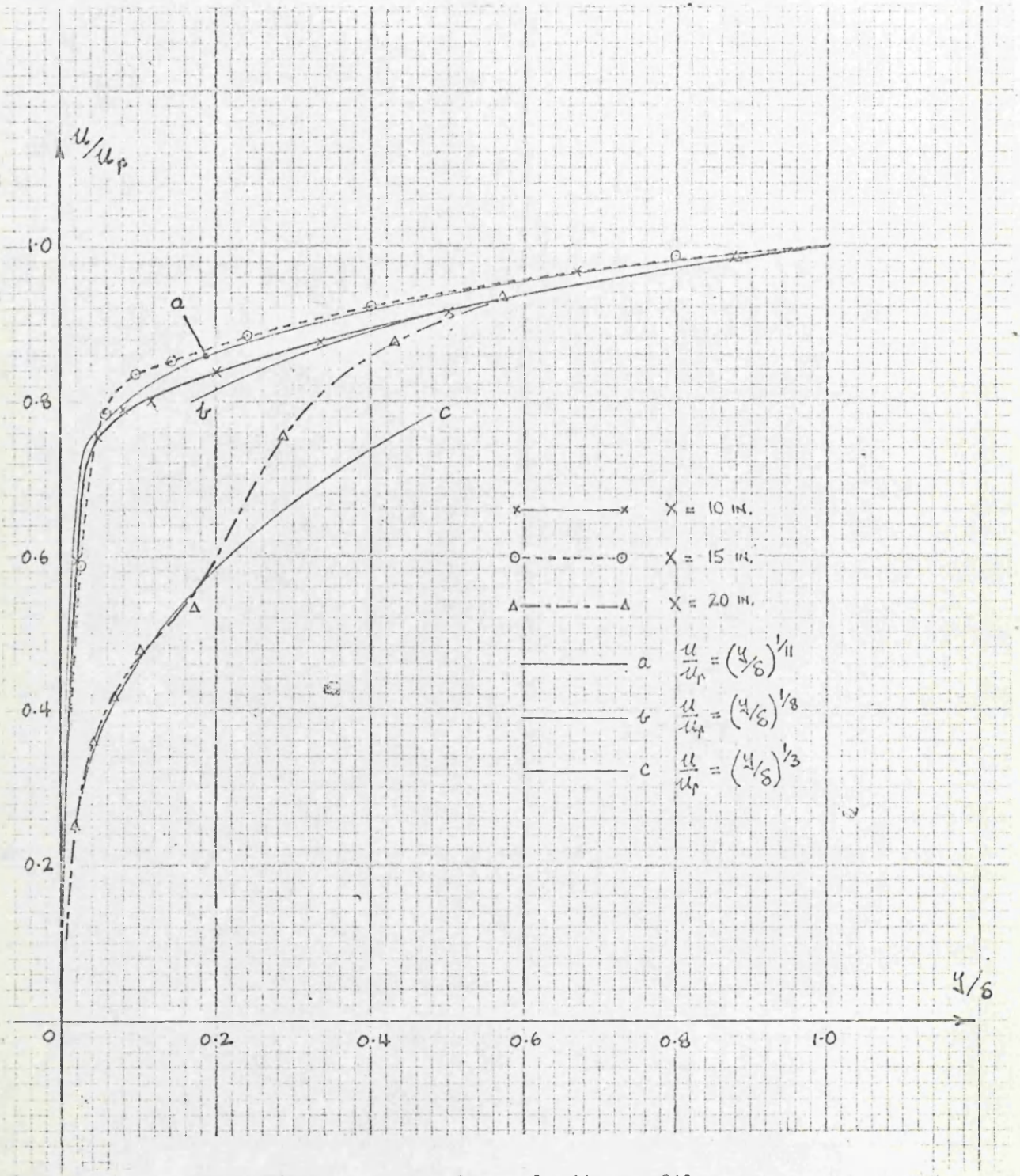

Figure 27: Power law velocity profiles.

boundary layer. However, no firm conclusions may be drawn on this matter without further study.

Full temperature profiles were measured at five planes within the duct, and are illustrated in Figure 23. These, of course, show no variation outside the boundary layer. The profiles at the first three planes, 6 in., 10 in. and 15 in. from the plate leading edge, were very similar, and in fact the 10 in. profile was omitted from Figure 23 for clarity. Points of inflexion appeared to be absent from the profiles further downstream, in contrast to the corresponding curves for velocity; the accuracy of that at x = 25 in., especially close to the wall, is however again doubtful. Rapid growth of the thermal boundary layer after separation is evident, the thicknesses of the thermal and velocity layers being closely comparable at all points.

The regularity of these velocity and temperature distributions was investigated by comparing them with power-law profiles. Experimental velocities were plotted in the form u/u_p, u_p being the local potential-flow velocity, to eliminate the effect of the mainstream velocity gradient. The velocity and temperature curves are given in Figures 27 and 28; the experimental velocity data refer to the boundary layer on the heated wall, and thus the flow conditions which produced the curves in Figures 27 and 28 were identical.

As will be seen from Figure 27, no single power-law curve was an exact fit to any of the experimental velocity curves. The profile for x = 10 in. was the most regular, ranging between a 1/10th power curve near the wall, to an 1/8th power curve over the outer half of the

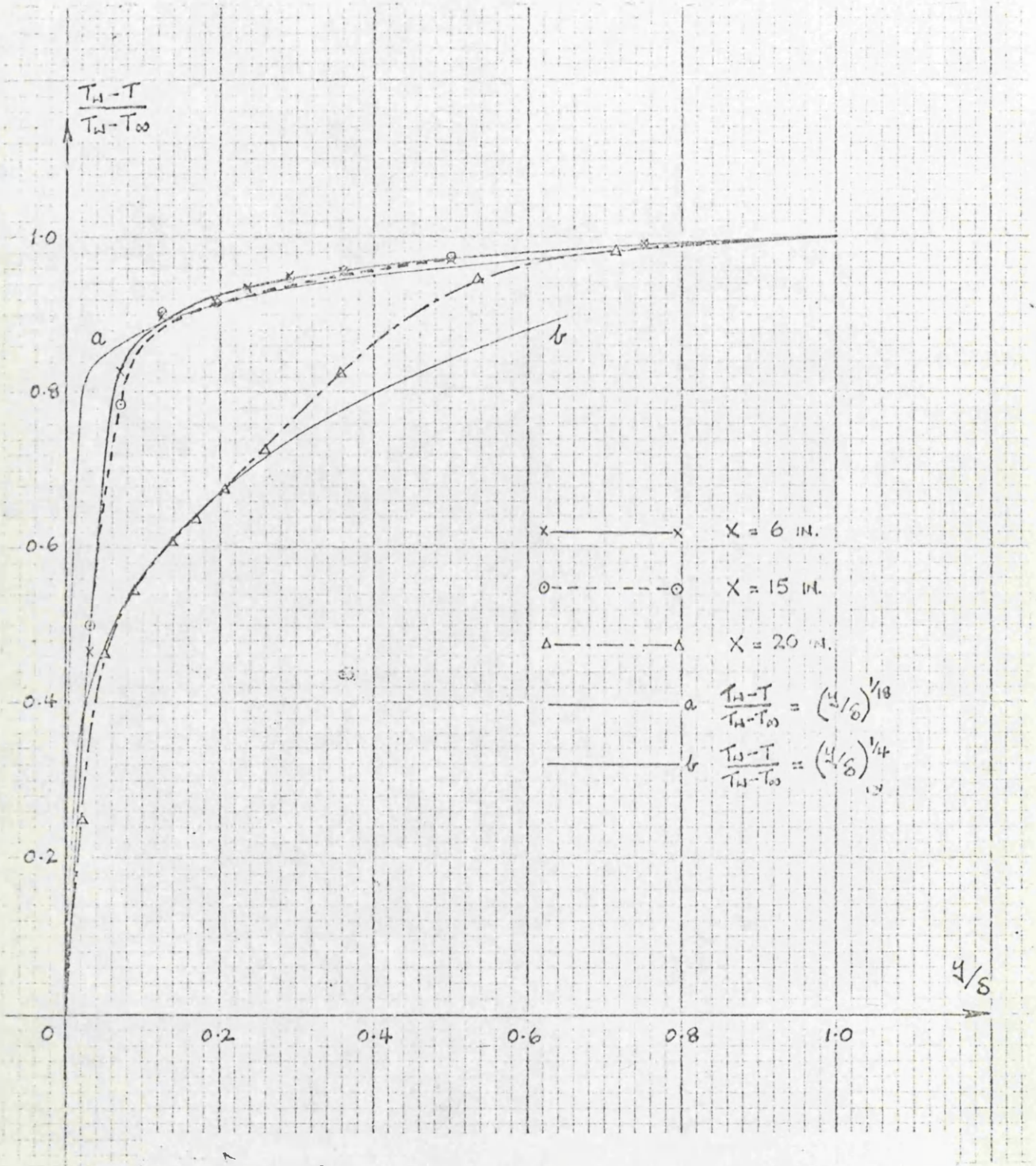

Figure 28: Power law temperature profiles.

boundary layer. At x = 15 in. the experimental data follow an 1/11th power curve in the outer boundary layer, but diverge near the wall due to the thickness of the sublayer. The inflected profile at x = 20 in. was obviously impossible to match; however, it followed closely a 1/3rd power curve over the inner 20% of the boundary layer, and an 1/8th power curve over the outer 40%.

A generally similar pattern was followed by the temperature profiles. Again, the experimental curves at x = 6 in., 10 in. and 15 in. were very similar, and the second of these has been omitted. As Figure 28 demonstrates, the thickness of the sublayers prevented any matching to a single power-law curve; this is even more pronounced than for the velocity data. At x = 6 in. and x = 15 in. the experimental points lay outside an 1/18th power curve for the outer boundary layer, but inside a 1/4th power curve very close to the wall. At x = 20 in., a slight inflexion in the experimental curve was observed, only made apparent by this method of plotting, and this led to difficulties in fitting. Outside the sublayer, the experimental points lay on the 1/4th power curve up to 20% thickness, and then rose to meet the 1/18th curve over the outer regions of the boundary layer.

The above serves to illustrate the wide variety of profiles observed in the curved duct. Flow conditions at the inner curved wall are of course stable; the radial pressure gradients act to retain the fluid in the boundary layer. Wall heating increases this stability by density stratification: the less dense the fluid, the smaller the centripetal force experienced by it. Thus a layer of

hot fluid will tend to build up against the inner wall. This behaviour is illustrated in the velocity and temperature profiles described above. It follows from this investigation that the use of predictions derived from power-law considerations in radial equilibrium flow problems should be approached with some caution, although in practice the errors involved may prove to be small.

4.6 The Parameters δ^*, θ and $\bar{H}$

As described in Section 3.4.4, velocity profiles in the boundary layer were measured at inch intervals from x = 10 in. to x = 20 in. From these, local values of displacement and momentum thickness, δ^* and θ, were obtained, both for adiabatic flow and for $T_{wall}/T_\infty = 1.42$. The corresponding Reynolds numbers, R_{δ^*} and R_θ, based on velocity u_{pw} and bulk fluid viscosity, were calculated, and are shown in Figure 22. Also, the local shape factor, $\bar{H} = \delta^*/\theta$, was calculated; this is also illustrated in Figure 22. The above quantities were derived graphically from the velocity profiles, and corrected as necessary for local density variations. A certain amount of inaccuracy was inevitable here, as very little change of profile was observed over most of the measuring range. The scatter was most marked in the R_{δ^*} and R_θ distributions; in the calculation of $\bar{H}$, the errors were to a large extent self-cancelling.

From Figure 22, it will be seen that, initially, both R_{δ^*} and R_θ fell with increasing x, to reach a minimum around x = 14 in. For adiabatic flow, this fall was quite marked, but was much less prominent with wall heating. In both cases, R_{δ^*} and R_θ increased from x = 14 in.,

with R_{δ^*} in particular rising very rapidly towards x = 20 in. This was reflected in the behaviour of $\bar{H}$, also illustrated in Figure 22, with a considerable rate of increase from about x = 16 in. The effect of wall heating was to increase $\bar{H}$ throughout the measuring range; however, this increase was small until the approach of separation, when the curves reflected the differing points at which this occurred. For the heated case, the value of $\bar{H}$ at separation (x = 20.0 in.) was 2.16.

4.7 Skin Friction

The same velocity profiles were used to derive C_f, the skin friction coefficient, for adiabatic flow and for $T_{wall}/T_\infty = 1.42$. The method used was the well-established one first suggested by Clauser (1). This involves the plotting of u/u_∞ against yu_∞/ν for a range of points on the profile. Velocity u_∞ was replaced by u_δ, the velocity immediately outside the boundary layer. In view of the irregularity of the velocity profiles, especially in the wall region (see Section 4.5), the method was adopted with some reservation, but no more direct method of local skin friction measurement was possible with the existing apparatus.

The resulting distributions are shown in Figure 21; both were approximately constant until x = 14 in., when they began to fall. The separation points (measured from local dynamic pressures) are indicated by points on the x-axis; it will be seen that the Clauser method appears about to predict separation (i.e. zero skin friction) at the measured points, until within two inches of them. Then C_f

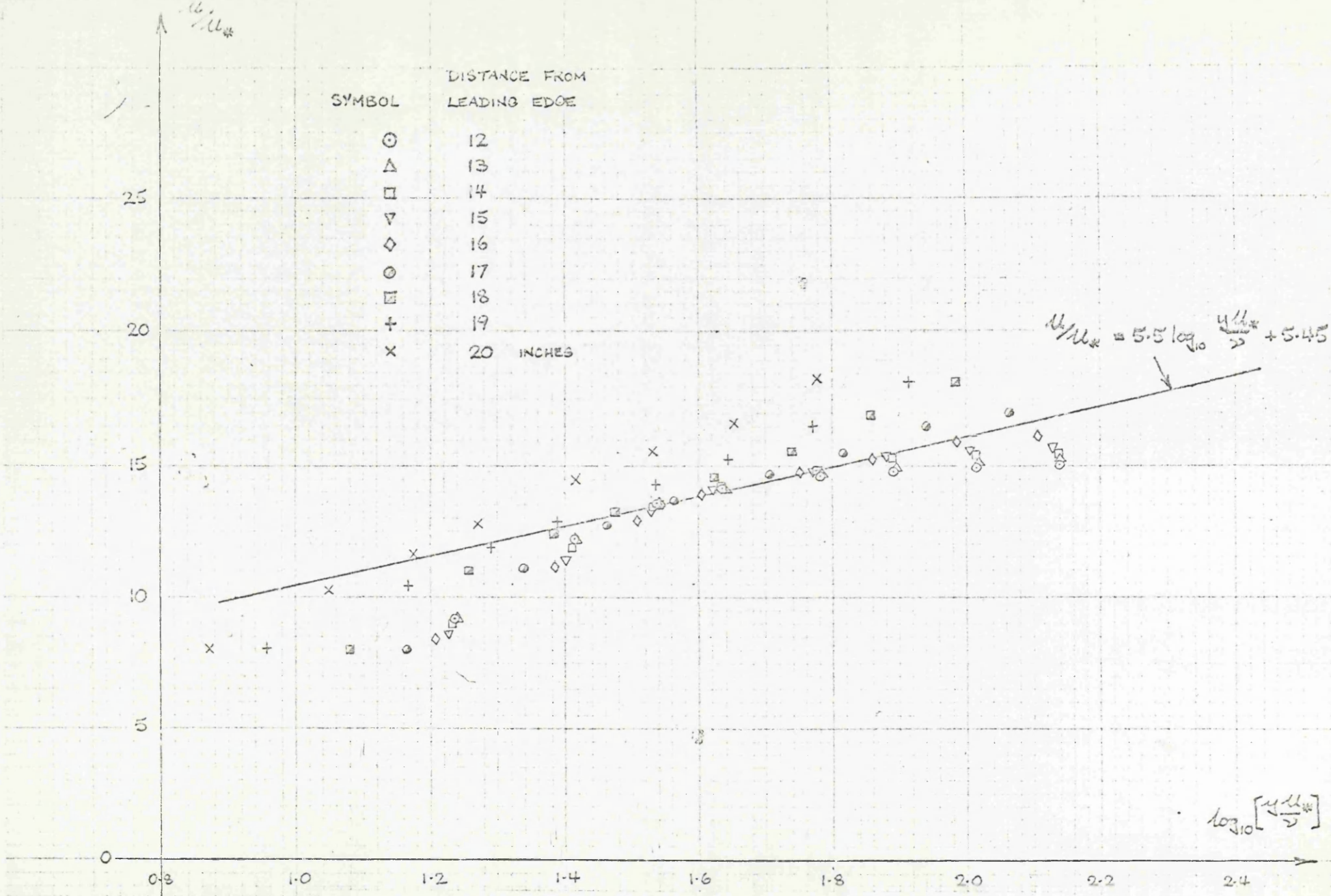

Figure 29: Universal velocity profile.

values too high to be consistent with the measured separation points are predicted; notably, in the heated case at x = 20 in., where observations suggest a value of zero, but the Clauser method gives 0.0015. This discrepancy may be attributable to the changes in the shape of the velocity profile prior to separation. For wall heating, both the 19 in. and 20 in. profiles show a marked point of inflexion.

The suitability of these velocity profiles for use on a Clauser chart was tested by plotting them on the "universal" profile of u/u_* against log $(y\ u_*/\nu)$, with particular reference to the linear section. This is illustrated in Figure 29. The experimental profiles exhibit a comparatively short linear section, but their fit is generally good until about x = 18 in., when increasing divergence from the "universal" form occurs. At x = 20 in. (the separation point), no matching linear section is apparent. In general, the closeness of fit to the "universal" profile was comparable to those observed by Patel (16) and So (29) from measurements in curved ducts with less extreme variations in streamwise pressure gradient.

It was therefore concluded that the Clauser chart method gave a very reasonable picture of the skin friction distribution, until running into increasing errors near separation. The absolute values of C_f calculated may be questionable in this application, because of the exaggerated sublayer thicknesses mentioned above. As described earlier, no direct skin friction measurement was attempted. The velocity gradient at the wall was estimated from the local velocity recorded by the innermost pitot tube (approximately 0.020 in. from

the wall), and local C_f values calculated. These were around 50% of the values given by the Clauser method, this discrepancy reducing very rapidly as separation approached. This indicated that the velocity profile in the sublayer was not strictly linear, which was to be expected from the considerable variations in local temperature in the heated boundary layer. Curvature was still present in the adiabatic sublayer; it was, however, less pronounced, and the calculated skin friction more closely approached the Clauser values. Velocity measurements closer to the wall were not attempted, as loss of accuracy due to interference was anticipated.

Further comments on the performance of the Clauser method are given in the following section.

4.8 Heat Transfer and Stanton Numbers

As described in Section 3.4.5, Stanton numbers for points between x = 10 in. and x = 20 in. were derived by four methods. The first was a simple flat-plate Reynolds analogy, with the equation from (22),

$$St.\ Pr^{0.4} = \frac{0.0296}{R_x^{0.2}\ (T_{wall}/T_\infty)^{0.4}}$$

with St and R_x evaluated at the freestream temperature T_∞. Wall temperature was taken as uniform and so no local data were employed. The resulting distribution is shown in Figure 24; variation of Stanton number with x was not great, with a mean value a little below 0.002. This method was not expected to give an accurate prediction, as it could not respond to changes in streamwise pressure gradient.

Secondly, temperature gradients at the wall were estimated from the local temperature profiles, in a similar manner to the wall velocity gradients in the previous section. Again, the presence of a non-linear sublayer was apparent; from the skin friction results of the previous section, it was expected that an underestimate of wall temperature gradient by about 50% would be made at x = 10 in., and that this underestimate would diminish as x increased. Local Stanton numbers were derived from these temperature gradients, and the distribution is again shown in Figure 24. Values were higher than for the Reynolds analogy, and showed a more marked fall towards separation. The value at separation (x = 20 in) was still considerable.

The third set of values was obtained using the method of Reynolds, Kays and Kline (22). This postulates the existence of a "universal" temperature profile similar (but not identical) to the accepted profile for velocity. A dimensionless temperature T_+ is defined by

$$T_+ = (T_{wall} - T_{bl}) \rho c_p \sqrt{\tau_{wall}/\rho} \; / \; q''_{wall}$$

where T_{bl}, the local temperature in the boundary layer varies with dimensionless distance y_+.

Heat transfer coefficients are calculated from the above equation after insertion of appropriate values for T_{bl} and τ_{wall}, which demands knowledge of skin friction distribution. T_+ is taken from the "universal" profile at the y_+ corresponding to T_{bl}, leaving q''_{wall} as the only unknown. Stanton numbers were calculated from the author's temperature and skin friction data, and are shown in Figure 24. The values of y_+

chosen were such as to place them on the inner part of the linear temperature profile.

The Stanton numbers produced by this method were almost double the "temperature gradient" values at x = 10 in. They fell very rapidly in response to the adverse pressure gradient, but levelled off the remain as high as 0.003 at x = 19 in. No value (other than zero) could be obtained at x = 20 in. as τ_{wall} disappeared with separation; however, this breakdown is in the nature of a discontinuity in the method, and does not appear to distort the Stanton number for very small values of wall shear stress. Thus an extrapolation is permissible up to the separation point, and gives a Stanton number of 0.0028.

From the comparisons drawn in the previous section between Clauser and "velocity gradient" methods for deriving local C_f, it was clear that the Reynolds, Kays and Kline method was the most accurate so far employed. Again, no direct-measurement method was available to give a clearer comparison. The method of Perry, Bell and Joubert (18) was also examined at this stage. This suggests a similar "universal" temperature profile for zero streamwise pressure gradient, but employs a parameter, $u_\tau^3/\alpha\nu$, to produce a family of profiles for other pressure gradients. The most severe adverse gradient quoted is for $u_\tau^3/\alpha\nu = 30$, for which it was estimated that the single Reynolds profile would predict Stanton numbers around 70% of their true value. The pressure gradients in the author's experiments, however, produced a minimum parameter value of 3900 (the lower the value, the greater the adversity of the pressure gradient), which required a negligible

movement from the Reynolds profile. Thus the Reynolds method would be expected to perform reasonably well in the author's flow conditions, up to the point of separation.

The fourth set of Stanton numbers were derived by a simple method developed by the author for use with a Clauser chart. The evaluation of skin friction coefficient from such a chart essentially determines $\partial u/\partial y$ at the wall, for the velocity profile in question. The similarity in shape between velocity and temperature profiles within stable laminar and turbulent boundary layers has long been recognised; hence, for example, the derivation of a "universal" temperature profile by Reynolds, Kays and Kline. Variation in thickness between thermal and velocity layers (a function of Prandtl number and relative starting points) frequently occurs, as does variation in profile shape under extreme conditions (see the profiles at x = 20 in. in Figures 20 and 23). However, under stable conditions it is suggested that the geometric shapes of the two layers are practically identical, and that the thermal layer retains its "stable" shape more successfully near to separation.

The calculation method, as stated previously, is a simple one. The local thermal boundary layer data, in the form

$$\frac{T_{wall} - T}{T_{wall} - T_{\infty}}$$

is treated exactly as if it were velocity data, u/u_{∞}, and plotted against yu_{∞}/ν on a Clauser chart. This yields a "dummy" value of C_f at the point in question, from which a corresponding $\partial u/\partial y$ may be found. This is translated into a temperature gradient, $\partial T/\partial y$,

after reference to the temperature and velocity ranges employed. From this $\partial T/\partial y$, local heat transfer coefficient and Stanton number are calculated in the usual way.

This was performed for the author's data, and the results shown in Figure 24. Stanton numbers generally lie very close to those from the method of Reynolds, Kays and Kline, being a little lower throughout the range. The value at separation is calculated to be 0.0027. The largest discrepancy is over the range from x = 10 in. to x = 14 in., being almost 5%.

Fundamental to the author's method is the assumption that the thermal and velocity layers behave essentially in the same way. Evidence in favour of this was provided by a "universal" plot using temperature instead of velocity data; the performance was in fact rather better than for the velocity plot. Similarity of thermal and velocity profiles at a given point on the surface is not assumed, nor is the existence of a "universal" temperature profile of the type proposed by Reynolds, Kays and Kline. These workers compared their profile with experimental results. The area of greatest discrepancy was the inner region of the linear section; the resulting predictions of Stanton number were up to 10% too high. It was this region into which the author's experimental data fell. The observed difference between the two distributions (Figure 24) suggests that the author's method may be the more accurate.

One advantage of the author's method is that it does not break down at the separation point. Indeed, there is no objection to extending predictions well into the separated region, if accurate

temperature data are available. Also, no knowledge of the skin friction distribution is required, and the only velocity information needed is the local value of u_ω. This does not have to be known to great accuracy. These points make the method very quick and simple to apply.

A fifth calculation of Stanton number, by the method of Moretti and Kays (13), is also illustrated in Figure 24. This was produced by computer calculations, and is discussed in Section 7.3.

To sum up, the four methods discussed here fell into two categories. The first was a prediction method, while the other three used experimental data at each point to calculate the local Stanton number. Two of the latter gave distributions which are believed to be reasonably accurate; the other methods, for various reasons, were not expected to give good results. Of the relative accuracy of the superior methods, nothing conclusive may be said, although there is a little evidence in favour of the author's in this application. For its simplicity and flexibility, it is suggested that the author's method may be useful in situations involving extreme pressure gradients, curvature or separation. Unfortunately, neither this method nor that of Reynolds, Kays and Kline lends itself to installation in boundary layer calculation programs.

4.9 Effects of Flow Velocity and Wall Temperature on Separation.

The method of separation point measurement has been described in Section 3.3.4. The results obtained, for a range of flow speeds and wall temperatures, are illustrated in Figure 18. This relates the

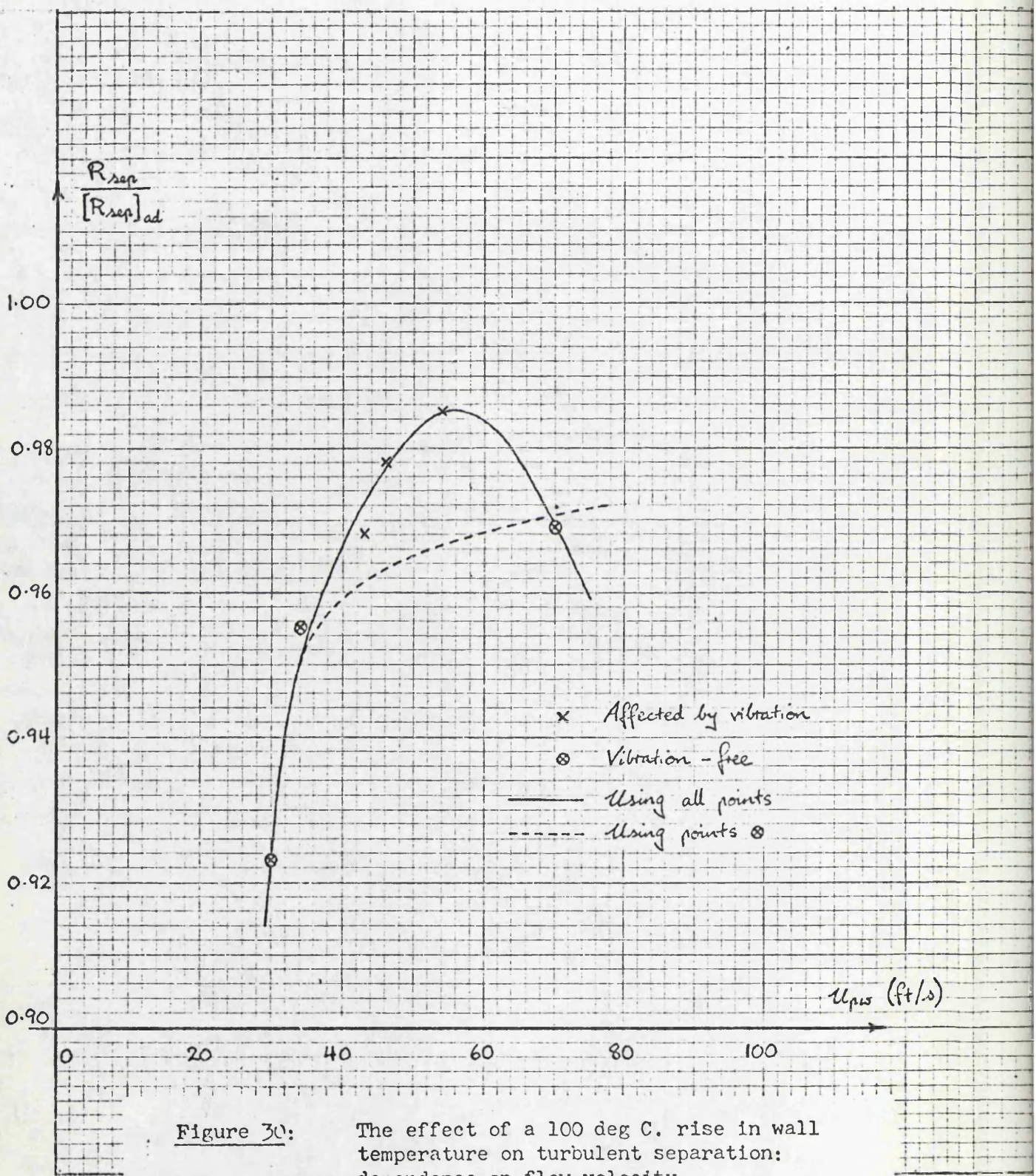

Figure 30: The effect of a 100 deg C. rise in wall temperature on turbulent separation: dependence on flow velocity.

Reynolds number at separation for a given wall temperature, to the adiabatic separation Reynolds number at the same flow speed, using bulk viscosity terms throughout. The ratio of the two Reynolds numbers is plotted against T_{wall}/T_{∞}, to produce a set of curves, one for each flow speed. It will be seen that the flow velocity exerted a considerable influence on the effect of a given increase in wall temperature. In general, the higher the velocity, the smaller was the effect of wall heating, although the latter appeared to reach a minimum and then rise in the upper velocity range. This behaviour is more clearly described by Figure 30, which illustrates the effect of a 100 deg C rise in wall temperature (T_{wall}/T_{∞} = 1.34) on movement of the separation point, for the range of flow speeds employed. The maximum on the curve (corresponding to a minimum distance moved) is clearly shown, and was confirmed by repeated measurements.

An explanation for this phenomenon was required, and flow conditions over the complete velocity range were examined once more. Attempts were made to locate the adiabatic separation point with more accuracy, but a scatter of $\pm$ 0.2 in. was the smallest which could be achieved. With these limitations the separation points at 30 ft/s and 70 ft/s - the limits of the speed range, were identical, but a slight advancement appeared to take place at intermediate speeds. This advancement, although very small, was considered sufficient to contribute to the maximum in Figure 30, and perhaps to be its sole cause.

In an attempt to find the reason for the above behaviour, the duct

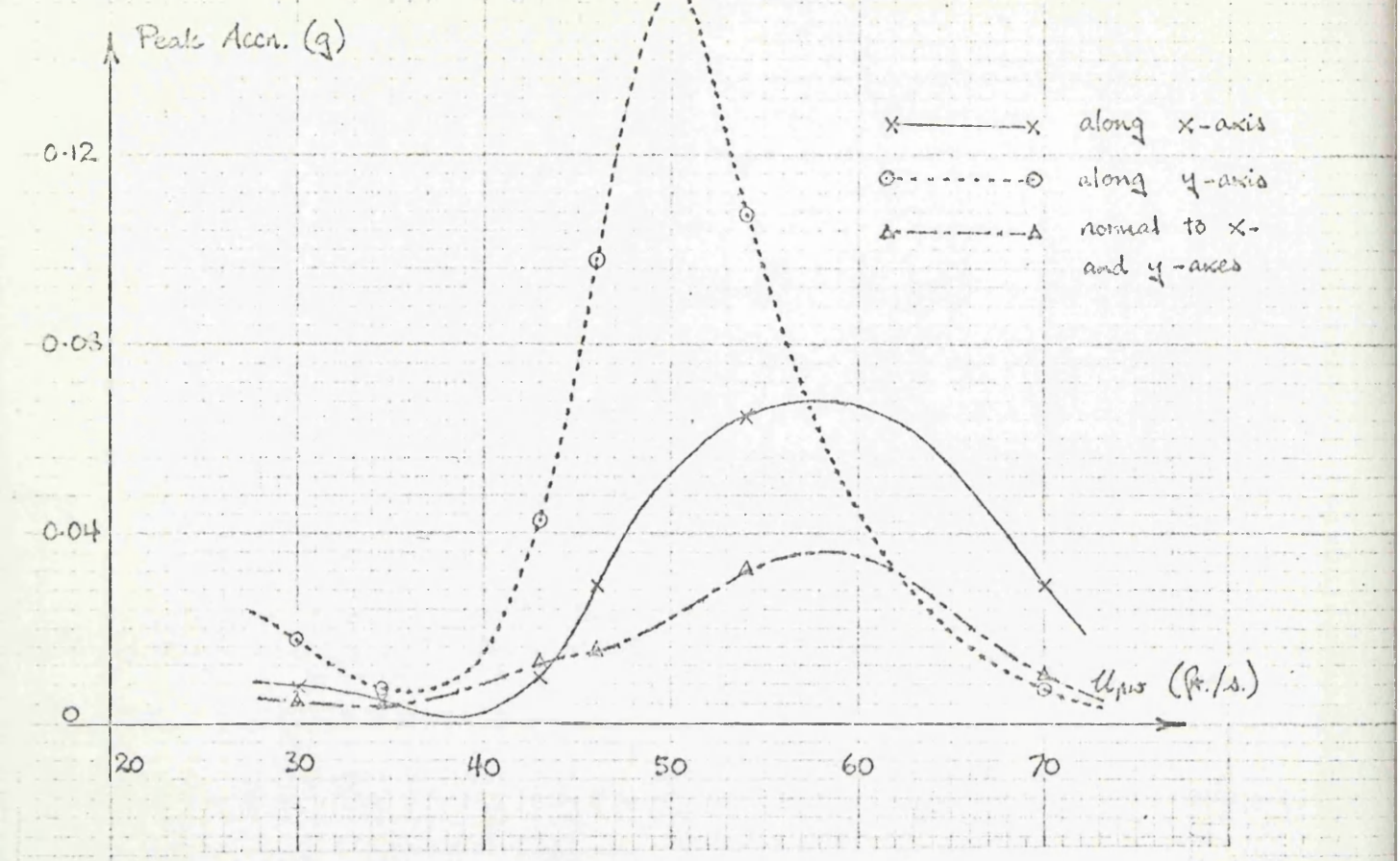

Figure 31: Plate vibration curves.

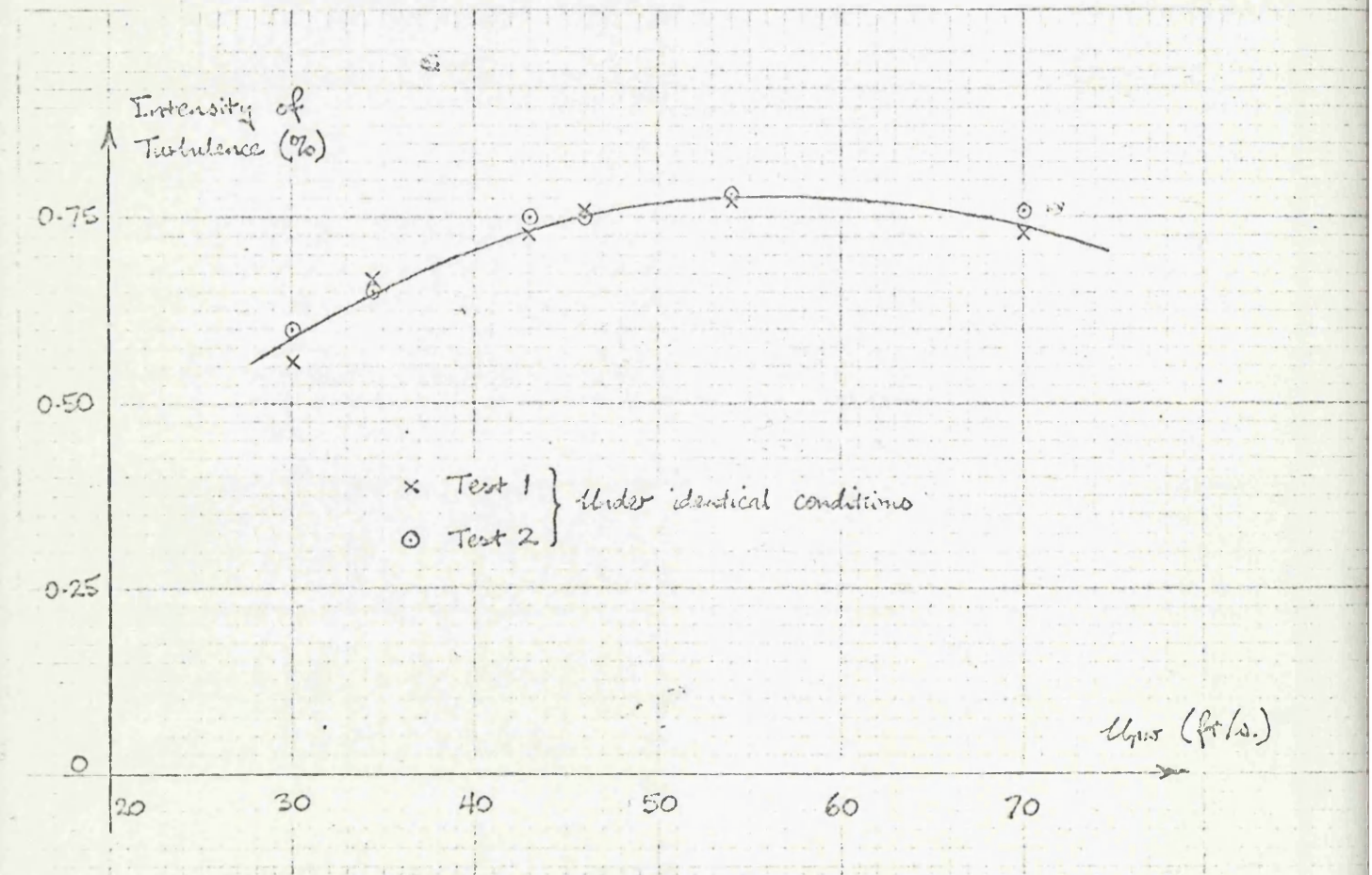

Figure 32: Variation of intensity of turbulence with flow velocity.

walls and the surface of the curved plate were tested for vibration over the tunnel speed range, using a small accelerometer connected through an amplifier to an oscilloscope. The results suggested an explanation for the observed shifting of the adiabatic separation point. At 30 ft/s and 70 ft/s, no detectable vibration was present, but between these velocities a resonant peak was observed (see Figure 31). This vibration was present in measurable quantity on all walls of the duct. A measurement at x = 20 in. on the curved plate, in the radial direction, disclosed a resonant frequency in the range 15 to 20 cycles per second, reaching a peak amplitude of 0.002 in. act a flow speed of about 55 ft/s. This is the distribution shown in the above figure.

A vibration of this nature could obviously interfere directly with the boundary layer on the curved surface; it could also generate turbulence in the mainstream, if present in the ducting of the tunnel itself. Further tests with the accelerometer showed that the vibration originated in the wind tunnel, presumably from the fan blades or motor, and was being transmitted in reduced intensity to the curved duct. Alterations to the joints and mountings of the latter failed to cure the problem, and it was suspected that the vibration was being transmitted through the floor.

The intensity of turbulence in the mainstream was then investigated, using a single hot wire normal to the flow. Intensity was found to be independent of position in the duct, within the bounds of the mainstream. However, variation with flow velocity was observed; maximum turbulent intensity was reached at about 55 ft/s, and thereafter

fell with increased velocity. This is illustrated in Figure 32, showing the results of two experimental tests. It will be seen that intensity was reasonably low, being below 1% throughout the speed range.

The effect of intensity of turbulence in the mainstream on the separation of a turbulent boundary layer is unknown; it is probable that intensities below a certain level have no significant influence. Still more difficult to assess is the effect of vibrations of the curved plate in the radial direction. These, unlike the intensity of turbulence, showed a very wide variation over the tunnel speed range, and may well have been the major cause of the problem.

Thus the existence of disturbing influences in the apparatus has been established, influences which attained a peak within the experimental velocity range. At the upper and lower velocity limits, vibration was practically absent. A study of Figure 31 shows that, if vibration is taken as being the major disturbing factor, measurements taken below 45 ft/s and at the peak velocity of 70 ft/s were largely free of these disturbing influences. Of the six experimental points in Figure 30, the first, second and sixth (in order of mainstream flow velocity) would fall within this undisturbed range. If the remaining points are ignored, an asymptotic curve may be drawn (dotted line), approaching a Reynolds number ratio of about 0.97. The experimental points furthest form this curve (the fourth and fifth) are in the velocity range over which the largest vibration amplitudes were recorded.

It is suggested that the effect of vibration on the boundary layer

would be greatly diminished by wall heating. On this (convex) wall, a stable thermal layer would be formed, which would tend to damp out disturbances in the radial direction.

To summarise, the accuracy of the original curve in Figure 30 was strongly doubted, this doubt being substantiated by the findings in the turbulent intensity and vibration tests. Vibration in particular was suspected of disturbing the boundary layer behaviour. The experimental points in Figure 30 were re-examined with this in mind, and a new curve was tentatively drawn, ignoring the points in the velocity range where vibration was large. It is suggested this second curve would more closely reflect behaviour in the absence of vibration. The curve indicates that the effect on separation of a given increase in wall temperature is diminished with increasing flow velocity, but that a measurable effect may still be present at very high velocities.

This is obviously unsatisfactory in the long term, and measurements with apparatus from which these undesirable effects have been eliminated would be most valuable. As mentioned earlier, such elimination from the author's apparatus would have involved very extensive modifications, which were not possible in the time available.

4.10 Radial Acceleration Parameters

Whether the second curve in Figure 30 is accepted or not, it is clear that the effect on separation of a given rise in wall temperature was strongly influenced by flow velocity in the duct. It was considered that further investigation would be facilitated by the use of a dimensionless parameter to describe the flow conditions, and in

particular the radial velocity or pressure gradient. Use of the Richardson number (23),

$$- \frac{g}{\rho} \cdot \frac{\partial \rho}{\partial y} \Big/ \left(\frac{\partial u}{\partial y} \right)^2_{wall}$$

was considered; however, the form of this number is such that the range of values covered experimentally was extremely small. A second parameter, of the form

$$\frac{r}{\rho u_\infty^2} \cdot \frac{\partial p}{\partial r}$$

was examined, but this is simply a check on radial equilibrium. When applied to the author's experimental conditions, therefore, it attained a value of unity shortly after entry to the duct, which was thereafter maintained.

A second parameter, of the form

$$\frac{\nu_\infty}{u_{pw}^2} \cdot \frac{\partial u}{\partial r}$$

with the velocity gradient measured in the mainstream, was then examined. This is essentially similar to the parameter K used by Moretti and Kays (13), with the exception that K contained the streamwise velocity gradient $\partial u_\infty / \partial x$. Accordingly, this second parameter was referred to as K_r. It was not suggested that K_r provided a sufficient description of the flow; however, no other acceptably simple parameters of this type were available.

The author's experimental separation data were then investigated. The Reynolds number ratios of Figure 30 were replotted against K_r in

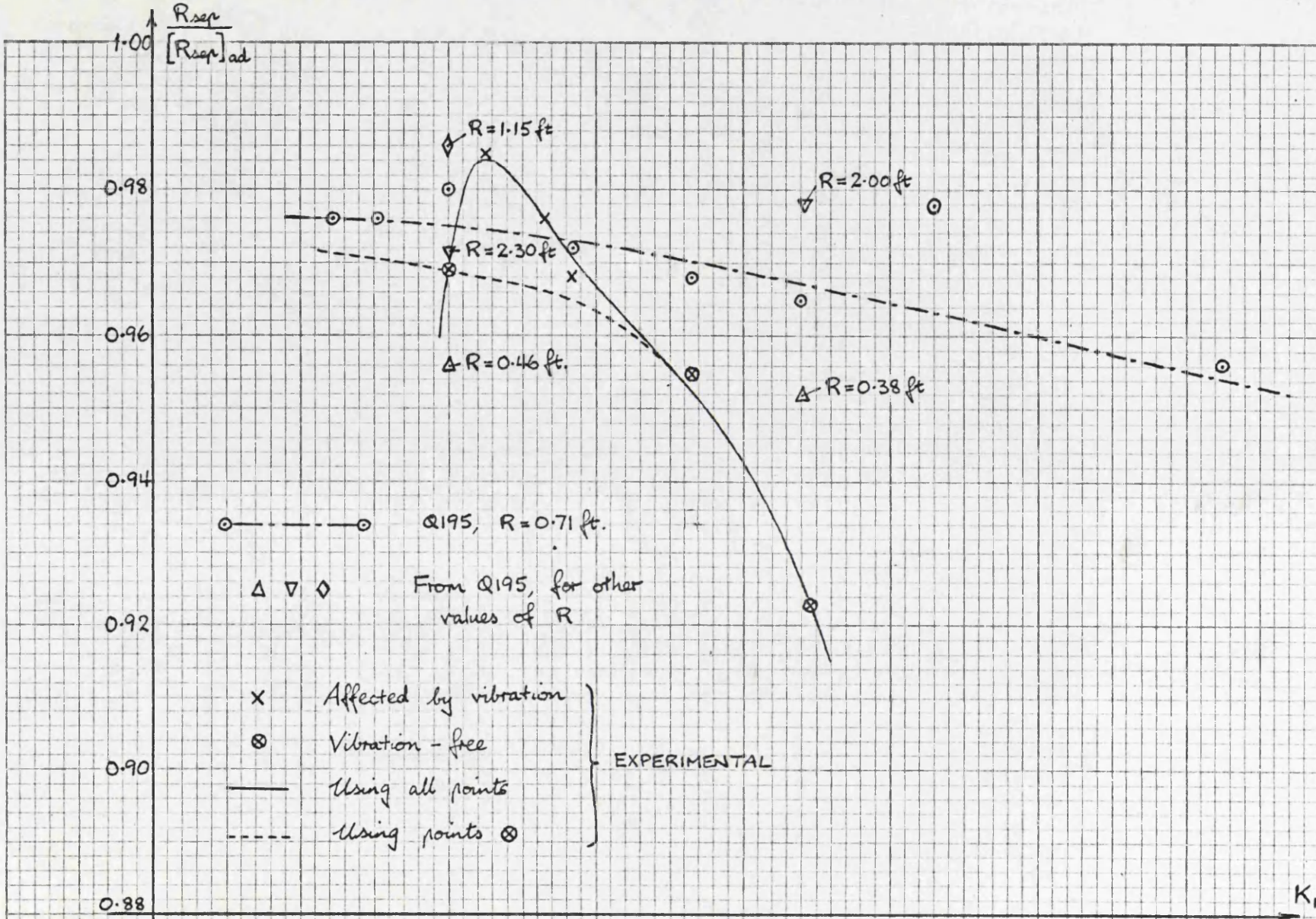

Figure 33: The effect of a 100 deg C. rise in wall temperature on turbulent separation: dependence on parameter K_r.

place of u_{pw}, and are shown in Figure 33. The maximum in the experimental points was accentuated by this change.

It is clearly possible to arrive at the same value of K_r using differing combinations of flow speed and radius of curvature. Comparisons of separation behaviour would then test the significance of K_r as a flow parameter. Experimental tests of this nature, which would of course require the construction of a series of curved ducts, were not possible in the time available. However, prediction procedures are more easily modified, and a series of tests on the validity of K_r was carried out using a digital computer program for calculation of the boundary layer properties. The theory behind this program, and the results obtained from it, are described in the following sections.

5.1 Reasons for Adoption

Shortly after the signing of the contract with Rolls-Royce, Ltd., discussions began on the choice of a prediction method to calculate a boundary layer development for the author's experimental conditions. It was considered that these conditions would provide an exceptionally severe test, combining as they did a strongly adverse pressure gradient and a high rate of heat transfer from the wall. Calculations based on the flat plate experiments were not required, and so the prediction of laminar boundary layers and transition were unimportant. The effects of surface curvature in the author's experiments could not be discounted, and so it was desirable that the adopted theory either allowed for surface curvature (this was unlikely) or could be modified to do so with reasonable facility. Finally, the adopted method had to predict with accuracy the rapid growth of the turbulent boundary layer nearing separation, and to locate this separation point.

Three established methods were considered at some length: those of Bradshaw, Ferris and Attwell (44), Spalding and Patankar (32) and Head (5). At a recent conference on boundary layer calculation (76), where a series of selected tests were applied on a large number of alternative procedures, the Bradshaw method was highly rated. However, its performance where heat transfer from the wall was large enough to affect the flow pattern was poor at that time, and its use was discouraged by Bradshaw (43). It is understood that this problem has now been overcome. Also, Patel and Head (67) have very recently reported a modified version of the method, for which it is claimed that calculation is simpler but no less accurate.

The same conference rated the Spalding/Patankar and Head methods rather less highly, placing them in the second of three classified groups. However, for the author's application, they were clearly more suitable in their tolerance of large heat transfer rates. Both were available as computer programs, the former from reference (32) and the latter from Rolls-Royce, Ltd. Each had its advantages: Head's method was attractively simple in its basic form, while that of Spalding and Patankar was less dependent on empircal data for its operation.

It was the necessity for modifications to the theory, to allow for surface curvature effects, which led to the adoption of Head's method; whether these modifications could be made without increasing the empirical content unduly remained to be seen. However, it was considered that the comparative ease with which curvature corrections could be made, in a theory which sacrificed nothing in working accuracy, was a significant advantage. Another factor was of course that Rolls-Royce staff had been working on Head's method, and would be available to give assistance; this advantage disappeared when, after the financial troubles of the company, these employees took their leave.

The computer program developed by Rolls-Royce was known as Q195. Although considerable modifications have been made to its theory (see Chapter 6), the name Q195 has been retained. The

name Q195 has been retained. The remainder of this chapter describes it in its original form.

5.2 General Description

The program Q195 was developed for use on aerofoils, principally turbine and compressor blading. A section of the program deals with laminar flow and transition; this is of little importance in the author's application. Turbulent flow calculation follows the method of Head (5) as developed for compressible flow by Green (4). Provision is made for suction or injection at the wall, and for increased wall temperatures, the resulting heat transfer calculation following the method of Moretti and Kays (13). Turbulent separation is predicted, and a wake calculation is also provided for aerofoil work.

Inputs

The general inputs (i.e. those independent of grid position) are as follows:-

Leading edge radius (aerofoil)

Number of grid points (both surfaces)

Axial chord

Stagnation temperature and pressure

γ, C_p, Prandtl number

Intensity of turbulence

Entry values: u_{in}, H and St.

A system of integer inputs allows a choice of suction, injection or solid wall; heated or adiabatic wall; and natural transition or turbulent flow from the leading edge.

At each grid point in turn, the inputs are as follows:-

Co-ordinates (x and y)

Velocity

Wall temperature

Injection ratio.

Outputs

For each grid point in turn, the laminar output consists of:-

Momentum thickness, θ

Corresponding R_θ

Polhausen parameter

Displacement thickness, δ^*

Shape factor, $H = \delta^*/\theta$

Skin friction coefficient, C_f

Stanton number, St

Heat transfer coefficient.

The turbulent output is similar, except that an incompressible shape factor replaces the Polhausen parameter. Also printed are transition point co-ordinates (where applicable) and the location of the separation point.

5.3 The Equations in Detail

While the laminar part of Q195 is used in most aerofoil calculations, only the turbulent section is used here for comparison with experiment; this section, in the form developed by Rolls-Royce, will now be described in more detail.

Calculation centres around the simultaneous evaluation of shape factor and momentum thickness, at each grid point in turn. The interval between adjacent grid points is divided into ten equal steps, which are then subdivided into four "sub-steps"; a second-order Runge-Kutta technique is employed over these four sub-steps. The print-out lists values at the grid points, avoiding intermediate values except in the case of flow separation, when a warning is printed at each application of the Runge-Kutta calculation (a maximum of 40 times between grid points).

The equations used to derive these values are listed by Green (4). A brief description of these is given below. The shape parameter,

$$H_1 = \frac{\delta - \delta^*}{\theta}$$

is calculated from Head's entrainment equation

$$\theta \frac{dH_1}{dx} = F - H_1 \left[\frac{C_f}{2} - (\bar{H} + 1) \frac{\theta}{u_\infty} \cdot \frac{du_\infty}{dx} \right] \qquad \ldots(1)$$

An empirical relation between the entrainment function F and H_1 is taken in the form

$$F = 0.0299 \, (H_1 - 3)^{-0.6169} \qquad \ldots(2)$$

which is a close fit to Head's original curve, and the relation between $\bar{H}$ and H_1 is assumed to be given by

$$\bar{H} = 1 + 1.12 \left[H_1 - 2 \pm \sqrt{(H_1 - 2)^2 - 3} \right]^{0.915} \qquad \ldots(3)$$

a negative value of the square root being taken for attached flow. Equations (2) and (3) differ slightly from those of Green's 1968

paper (4), and follow Green's later recommendations as reported by Perry (19). $\bar{H}$ is the incompressible shape factor δ^*/θ; the compressible shape factor, H, is calculated from $\bar{H}$ by the equation

$$H = \frac{T_w}{T} \bar{H} + \frac{T_r}{T} - 1$$

where T, T_w and T_r are the static, wall and adiabatic wall temperatures respectively.

Skin friction values are calculated from

$$\left(\frac{C_f}{C_{fo}} + 0.5 \right) \left(\frac{\bar{H}}{\bar{H}_o} - 0.4 \right) = 0.9,$$

where the suffix o refers to flat plate values, to fit the values of Nash and Thompson (35). The flat plate C_{fo} is given by

$$C_{fo} = \frac{0.012}{\log_{10} R_\theta - 0.64} - 0.00093,$$

giving a good fit with the values of Spalding and Chi (31). Finally, the flat plate $\bar{H}_o$ is derived from

$$\frac{1}{\bar{H}_o} = 1 - 6.8 \sqrt{\frac{C_{fo}}{2}}$$

An additional term in $\frac{\rho_w u_w}{\rho_\infty u_\infty}$ is required if suction or injection is to be simulated. For the present application, a solid wall was used at all times.

For calculation of momentum thickness, the integral equation is written in the form

$$\frac{d\theta}{dx} = \frac{C_f}{2} - (H + 2 - M^2) \frac{\theta}{u_\infty} \cdot \frac{du_\infty}{dx}$$

However, Perry (20) incorporated modifications for surface curvature, along the lines suggested by Patel (16), who wrote the equation in polar co-ordinates:

$$\frac{d\,\textcircled{H}}{d\phi} + (\Delta^* + 2\,\textcircled{H})\,\frac{1}{\Omega}\,\frac{d\Omega}{d\phi} - \frac{\tau_w R^2}{\rho \Omega^2}$$

$$= \frac{1}{2}\,\frac{d}{d\phi}\left\{\tfrac{1}{2}\rho\Omega^2 \ln\frac{R_1}{R} + \int_R^{R_1} \mathrm{Pr}\,dr\right\}$$

for flow over a wall of constant radius R. R_1 refers to a line of constant radius immediately outside the boundary layer. Δ^* and $\textcircled{H}$ are related to the familiar δ^* and θ by the equations

$$\Delta^* = \delta^*/R$$

and $$\textcircled{H} \doteq (1 + \delta/R)\,\theta/R.$$

Perry expressed Patel's equation in curvilinear co-ordinates, for $\partial P/\partial r = 0$, i.e. for no static pressure variation across the boundary layer. Neglecting multiples of small quantities, and with an additional Mach number term for compressibility, the equation becomes

$$\left(1 + \frac{\delta}{R}\right)\frac{d\theta}{dx} = \frac{C_f}{2} - \left[H + 2\left(1 + \frac{\delta}{R}\right) - M^2\right]\frac{\theta}{u_\infty}\cdot\frac{du_\infty}{dx}$$

$$+ \left[\ln\frac{R_1}{R} - \tfrac{1}{2}\left(1 - \frac{R^2}{R_1^2}\right)\right]\frac{\theta}{u_\infty}\cdot\frac{du_\infty}{dx} \qquad \ldots(4)$$

It was this form of the momentum integral equation with additional terms to deal with variable radius of curvature, that was employed by Rolls-Royce in their aerofoil calculations.

Wall heating makes itself felt in the entrainment and momentum integral equations through the variation of H, the compressible shape factor, which varies widely with wall temperature. As mentioned earlier, Stanton numbers and heat transfer coefficients are calculated by the method of Moretti and Kays, and calculation is exactly as described in their paper (13).

Turbulent separation is indicated in either of two ways: negative values of skin friction coefficient, after which calculation ceases, or repeated warnings if H_1 falls below a certain figure. In the Rolls-Royce version, this figure was 3.74 (lower values causing breakdown of equation (3)), equivalent to an $\bar{H}$ of 2.86; this could, of course, be adjusted.

It was in the form described above that the program Q195 was made available to the author.

CHAPTER 6

PREDICTION PROGRAM Q195 - TESTING AND DEVELOPMENT

6.1 Computing Facilities

The Rolls-Royce version of Q195 had been written for use on an IBM 360 computer in Derby. It was decided, on the grounds of convenience, to employ facilities nearer to hand, and the listing was modified for use on the Univac 1108 at the National Engineering Laboratory at East Kilbride. Considerable teething troubles were experienced, especially as this development coincided with the departure from Rolls-Royce of the two employees most familiar with the program.

6.2 Schubauer and Klebanoff's Data

For an initial evaluation of Q195, the experimental data of Schubauer and Klebanoff (28) were applied. Their experiment featured measurements in the adibatic boundary layer (predominantly turbulent) over a wing section, the working side of which consisted of two curved sections of constant radius, joined by a flat surface. Pressure gradient was favourable at entry, becoming adverse around 30% chord, and increasing in adversity further downstream. Separation of the turbulent layer was noted a short distance upstream of the trailing edge. Entry flow speed was around 100 ft/s, so compressibility effects were small.

For the comparison, attention was concentrated on the two primary outputs from Q195, the momentum thickness θ and shape parameter H_1, which led to the more usual shape factor H. Calculation of θ was

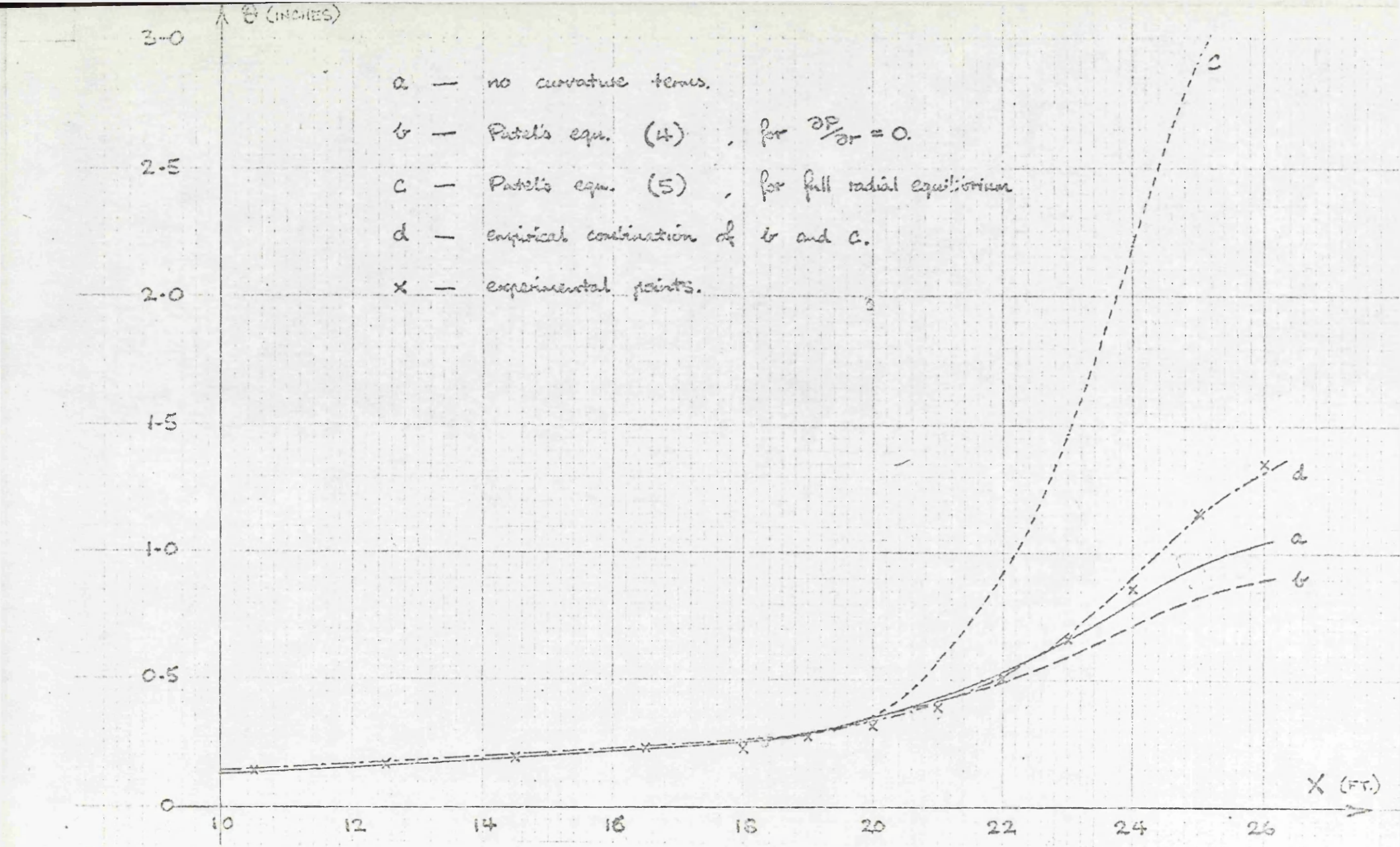

Figure 34: Momentum thickness distributions, from the data of Schubauer and Klebanoff (28).

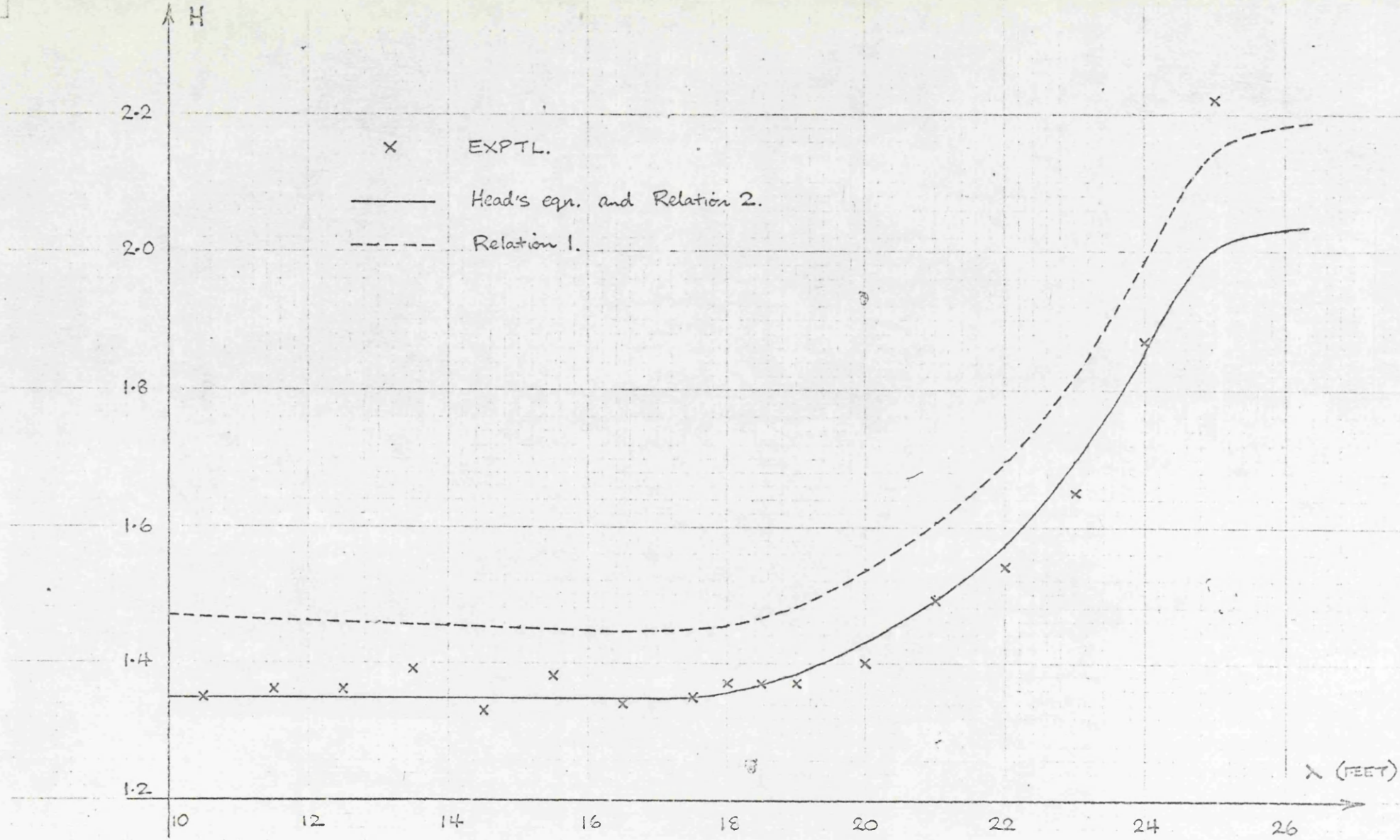

Figure 35: Shape factor distributions, from the data of Schubauer and Klebanoff (28).

performed firstly by the simple momentum integral equation and then by equation (4) with the added curvature terms. The results are shown in Figure 34, along with Schubauer and Klebanoff's experimental points. It will be seen that agreement is very satisfactory until around x = 22 ft, where Q195 begins to under-predict, the discrepancy increasing progressively towards the trailing edge. Curiously, the simpler momentum integral equation gives a better fit over this region, but cannot be accepted as satisfactory. Values of $\bar{H}$ calculated from the entrainment equation and equation (3) were generally a little low, and again this discrepancy increased near the trailing edge, where the experimental values reflected the approach of separation (Figure 35).

In an attempt to achieve better prediction of Θ development, Patel's (16) momentum integral equation for constant radius of curvature was examined once more. One relatively simple adjustment, suggested by Patel, was the introduction of the radial equilibrium equation,

$$\frac{u^2}{r} = \frac{1}{\rho} \cdot \frac{\partial p}{\partial r}$$

to describe the static pressure distribution in the boundary layer. After evaluation of the integral term and reversion to curvilinear co-ordinates, Patel's equation becomes

$$\left(1 + \frac{\delta}{R}\right) \frac{d\Theta}{dx} = \frac{C_f}{2} - \left[1 + \frac{\delta}{R} - M^2\right] \frac{\Theta}{u_\infty} \cdot \frac{du_\infty}{dx} + \frac{1}{2}\left[\frac{R^2}{R_1^2} - 1\right] \frac{\Theta}{u_\infty} \cdot \frac{du_\infty}{dx} \qquad \ldots(5)$$

With this equation, it was quickly apparent that the choice of R_1

had a considerable influence on the θ distribution predicted, and allowance had to be made to adjust R_1 to be immediately outside the boundary layer at each grid point. This of course gave a stepwise variation; the calculations using equation (5), made between these steps, were made at a constant value of R_1. A predicted θ distribution for Schubauer and Klebanoff's data is shown in Figure 34; it will be seen that greatly accelerated boundary layer growth is indicated, considerably in excess of the experimental observations. If equation (5) is taken as accurate for a radial equilibrium boundary layer (an assumption which has yet to be justified), the indications are that static pressures within the boundary layer were uniform over the greater part of the aerofoil, but that some variation set in some 22 feet from the leading edge; this variation at no time approached that which would arise in radial equilibrium flow. The above conclusions seem reasonable from a study of the experimental data.

The performance of the entrainment equation could not be assessed in company with an inaccurate momentum integral equation, as the two are interlinked; accordingly, the latter was modified empirically to give an acceptable fit with the experimental results near the trailing edge. This curve is also shown in Figure 34. However, the corresponding entrainment equation was not entirely satisfactory, the $\bar{H}$ distribution levelling off towards the trailing edge rather than rising steadily to separation (Figure 35).

6.3 The Author's Data - Modifications for Duct Flow

The present author's experimental data for adiabatic conditions were then used in further testing of the predictions. It was hoped that these would determine the accuracy of equation (5) for radial equilibrium flow, and throw more light on the need for changes in the entrainment relations. The θ development was therefore the first concern. Allowance was made for the experimental method of boundary layer tripping, and the resulting thicker layers, by introducing an extra "starting length" of flat plate on the prediction model. A length was selected to give matching θ at x = 10 in., and the distribution compared with the experimental over the following ten inches.

A problem arose in choosing a local velocity, to be specified at each grid point. The calculation is extremely sensitive to these velocities, from which the local streamwise pressure gradients are calculated. Patel's velocity u_{pw} was used initially, but with poor results, and was replaced by u_δ, the velocity just outside the boundary layer. However, this was only a limited improvement. The predicted growth of the boundary layer was generally too slow; calculations of mass flow for the experimental duct dimensions showed that the displacement thickness and mainstream velocity distributions were inconsistent, even with generous allowance made for boundary layer growth on the remaining three walls.

In order to obtain consistency between local duct blockage and mainstream velocity, and to avoid the necessity of specifying a

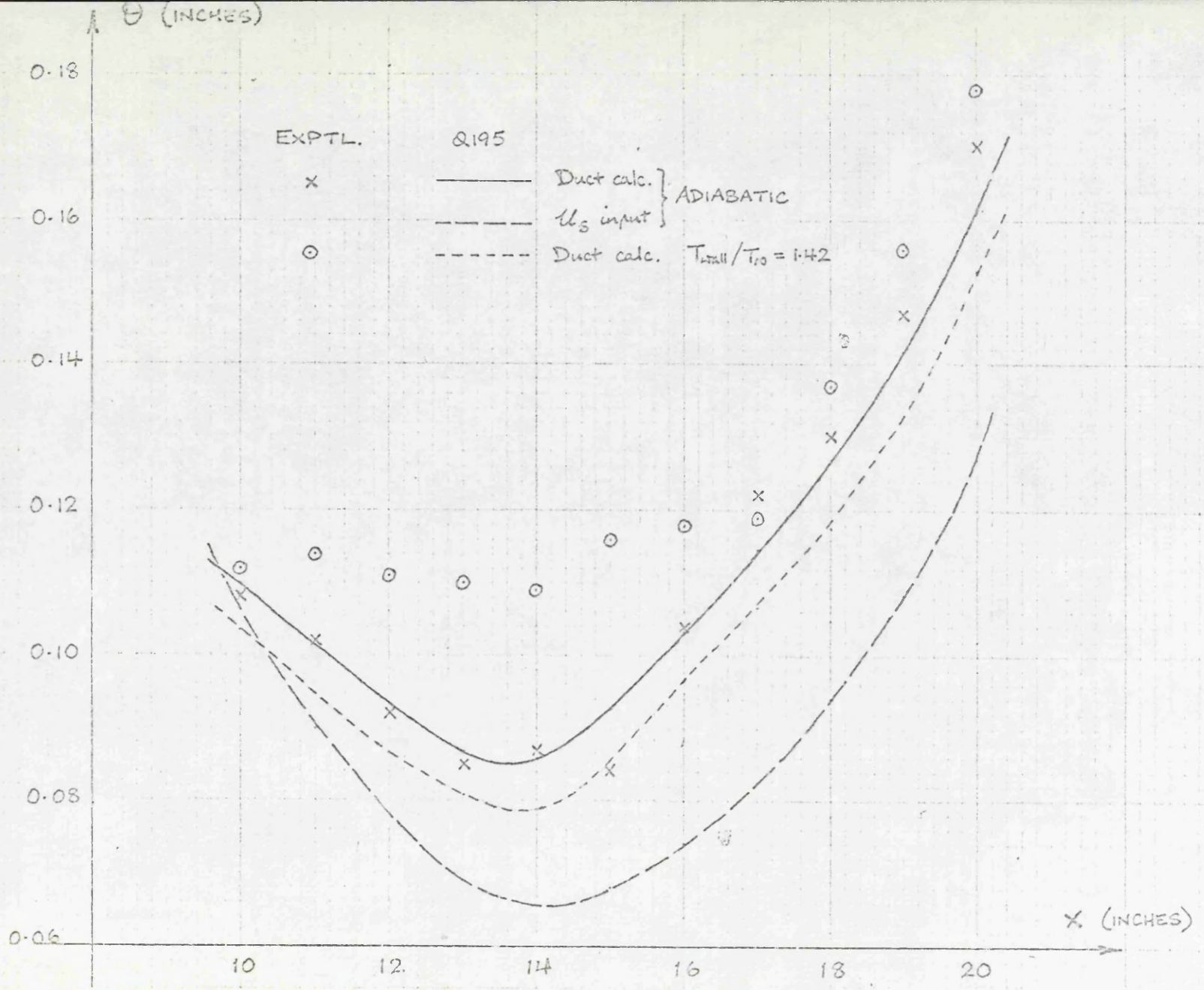

Figure 36: Momentum thickness distributions, from the author's data.

somewhat arbitrary local velocity input, a new subroutine was written into Q195. This puts the entire program through several iterations: the first uses velocity inputs calculated from duct geometry alone, the second adds a factor accounting for blockage due to boundary layer growth, as do the subsequent iterations. In practice, six runs gave a very reasonable convergence of calculated values. For straight ducts, the blockage is easily evaluated, as all surfaces have similar boundary layers upon them; the curved duct obviously poses more of a problem. Lack of measurements on all but the inner wall made an estimate necessary, a figure of two to three times the inner wall blockage seeming reasonable in view of the rapid boundary layer growth on the latter. A figure around 2.5 was decided upon, falling slightly with x as a further concession to the above growth rate.

An obvious advantage of this approach is that no velocity or pressure gradient data are required for duct problems. Also the dimensions of a duct are usually measurable to a much greater degree of accuracy than are local flow velocities, and so form a more satisfactory input. Results from the author's duct geometry were most encouraging; the calculation of momentum thickness used all three forms of the integral equation. After the flat plate entry section, equation (4) was used for approximately four inches of curved surface before the radial equilibrium equation (5) was introduced. The resulting θ distribution, after matching at x = 10 in., was an almost perfect fit with the experimental values. This is illustrated in Figure 36, along with an earlier calculation using velocity input u_δ.

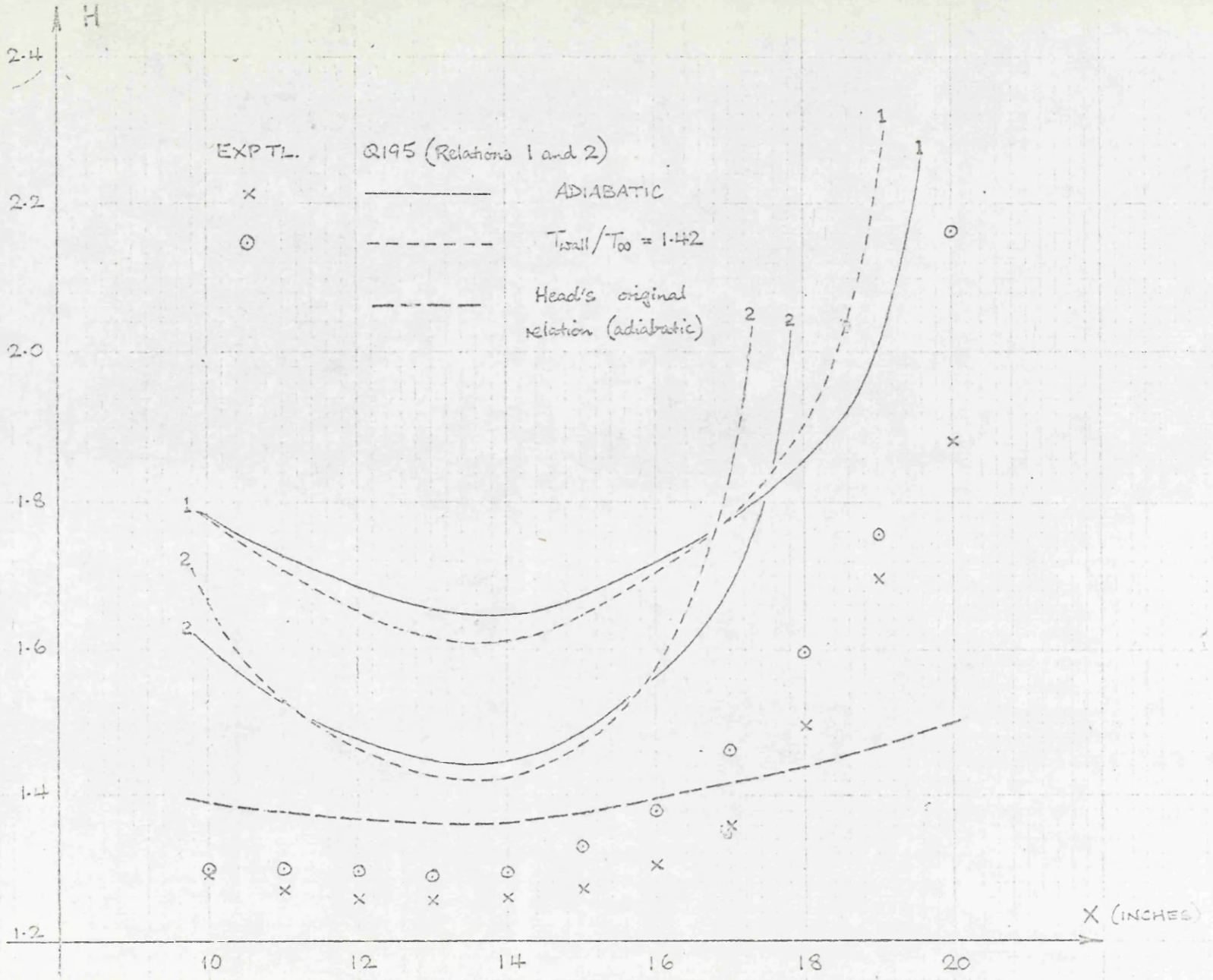

Figure 37: Shape factor distributions, from the author's data.

It is emphasised that these results are for adiabatic conditions throughout.

6.4 The Author's Data - Modifications to Entrainment Theory.

Performance of the entrainment equation was much less satisfactory. Predictions of $\bar{H}$ were too high up to approximately $x = 17$ in., after which they fell below the experimental values. Separation was predicted, but well downstream of the observed separation point. The discrepancies in $\bar{H}$ are shown in Figure 37.

Clearly, this entrainment theory was in need of modification. Thompson (35) has suggested that Head's original $H_1(\bar{H})$ relation required adjustment for local values of R_θ, and has computed curves for a range of R_θ. Patel (16) has also mentioned corrections to this relation for surface curvature, mentioning δ/R as a possible parameter. For his experiments, the R_θ corrections outweighed those for curvature. Accordingly the $H_1(\bar{H})$ relationship was examined with a view to modification.

As mentioned before, the equation used in Q195 is in the form

$$\bar{H} = 1 + 1.12 \left[(H_1 - 2) - \sqrt{(H_1 - 2)^2 - 3} \right]^{0.915} \quad .. (3)$$

For convenience, certain of the numerical constants may be labelled, to give

$$\bar{H} = 1 + A \left[(H_1 - C) - \sqrt{(H_1 - C)^2 - 3} \right]^B$$

It was found that if A and B were transformed into functions of R_θ and C remained as 2, the R_θ-dependent curves of Thompson could be reproduced. Further, if C became a function of δ/R (and equalled 2

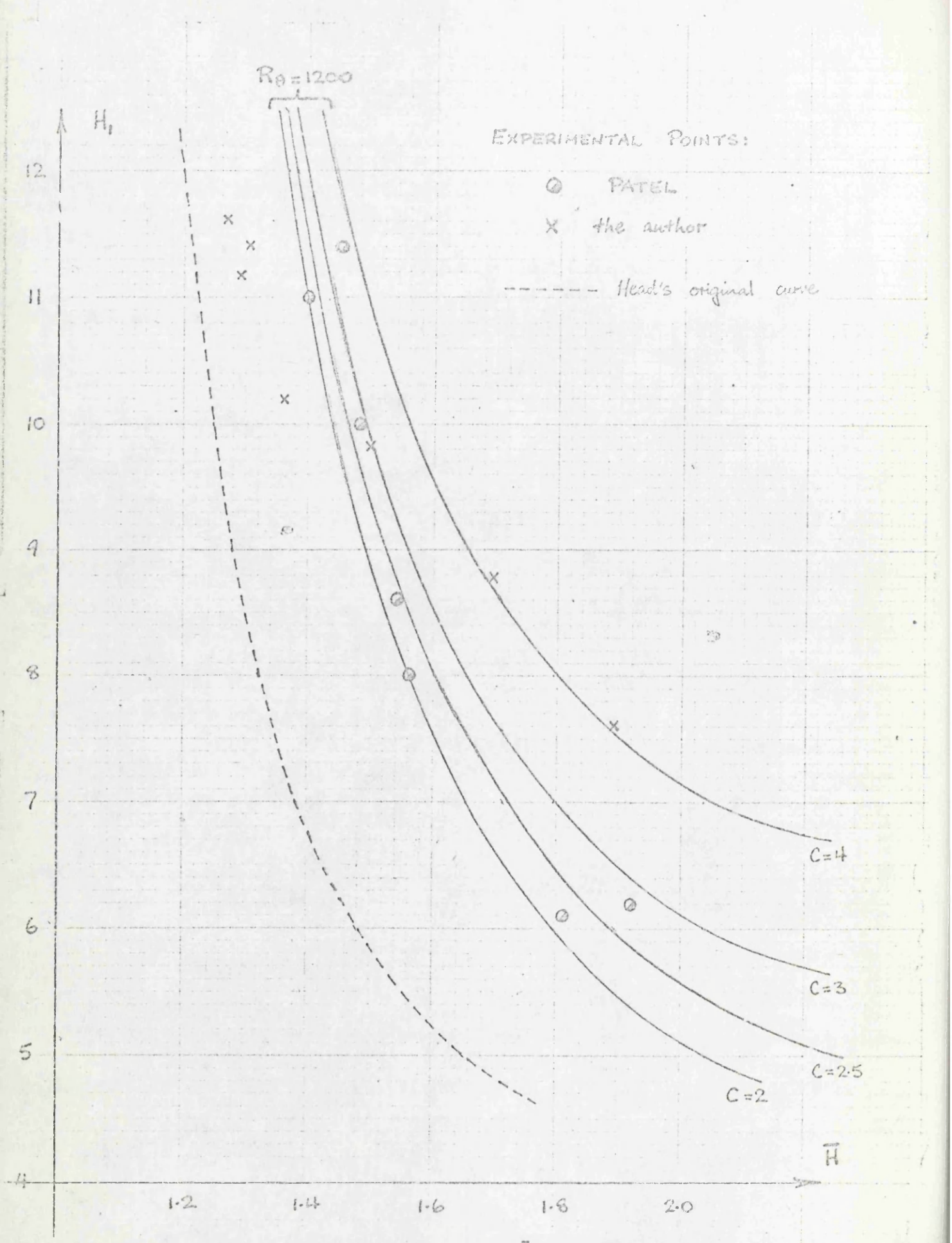

Figure 38: Thompson's (35) H_1 ($\bar{H}$) curve family, with added curvature correction.

when $R = \infty$), curvature-corrected curves were produced to fit Patel's experimental points. The values selected for A, B and C were as follows:-

$$A = \frac{35}{\ln R_\theta + 14}$$

$$B = \frac{25 + \ln R_\theta}{40}$$

and $$C = 2 + \frac{8\delta}{R}$$

this last relation being chosen empirically. A family of curves for $R_\theta = 1200$ and C in the range 2 to 4, is shown in Figure 38. Both Patel's and the author's measured R_θ were close to the above value, so it would be expected that the curves fit both sets of experimental points. However, this is not the case; while Patel's points are a most acceptable fit, the author's are not, and appear to dispute the need for R_θ correction terms A and B above. At this point it should be mentioned that Patel's values of δ/R were very small, and the choice of C (above) was not critical. The relation was selected with reference to the author's experimental points, which are for much larger δ/R.

An indication of the curve family produced if A and B are returned to their values in equation (3), is given in Figure 38 by the broken line, which represents the original curve taken by Head. This would become the curve for C = 2, and the other curves in the family would be placed accordingly. With a new curvature relation,

$$C = 2 + \frac{12\,\delta}{R}$$

this curve family gives a good fit with the author's experimental points. However, Patel's data are not satisfactorily represented.

To sum up, two alternative forms of the $H_1(\bar{H})$ relation have been described. The first incorporates terms in R_θ and δ/R, and is an excellent fit with the experimental data of Patel; the second has no terms in R_θ, but is more heavily weighted in favour of δ/R. This fits the author's experimental points. The two sets of experimental data are such that no $H_1(\bar{H})$ relation can be found to fit both, without radical (and highly empirical) departure from the form of equation (3). Obviously, more data are required before the position may be clarified.

It was therefore decided to employ both forms of the $H_1(\bar{H})$ relation for prediction of the author's experimental results, in the hope that more light would be thrown on the relative merits of the two. Details of the input conditions and results obtained are given in the following section. It will be noted that Green's original $F(H_1)$ relation (a single curve) was left unaltered. Calculation of momentum thickness was by equation (5) over the curved surface, with the exception of a 4 inch section at entry, where equation (4) was used. Over the flat lead-in section (up to x = 6 in.), the simple flat-plate equation was of course employed. Finally, velocity inputs were based on duct geometry, and six iterations for blockage calculation were specified, the output for the last two being identical.

6.5 The Author's Data with Heat Transfer - Predictions from Modified Q195.

The first series of predictions was designed for comparison with the author's low speed tests, during which detailed measurements of θ, H, C_f and St had been made (see Sections 3.4.4 and 3.4.5). Grid points were spaced every inch over most of the curved surface, and at two-inch intervals elsewhere. Entry velocity was 24 ft/s, and stagnation temperature 300 K. Wall temperatures (uniform) varied from 300 K to 425 K, at 25 deg K intervals. For ease of reference, the first form of the $H_1(\bar{H})$ relation, which involves R_θ terms, will be known as Relation 1. The second form with curvature variables only, will be known as Relation 2.

6.5.1 Adiabatic Conditions

For both Relations, prediction of momentum thickness was most satisfactory, as was mentioned earlier. This is illustrated in Figure 36; the curves for Relations 1 and 2 were practically identical. Prediction of shape factor, however, was less promising (see Figure 37). Relation 1 gave a distribution in which $\bar{H}$ was at all times too large; the discrepancy reduced a little as x increased. Separation was predicted 1.5 in. upstream of the experimentally-observed point. Use of Relation 2 reduced $\bar{H}$ in the early stages (but not nearly enough), and gave a curve of somewhat better shape; however, $\bar{H}$ increased very rapidly around x = 17 in., and separation was predicted a full 3.5 in. upstream of the experimental point. Included for comparison in Figure 37 is an $\bar{H}$ distribution calculated from the single-curve

relation of equation (3).

Skin friction coefficients (Figure 21) generally reflected the over-predicted values of $\bar{H}$, from which they were calculated. Thus they began at around 50% of the experimental values and did not recover, although their progressive reduction towards separation was reasonably satisfactory. Relation 2 was perhaps the more successful, in that it predicted coefficients which more nearly approached the experimental values. Stanton numbers were not measured experimentally for adiabatic flow conditions.

6.5.2 Wall temperature 425 K

For flow with wall heating, Q195 predicted a slight reduction in momentum thickness, compared with adiabatic values, at each point on the wall. Again, the two $H_1(\bar{H})$ relations produced similar results. As will be seen from Figure 36, this is not consistent with experimental observations, in which Θ showed a slight increase on heating, in the range x = 10 in. to x = 18 in.

Prediction of shape factor was also influenced by the choice of $H_1(\bar{H})$ relation, as would be expected. However, both Relations 1 and 2 predicted values of $\bar{H}$ at x = 10 in. which were greatly in excess of the experimental values, and comparison further downstream suffered as a result (see Figure 37). When referred to the corresponding adiabatic figures, the results of wall heating were similar for both relations. The heated distribution appeared to be more responsive to streamwise pressure gradient, falling below the adiabatic curve before crossing it at the approach of separation.

The predicted separation points differed markedly, as Figure 37 suggests. In this field, Relation 1 was clearly superior. However, the upstream movements of separation point for 125 deg C of wall heating were similar; 0.75 in. for Relation 1 and 0.70 in. for Relation 2. This compares with the experimentally observed movement (at this flow speed) of 1.6 in.

Both relations predicted that skin friction coefficients would show a small reduction from their adiabatic values. This agrees with experiment (see Figure 21), although again the experimental and predicted values compare poorly.

Stanton number predictions, which as described earlier follow the method of Moretti and Kays, are not dependent on the $H_1(\bar{H})$ relation specified. The predicted distribution is shown in Figure 24, along with other distributions derived from the experimental results. As will be seen, it seriously under-estimates the Stanton number throughout the range of x considered, and shows little or no response to changing pressure gradients. In this application, the method is no better than a simple, flat-plate equation derived from Reynolds analogy (also shown in the Figure).

6.5.3 Separation points for u_{in} = 24 ft/s.

A set of predictions, using Relation 1 and Relation 2 in turn, was then completed for a range of intermediate wall temperatures. Of primary interest was the movement of the separation point. A table of separation points, including those for adiabatic flow and for a wall temperature of 425 K was drawn up and is given below.

Wall Temperature	Separation Point (inches from LE)	
	(Relation 1)	(Relation 2)
300 K (adiabatic)	20.10	18.00
325 K	19.65	17.55
350 K	19.55	17.50
375 K	19.50	17.40
400 K	19.40	17.35
425 K	19.35	17.30

Table 2: Separation Points at u_{in} = 24 ft/s.

6.5.4 Separation points at other entry velocities.

The duct entry velocity u_{in}, which had remained at 24 ft/s for all previous runs using the author's data, was then increased to 60 ft/s to represent conditions at the maximum flow velocity obtained experimentally. Separation points were again calculated for a range of wall temperatures, using the two $H_1(\bar{H})$ relations in turn, and the results are tabulated below.

Wall Temperature	Separation Point (inches from LE)	
	(Relation 1)	(Relation 2)
300 K (adiabatic)	20.90	19.25
325 K	20.80	19.00
350 K	20.70	18.55
375 K	20.60	18.50
400 K	20.50	18.45
425 K	20.40	18.40

Table 3: Separation Points at u_{in} = 60 ft/s.

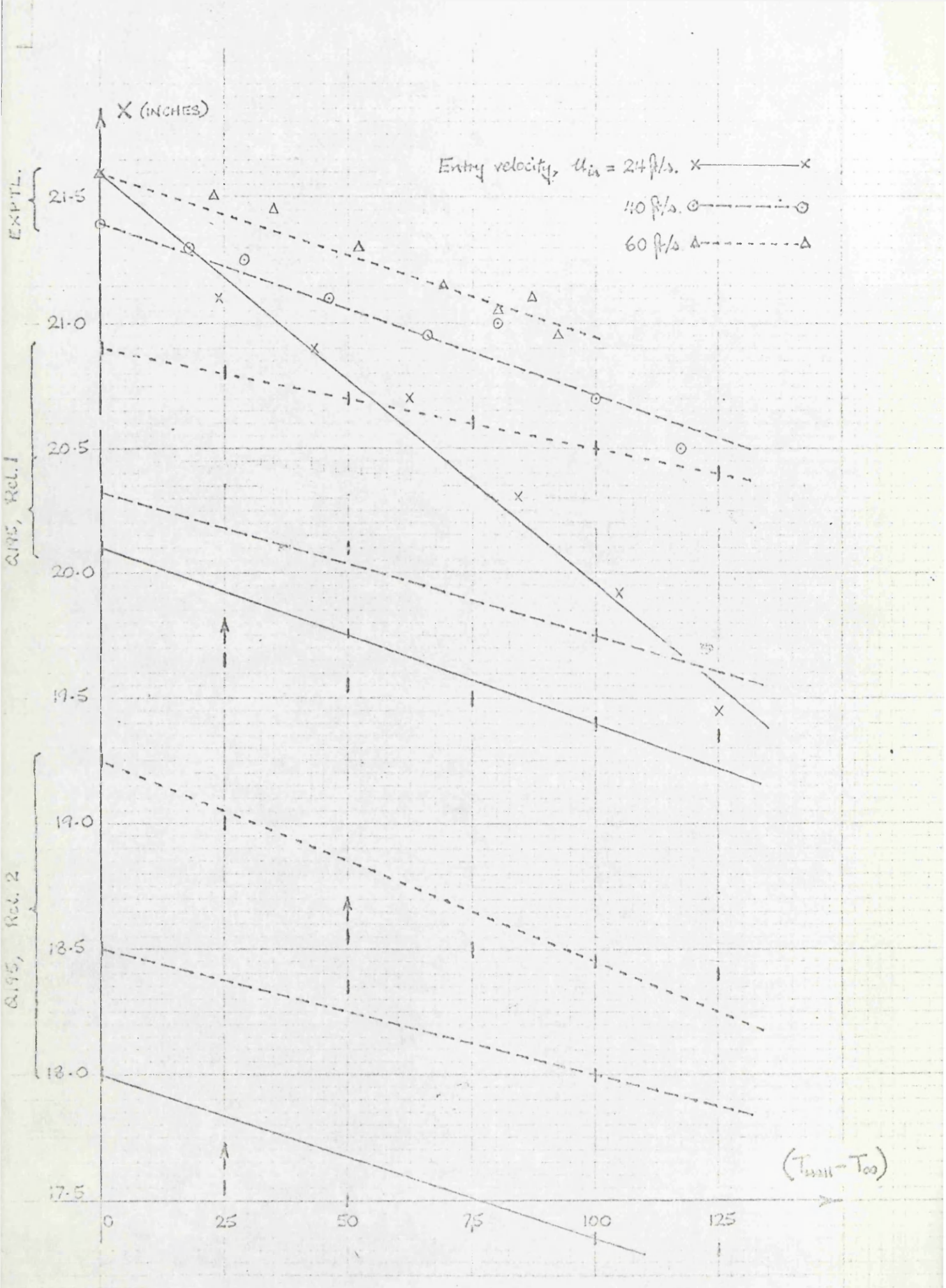

Figure 39: Experimental and predicted separation points.

A further series of predictions, at an entry velocity of 40 ft/s, was then completed. This was less detailed than the previous two, and only covered two wall temperatures other than adiabatic. The results are tabulated below.

Wall Temperature	Separation Point (inches from LE)	
	(Relation 1)	(Relation 2)
300 K (adiabatic)	20.325	18.50
350 K	20.10	18.35
400 K	19.75	18.00

Table 4: Separation Points at u_{in} = 40 ft/s.

A similar prediction was performed for an entry velocity of 100 ft/s. (see table below).

Wall Temperature	Separation Point (inches from LE)	
	(Relation 1)	(Relation 2)
300 K (adiabatic)	21.20	19.55
350 K	20.90	19.40
400 K	20.70	19.15

Table 5: Separation Points at u_{in} = 100 ft/s.

6.5.5 Discussion of Results

The results in Tables 2, 3 and 4 were plotted against wall excess temperature, along with the experimental results under the same conditions (Figure 39). The results at 100 ft/s had of course no experimental equivalent, and for clarity were omitted from this

figure. However, they are included in Figure 33. For both experimental and predicted results, straight-line distributions have been drawn; these are a good fit to the former, but less satisfactory for the latter. It had been expected that the movement of the predicted separation point would be reasonably pregressive; that this was not so (for some conditions, at least) was considered to be largely due to the coarseness of the grid spacing, compared with the distances to be measured. Evidence to support this conclusion is given in Section 6.8.

The predicted large response of the adiabatic separation point to changes in flow speed was not observed experimentally. This may have been the result of experimental entry conditions, or the prediction theory may be in error. It seems not unreasonable to expect some response to variation of flow speed, and that this response be progressive, which throws suspicion on the experimental results. However, the inconsistencies in the latter may have been entirely due to vibration (see Section 4.9), indicating negligible separation point movement for vibration-free adiabatic flow. Thus no conclusions may be drawn. Relation 1 predicted less adiabatic point movement than did Relation 2.

Both predictions under-estimated the value of x at separation, for all wall temperature, the discrepancy being greater for Relation 2. At an entry velocity of 24 ft/s, both Relations predicted a rate of movement in response to wall temperature increase around 50% of the experimental value. At 40 ft/s, the predicted rate was close to the experimental one, but the latter was regarded as suspect because

of plate vibration. At 60 ft/s, the two predictions differed; Relation 1 gave a response rate around 60% of the experimental, while Relation 2 predicted a rate slightly greater than the experimental one.

Comparing the overall performances of each Relation, it will be seen that Relation 1 predicted a progressive reduction in response rate as velocity rises, while Relation 2 gave a fall and then a rise in response rate with increasing flow velocity. The expected behaviour of the boundary layer on a vibration-free plate (discussed in Section 4.9) suggests that the predictions from Relation 1 are possibly correct, while those from Relation 2 are most unlikely to be.

The performance of Relation 1 was further investigated for other entry velocities, of 15, 20, 30 and 80 ft/s. The effect of an increase in wall temperature of 100 deg C was examined, and a table drawn up to include all the entry velocities so far employed.

This table is shown overleaf.

Entry Velocity	Separation Points (inches from LE)		K_r
(ft/s)	300 K (adiabatic)	400 K	(x 10^6)
15	19.45	18.60	7.24
20	19.65	19.25	5.32
24	20.10	19.40	4.42
30	20.20	19.55	3.65
40	20.325	19.75	2.84
60	20.90	20.50	2.01
80	21.10	20.60	1.54
100	21.20	20.70	1.22

Table 6: Separation Points Predicted by Relation 1.

The right-hand column lists the parameter K_r (see Section 4.10). For each flow speed, the ratio of heated to adiabatic Reynolds number at separation was calculated, based on ν_∞ throughout, and plotted against K_r in Figure 33. This gave a comparison with the experimental points obtained, and the expected curve for a vibration-free plate. The result was inconclusive; the predicted Reynolds number ratio generally exceeded the experimental value, but did exhibit the same tendency towards falling with increasing K_r, and (more important) tending towards a steady figure of low values of K_r. This figure was around 0.98, which was reasonably close to the experimentally-derived value. However, the scatter of the predicted points was very great, especially for higher values of K_r. Modifications to Q195, to reduce this scatter at the cost of a modest increase in required storage space are under consideration.

6.6 Further Predictions using Schubauer and Klebanoff's Data

This completed the predictions based on the author's data. Further investigations using Q195 were then made to check the validity of the parameter K_T, and to predict the movement of the separation point on a typical aerofoil; these are described in Sections 6.7 and 6.8. A final set of predictions was made with the data of Schubauer and Klebanoff, as used previously; this employed the empirical modifications to the momentum integral equation, described in Section 6.2, to give an accurate fit to the experimental Θ distribution. In the entrainment calculations, the $H_1(\bar{H})$ relation included corrections for R_θ and curvature as in the Relation 1 used in prediction of the author's results. However, the curvature correction was empirically reduced, to reflect the assumed reduced static pressure difference across the boundary layer, compared with the radial equilibrium case. The resulting $\bar{H}$ distribution is shown in Figure 35, and will be seen generally to lie above the experimental values. However, this position was reversed before the trailing edge was reached, and separation was not predicted.

In view of this rather poor performance, a further prediction was made for the same data, using entrainment Relation 2. The results are not given in Figure 35, as they showed practically no change from the predictions of Head's original $H_1(\bar{H})$ relation, indicating that the curvature corrections were very small. This was, of course, to be expected in view of the large radii of curvature of the Schubauer/Klebanoff wing.

6.7 Investigations of the Parameter K_r

It has already been mentioned (see Section 4.10) that equal values of the parameter

$$K_r = \frac{\nu_\infty}{u_{pw}^2} \cdot \frac{\partial u}{\partial x}$$

may be obtained by different combinations of flow velocity and streamline curvature. The relevance of the parameter may therefore be tested by comparing behaviour of the boundary layer at the same K_r but different flow velocity. Experimentally this would be time-consuming, requiring the construction of several ducts of various radii of curvature. However, computer predictions for these conditions present no problem.

Two values of K_r were chosen for investigation, these being -2.01×10^{-6} and -4.42×10^{-6}, representing the upper and lower limits of the experimental range. These values were obtained experimentally at entry velocities of about 60 and 24 ft/s respectively. In the predictions, the entry velocities were first set at 40 and 15 ft/s, and the plate radius of curvature reduced to obtain the same values of K_r. Then, with velocities of 200 and 80 ft/s, and increased radii of curvature, the tests were repeated. The effect of wall heating, at 50 and 100 deg C above ambient, was then examined. The predicted separation point movements were expressed as Reynolds number ratios, as before, and the results for a 100 deg C rise in wall temperature are shown as single points in Figure 33.

These demonstrated reasonably clearly that K_r alone is not an adequate parameter for describing the effects of flow velocity and

radius of curvature. At $K_r = -4.42 \times 10^{-6}$, the three calculated points indicated a reduced separation point movement for increased radius of curvature (or increased flow velocity). At $K_r = -2.01 \times 10^{-6}$, the picture was not so clear, possibly because one of the points (labelled R = 2.30 ft) was calculated at a flow speed of 200 ft/s, at which compressibility effects could not entirely be ignored. It appeared that these effects tended to increase the separation point movement, compared to the incompressible case, and this was confirmed by the inclusion of a fourth calculated point, for a flow speed of 100 ft/s (labelled R = 1.15 ft). Compressible flow and its effects are discussed at greater length in Section 8.5.

From the above, it is seen that the parameter K_r falls short of its prime objective, to produce a single predicted curve in Figure 33. Investigations into the validity of further parameters are planned, but modifications to Q195, to improve its precision in fixing the separation point, are required before such work is undertaken.

6.8 Aerofoil Predictions

The program Q195 was then put to its original use, in a series of predictions of flow over an aerofoil. For the majority of these calculations, the iterative process for duct flow was omitted, after it was shown that the boundary layers were sufficiently thin to make duct blockage corrections unnecessary; this of course saved a considerable amount of computing time. The aerofoil model was of 2 in. chord, with grid points spaced at 0.1 in. intervals. The static pressure distribution, applied by specifying local freestream velocity,

was varied from run to run, but was generally typical for compressor blading. The first tests were made for a completely turbulent boundary layer on the suction surface (a common assumption in the aerodynamic study of compressor blades) and employed four different combinations of the momentum integral and entrainment equations. These were as follows:-

1. The momentum integral equation was written with no correction terms for surface curvature, and the entrainment $H_1(\bar{H})$ relation was the unique single-curve type given in Equation (3). This effectively treated the aerofoil as a flat plate with variable pressure gradient.

2. The momentum integral equation was unchanged, but the $H_1(\bar{H})$ relation was modified to include corrections for R_θ, as described in Section 6.4. This was still a flat-plate treatment.

3. The momentum integral equation was re-written to include curvature terms, but with negligible static pressure variation across the boundary layer (Equation (4)). The suction surface radius of curvature was uniform at 1 ft. The entrainment theory was unchanged from test 2. This combination represented the theory used in the Rolls-Royce version of Q195 made available to the author, with the addition of R_θ corrections to entrainment.

4. The momentum integral equation was written with curvature terms for full radial equilibrium, as in Equation (5), with the same radius of curvature on the suction surface.

The $H_1(\bar{H})$ relation included correction terms for R_θ as before, but also contained curvature terms, to make the entrainment theory that of Relation 1 in the predictions of the author's results.

The flow on the pressure surface of the aerofoil was not studied in detail, as the main concern was the growth towards separation of the suction surface boundary layer. For each of the above four theories, the same procedure was adopted. Adiabatic testing took place with varying static pressure gradients over the last few grid points on the blade, until separation was established just upstream of the trailing edge. Then, for the same pressure gradient, the effect of wall heating on movement of the separation point was calculated, for uniform wall temperatures 50 and 100 deg C above the stagnation temperature of the freestream. No detailed examination was made of the separation points predicted by the four theories under identical flow conditions.

The inlet velocity for all tests was 780 ft/s. Local Mach numbers remained below unity throughout. A table of separation points for the four theories is given below. The adiabatic points are, of course, arbitrary as they are the result of variations in pressure distribution.

The temperature T_r refers to the adiabatic wall temperature, which for these calculations was within a few degrees of the stagnation temperature T_o.

	Separation Point (inches from LE)		
Theory	Adiabatic	$(T_{wall} - T_r) = 50\ C^\circ$	$(T_{wall} - T_r) = 100\ C^\circ$
1.	1.905	1.835	1.775
2.	1.990	1.915	1.850
3.	1.955	1.880	1.8125
4.	1.970	1.895	1.800

Table 7: Separation Points on Aerofoil, Fully Turbulent Boundary Layer.

Expressed as percentages of the value of x at separation, these are reductions of 6.8%, 7.0%, 7.2% and 8.6%, for an increase in wall temperature of 100 deg C above the adiabatic value. It will also be seen that the movement of the separation point is approximately linear with wall excess temperature. This was not readily apparent in the tests for the curved duct, where the grid spacing was somewhat coarse. The above suggests that the straight-line profiles, drawn in Figure 39 through the very scattered predicted separation points for the curved duct, are not seriously in error.

A second set of predictions was then made for an initially laminar boundary layer, with the turbulent section following theories 3 and 4. Again, the streamwise velocity distribution was arranged to produce turbulent separation just short of the trailing edge, for adiabatic flow. It was found that for a 1% intensity of turbulence, laminar separation was predicted, with turbulent reattachment a short distance downstream. With an intensity of 4% (probably a more realistic figure), the laminar layer went into transition in the usual way. The results quoted below are for the latter figure.

Turbulent Theory	Adiabatic	Separation Point (inches from LE) $(T_{wall} - T_r) = 50$ deg C	$(T_{wall} - T_r) = 100$ deg C
3.	1.930	1.860	1.795
4.	1.9075	1.860	1.775

Table 8: Separation Points on Aerofoil, Laminar/Turbulent Boundary Layer.

Expressed as percentages of the value of x at separation, these are reductions of 7.0% and 7.0%, for an increase in wall temperature of 100 deg C above the adiabatic value. The transition point was not greatly affected by the wall heating; indeed, the position of the end of transition was not altered at all.

Thus it will be seen that, for an increase in blade temperature of 100 deg C above the adiabatic value, the value of x at separation was reduced by between 6.8% and 8.6%, indicating that the effect of wall heating is not significantly influenced by the choice of prediction theory.

For a given mainstream velocity distribution, the position of the adiabatic separation point is of course highly dependent on the prediction theory used. In general, the corrections for curvature tend to advance the predicted point; put another way, the effect of curvature is to make the boundary layer less tolerant of adverse pressure gradients.

The implications of these results, regarding the transient performance of an axial compressor, will be discussed in Chapter 8.

CHAPTER 7

PREDICTION PROGRAM Q195 - DISCUSSION

The modifications made by the author to the turbulent section of Q195 have already been described. Briefly, these attempted to correct the calculations of momentum thickness and shape factor for surface curvature and Reynolds number effects. Also, the scope of the program was widened to include duct problems. Several other alterations were made, but these were to improve its ease of handling rather than its versatility or accuracy.

In its current form, Q195 is capable of predicting boundary layer parameters on flat or curved surfaces for a wide variety of pressure distributions. Suction and injection at the wall are permissible; this section of the program was not investigated by the author, and remains in the form drawn up by Rolls-Royce Ltd. Wall temperature variations over a generous range are also catered for, as is the effect of surface roughness (again ignored by the author). Transition, laminar separation and turbulent separation are all included in the prediction theory.

7.1 Momentum Integral Equation

The form of the momentum integral equation is now considered satisfactory. This permits any of three conditions: no streamline curvature, curvature with no radial pressure gradient and curvature with full radial equilibrium. One possible extension is to cover radial pressure gradients below the equilibrium value, as exemplified by the Schubauer

and Klebanoff tests (28): however, this is probably best done to suit the individual case. The radial equilibrium equation performed well with the author's data, given a matched starting value. Further comparison with experiment of all forms of the equation would, of course, be valuable.

7.2 Entrainment Theory and Skin Friction

Prediction of shape factor was a more limited success. Here, the extra empirical content of the corrections for curvature and R_θ must be weighed against the accuracy gained. Comparison with the author's results, with very rapid boundary layer growth and separation, was an extremely severe test for the theory. The need for a correction term for surface curvature in the $H_1(\bar{H})$ relation was clear; without one, separation would not have been predicted. However, the magnitude of this correction depended on whether the terms in R_θ from Thompson (35) were included. Accordingly, two forms of the $H_1(\bar{H})$ relation were drawn up, and tested simultaneously.

The results were inconclusive. The R_θ terms resulted in early values of $\bar{H}$ which were much too large; however, the separation predictions from this version were generally superior. Returning to the data of Schubauer and Klebanoff, it was seen that the R_θ terms again produced a considerable discrepancy over most of the surface. The radius of curvature was too great for the curvature correction to be assessed.

Clearly, a great deal remains to be done before this situation may be resolved. At present, the original $H_1(\bar{H})$ relation of Head (5)

is adequate for many situations, and the effects of surface curvature are small for values of δ/R below about 0.05. Experimental work, with large values of δ/R, is necessary to evaluate the curvature correction terms, and more comparisons with general experimental results are needed to determine the usefulness of the terms in R_θ. All this applies to Head's G relation; a similar examination of his F relation was not carried out. It may be that correction terms are required here also; in view of the already high empirical content of the method, it is to be hoped not.

Predictions of skin friction were largely dependent on the local shape factor, and therefore suffered from the inaccuracies in prediction of the latter. As far as may be judged, acceptably accurate skin friction values are calculated when the shape factor is not seriously in error.

7.3 Stanton Number

As mentioned earlier, the predicted Stanton numbers from the author's data were not satisfactory. In their original paper, Moretti and Kays (13) tested their method in zero or favourable pressure gradients, for a range of wall temperature distributions; the results were encouraging. However, the more severe test of predictions for adverse pressure gradients was not attempted. For the author's experimental conditions, the method responded poorly to changes in pressure gradient, and gave predictions generally similar to those for a flat plate at zero incidence, as will be seen from Figure 24. Modifications to the method to remove this objection are not possible.

Of the alternative calculation procedures discussed in Section 4.8, the method of Reynolds, Kays and Kline (22) may prove useful as a basis for a replacement, although certain assumptions regarding temperature profile shape will have to be made.

The other sections of Q195, dealing with the laminar boundary layer, transition and laminar separation, were not modified by the author.

7.4 Future Developments.

Proposals for future work on the Rolls-Royce version of Q195 have been described by Ntim (14). Briefly, these include modifications to laminar heat transfer and separation bubbles, while for the turbulent section, the main topics are surface roughness, Taylor-Görtler vortices and flow relaminarisation. Meanwhile, Perry (21) has expressed his dissatisfaction with the current performance of Head's entrainment theory, and is considering the use of an alternative method.

Certainly, the greatest weakness of Q195 in its present form is its indifferent performance in shape factor prediction, but the same can be said for many boundary layer methods. It is considered by the author that further comparison with experiment is advisable before judgement is passed on Head's theory. Radial equilibrium flows provide the most severe test, especially if the curvature is severe; calculations for these flows would provide more information on the

subject of curvature corrections. It should be emphasised, however, that the entrainment theory in its present form gives very satisfactory predictions for the majority of cases, and it is only in extreme conditions that its performance suffers.

CHAPTER 8

FINAL DISCUSSION AND CONCLUSIONS

8.1 Comparison with Published Work

The author's flat plate results are well supported by those of Liepmann and Fila (10), Higgins and Pappas (6) and others. The conclusion reached is that on a flat plate, heat transfer to the laminar boundary layer brings about transition at a lower Reynolds number (based on x). For a 100 deg C rise in plate temperature, the Reynolds number is reduced by about 50% for an unstable buoyancy condition, and the reduction is approximately linear.

For curved ducts, no other investigations of wall heating effects have been found. Even the author's adiabatic results were not directly comparable with those of other authors, although various aspects are covered in the papers below. Wilcken (37) and Schmidbauer (27) have measured the flow in curved ducts for adiabatic flow and approximately zero streamwise pressure gradient. More recently, So (29) and Patel (16) have conducted similar experiments. Schubauer and Klebanoff (28), von Doenhoff and Tetervin (3) and Stratford (33) have employed curved surfaces in the investigation of pressure gradient effects, with separating or near-separating flow, but have not approached radial equilibrium conditions in the boundary layer. Thomann (34) has measured Stanton numbers on curved surfaces in supersonic flow, but without detailed boundary layer measurements.

8.2 The Author's Results for the Curved Duct

In the author's experiments, the curved duct was found to be notably free from three-dimensional flow, and the position of the separation point was confirmed using surface films and tufts. The method used to obtain a tripped boundary layer was not considered entirely satisfactory, and in future experiments, natural transition or tripping in an adiabatic straight duct is recommended. Nevertheless, the momentum thickness distribution followed closely predictions from the radial equilibrium equation of Patel, once starting values had been matched.

Separation point measurement was hampered by a vibration period in the tunnel. Also, considerable strain was placed upon instrument accuracy, which produced some scatter of results. The position of the separation point was found to be dependent on both wall temperature and flow velocity; a parameter K_T was introduced to simplify matters, but was found to be inadequate. Predictions of shape factor (and also of the separation point), using relations corrected empirically for R_θ and surface curvature, were not entirely successful; shape factors were generally higher, and separation earlier, than in the experiments. However, movement of the separation point on heating was more accurately predicted, especially at the higher flow speeds. Considerable scatter was present in the predicted points, future work with Q195 would be aided if this could be reduced.

8.3 Flow in Compressor Blading during Thermal Transients

The purpose of the above experiments was, of course, to estimate

the boundary layer behaviour on a compressor aerofoil. The flow within an axial compressor is extremely complex. The turbulence structure and its likely effects upon the boundary layer are discussed in Appendix A. Typical intensities of turbulence have been quoted at 1% to 3.4% by Sohn (30). Measurements of up to 8% intensity were reported by Schlichting and Das (73), but on a compressor with too high an inlet turbulence to be representative.

On the pressure surface of the aerofoils, it is likely that vortices of the Taylor-Gortler type will be formed, as a result of the velocity instability. These have been observed in the turbulent boundary layer on a concave wall (17), but no experimental cases on aerofoils have been measured. It further seems likely that the additional thermal instability, when the blade surface is hotter than its surroundings, will intensify these vortices, although again no experimental evidence is available. The velocity profile shape (for velocity components in the streamwise direction) is uncertain. Wilcken (37) performed measurements on a concave surface without establishing the presence of vortices, and observed steep velocity gradients at the wall. Further out, stagnation pressure was almost uniform at a value a little below that in the freestream. Thomann (34) has noted an increase in Stanton number for concave surfaces, indicating that the temperature gradient at the wall is also steeper than normal.

It is now generally accepted that the boundary layer in such cases grows in thickness much more rapidly than it would upon a flat surface, but the comparative growth rates for displacement thickness have not

satisfactorily been determined. The effect of heating on the growth of a concave-wall boundary layer is another topic on which no information is available; experimental investigations are extremely difficult, because of the three-dimensional nature of the layer. An increase in boundary layer thickness on heating, which would be expected from behaviour in other circumstances, would contribute to duct blockage, and reduce the mass flow through the compressor for a given rotational speed.

Velocity and thermal instability will also occur in the boundary layer formed on the outer wall of the annulus, which presents a concave surface to the flow (see Figure 2). Growth in duct blockage from this source is potentially more dangerous than that from the aerofoils, in view of the greater Reynolds number (based on distance covered) which are attained. However, the disturbances to this flow as it moves through the blading are such that it is doubtful whether vortex growth, and subsequent thickening of the boundary layer, will be allowed to take place.

On the suction surface of the aerofoils, the boundary layer is more regular. Large areas exist where the flow is largely two-dimensional, although at the blade root and tip three-dimensional flow patterns are known to exist. It is generally accepted that a laminar boundary layer forms from the leading edge, and persists up to a point of minimum static pressure (30). The turbulent layer which follows grows rapidly in the adverse pressure gradient; the maximum permissible gradient is governed by the tendency of the boundary layer towards separation. Premature separation on a compressor

aerofoil can be disastrous, since not only is the boundary layer thickened and duct blockage greatly increased, but the outlet angle of the airstream is altered. This outlet angle of course determines the inlet angle for the next blade row, which will in turn perform differently under its new entry conditions. Thus the disturbance is transmitted downstream; a study of the blade geometry suggests that stall (if it occurs) will take place at a point an even number of blade rows downstream from the row at which the disturbance originated.

The blade designer therefore chooses an aerofoil shape which produces a large static pressure increase across the blade, but which avoids boundary layer separation from the suction surface, at least until very near the trailing edge. Care is taken to provide a certain safety margin at normal running conditions.

8.4. The Transition Point

The experimental and calculation procedures concentrated on the prediction of boundary layer behaviour on the suction surfaces of compressor blades, as it was there that the potentially most damaging aerodynamic effects were likely to occur. From the measurements of laminar transition, three conclusions were drawn:

1. Wall heating generally moves the transition point upstream.
2. This movement is roughly proportional to the excess wall temperature.
3. For a given excess wall temperature, the movement is strongly dependent on buoyancy conditions.

The third conclusion arises from comparison of the author's experimental results with those from references (2), (6), (9) and (10). Of the flat plate experiments, the author's and (6) were performed with the plate horizontal, and the boundary layer on its upper surface (an unstable configuration when the plate was heated). The third flat plate experiment (10) avoided buoyancy forces by mounting the plate vertically. Comparison of results indicates that a given transition point movement, with no buoyancy, is approximately doubled by the addition of unstable buoyancy forces. This is discussed further in Appendix B.

The effect of freestream turbulence on the transition point was not examined in the author's experiments. It is, however, known to be considerable, and the implications for boundary layers on blading are discussed in Appendix A.

8.5 The Turbulent Layer - Flow Relaminarisation

Of the experimental studies performed by other authors, of flow separation from continuous surfaces, none have included departure from adiabatic conditions. The author's measurements were performed on the inner wall of a curved duct, for which wall heating gave rise to stabilising buoyancy forces of considerable magnitude. It would seem reasonable to suggest that buoyancy conditions would have a strong influence on the development of the heated turbulent layer, but that comparison with their effect on laminar transition may be misleading.

It has been established (38) that stabilising buoyancy forces due to gravity in the turbulent boundary layer counteract the source of turbulent energy and work towards laminarisation of the flow. However, the centripetal field in the boundary layer on a convex

surface exerts a stabilising influence even in adiabatic flow (see Appendix B). If this surface is heated, turbulent decay may take place, and the flow will laminarise.

The study of laminarisation, or reverse transition, is a research field in its own right. Although considerable work has been doen using favourable pressure gradients (see Section 1.4), the effects of curvature and normal density gradient have received little attention. It is suggested that in the author's experiments, the arc length of the curved surface was insufficient for reverse transition to occur, and that the boundary layer at separation was turbulent. Further discussion on this topic is contained in Appendix B.

8.6 The Turbulent Layer - Separation

From the author's experiments, three observations were made:

1. For all cases investigated, the turbulent separation point was advanced by wall heating.
2. This advancement was roughly proportional to the wall excess temperature applied.
3. The separation behaviour on the curved plate was also dependent on flow velocity.

This third observation made the prediction of aerofoil conditions somewhat hazardous. Further complications arise from two more

observations, drawn from previous remarks in this section:

4. Turbulent boundary layers on convex surfaces may relaminarise, and this tendency may be increased by heat transfer into the boundary layer.

5. The above tendency may also be affected by the intensity of mainstream turbulence in the duct.

Predictions from the calculation program Q195 supported the experimental observations, although agreement could have been improved. The velocity dependence was clearly only a symptom of dependence on a more comprehensive parameter, including radius of curvature and other terms in addition to flow velocity. One such parameter, K_r, was investigated using Q195, but did not perform well.

Examination of the experimental and predicted separation behaviour, whether based on K_r or flow velocity, suggests that as the centripetal field is increased, the effect of a given rise in wall temperature is diminished. Thus for very strong fields, such as are present in the flow through compressor blading, the effect is expected to be small. However, the flow velocities in a compressor are well into the compressible range, while the author's experiments were in conditions for which compressibility effects could be neglected. This prevents a direct comparison from being made.

An illustration may be given by comparing the effects of an increase in wall temperature of 100 deg C above its adiabatic value. The incompressible data, both experimental and predicted, suggest a reduction in the value of x at separation of at most 2% (see Figures 30 and 33). For compressible flow, however, the predicted

reduction is in the range 6.8% to 8.6%, depending on the assumptions made (see Section 6.8). In practice, a temperature difference of this magnitude is unlikely to occur; Maccallum (12) has calculated that one of 50 deg C is more typical. It has been established that the separation point movement is approximately linear with wall temperature, so for 50 deg C the predicted movements are at most 1% (incompressible) and around 4% for compressible flow. This last figure is largely independent of the assumptions made in the calculation: whether a substantial region of laminar flow is present, or whether corrections are made for R_θ or curvature.

On a compressor blade, it is unlikely that radial equilibrium conditions are attained. However, it is possible that an appreciable pressure gradient across the stream is developed towards the trailing edge; this type of behaviour is discussed in Section 6.2, with reference to the experiments of Schubauer and Klebanoff (28). The accuracy of predictions in compressible flow for such a situation is uncertain, with the entrainment theory in particular being of doubtful validity. The corrections for R_θ from Thompson (35) are for incompressible flow, while the author's curvature corrections were empirically calculated to fit the low-speed experimental data.

8.7 Conclusions

From the experimental and predicted results, the following conclusions were drawn:-

1. The transition point is advanced by wall heating, for conditions of unstable or zero buoyancy; the advancement is approximately linear with wall temperature.

2. On the suction surface of a compressor blade, where stable buoyancy forces prevail, the transition point may be delayed by wall heating. However, this effect is expected to be small compared with that of the streamwise static pressure distribution, and significant movements of the transition point are not expected. This was confirmed by computer predictions for aerofoil boundary layers (Section 6.8).

3. The point of turbulent separation is advanced by wall heating, even in stable buoyancy conditions; again, the advancement is approximately linear with wall temperature. The effect was also dependent on flow velocity and surface curvature, in a complex manner. None of the parameters introduced was satisfactory in describing this dependence.

4. In a compressor, the most likely areas for boundary layer separation are the blade suction surfaces, near to the trailing edges, especially in the regions of three-dimensional flow near the blade root and tip (39). On the blades, the separation movement is unlikely to be great (5% is probably a generous estimate for the most extreme conditions), but the possible amplification of disturbances in successive blade rows may make an initial movement of this order a serious matter.

5. It may therefore be concluded with reasonable confidence that the advancement of separation points due to heat

transfer within the compressor is a significant factor in promoting stall during the "hot re-slam" test procedure. Stall may be avoided, as has already been observed, by maintaining the engine at idling speed for a longer period. However, for elimination of the problem, a new design point with a greater surge margin (bringing an inevitable reduction in performance) must be adopted.

8.8 Future Work

The qualitative nature of many of the remarks in this Chapter reflects the considerable scope for future research in this field. Above all, detailed experimental data are required on boundary layer behaviour in all conditions, but especially those involving curvature, adverse pressure gradients or a combination of these. Only then may prediction methods be tested under the adverse conditions which are required if firm conclusions are to be drawn.

One useful exercise would be to examine the effect of curvature in promoting radial pressure gradients, both in the mainstream and the boundary layer. The severity and duration of streamline curvature required to produce radial equilibrium flow could be measured, and this would throw light on the conditions obtaining in compressor and turbine blading.

Appendix A - The Effects of Free-Stream Turbulence

The experimental work described in the main text was performed at a low level of freestream turbulence (below 1% intensity at all times), whereas typical intensities for a compressor are considerably greater. The creation of turbulence conditions more representative of compressor flows was considered during the design of the experimental equipment. However, it was decided that for this initial investigation of a phenomenon which had apparently received no previous studies in detail, measurements at low turbulence levels would be more helpful. An attempt would then be made to assess the effect of an increase in turbulent intensity on the data obtained, and such an attempt now follows.

The Turbulent Energy Spectrum

It is now accepted that the turbulent energy of any flow may be described as a function of wave number by a unique distribution (see Figure). This distribution may be divided into a series of sub-ranges by wave number, each of which exhibits its own characteristics, as described in detail by Hinze (57).

In the present author's experiments, where the stream was passed through fine gauzes and a contraction before entering the working section, the scale of the eddies in the freestream would be small. Contributions to turbulent energy from the low wave number (large scale) end of the distribution would therefore be absent, and the energy spectrum might commence at point X in the figure. In a compressor, it is suggested that large-scale turbulence

would be generated by the first blade rows, and that this scale would progressively diminish as the air passed downstream. However, even at the high pressure stages, the turbulent eddies would be much larger than their counterparts in the wind tunnel. The energy distribution might commence at point Y in the figure and include region A which covers the main bulk of energy-containing eddies. Thus it is seen that the two flows might share the same energy spectrum above a certain wave number, but that the wind tunnel flow is deficient in the low wave number region.

It is possible that this deficiency may be unimportant. The experiments of Evans (51) on the effects of freestream turbulence on transition, indicated that an increase in intensity moved the transition point upstream. In addition to this, it was observed that the scale

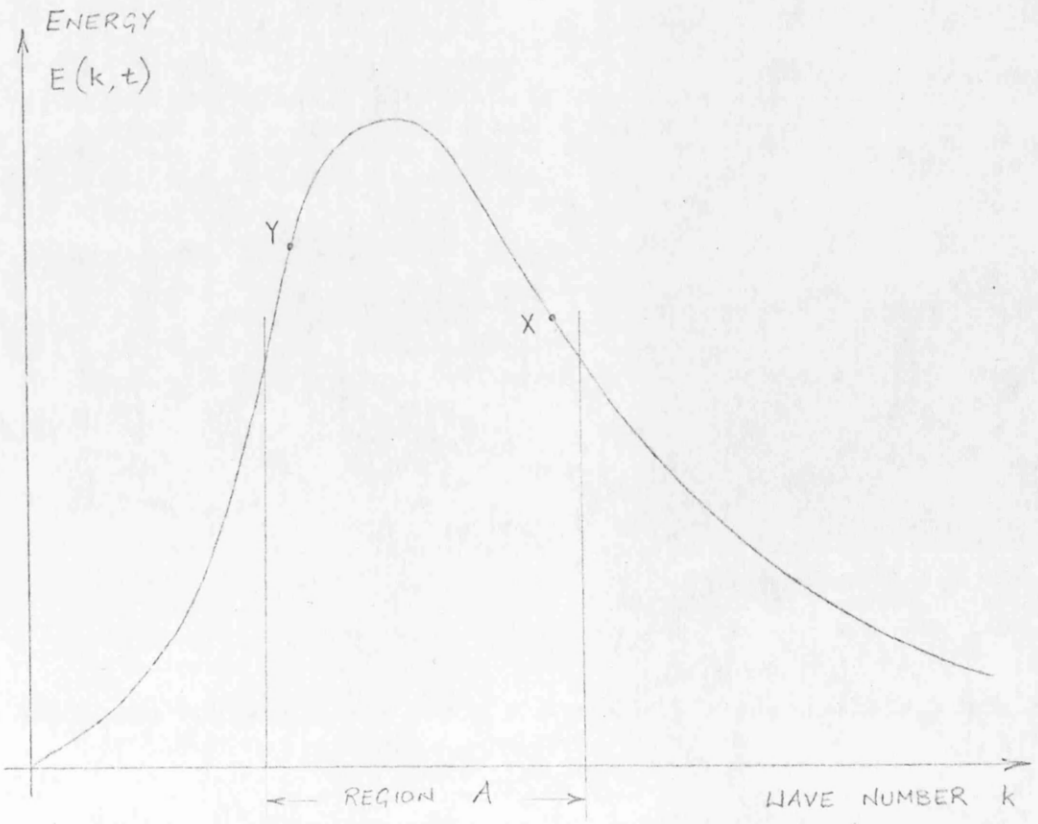

of the turbulence was also important, and that a decrease in scale at the same intensity produced a further upstream movement of the transition point. This suggested that the most effective interaction between freestream and boundary layer takes place in the small-scale (high wave number) region of the energy spectrum, and that the influence of the large-scale compressor eddies on the boundary layer may be of relatively little significance.

Further information on this subject was clearly desireable, and an examination of the literature was made (see also Section 1.4), to assess the effects of freestream turbulence on the general development of the boundary layer. The discussion of this which now follows considers laminar, transition and turbulent layers in turn.

In the laminar boundary layer region, Buyuktur, Kestin and Maeder (45) noted a slight increase in heat transfer for an accelerated boundary layer, and Kestin (60) in his review postulates some interaction between turbulence effects and pressure gradient. This, and his further suggestion that the laminar layer at zero pressure gradient is largely independent of freestream turbulence, is supported by the later work of Junkhan and Serovy (58). The broad conclusion from this is that while the boundary layer is laminar, it is little influenced by freestream turbulence.

In contrast, the location of the transition point is markedly effected by the turbulence intensity. This is not unexpected, since transition is a consequence of amplification of small disturbances within the laminar layer, as evidenced by the experimental work quoted by Kestin (60).

Further support for this may be found in the recent work of Evans (51), who demonstrated the same phenomenon in the boundary layer of an aerofoil in a cascade.

Worthy of note is the flat plate experiment of Liepmann and Fila (10) where the effect of heat transfer on subsonic transition was measured at two freestream turbulence levels. The results indicate that the effect of a given temperature ratio is greater at the higher turbulence level. The relevance of this finding, if confirmed, is obvious; however, no subsequent attempt at confirmation appears to have been made, and its validity is difficult to assess.

Thus it may be concluded that transition is very sensitive to changes in freestream turbulence, in a zero pressure gradient configuration. Other factors influence transition (for example, the onset of an adverse pressure gradient), and here the effect of turbulence intensity may well be reduced.

Of particular relevance to the present study is the response of turbulent boundary layers to changes in freestream conditions. If such changes have a substantial effect, then clearly it will be less easy to relate the author's curved plate results (at low intensity of turbulence) to the somewhat higher turbulence environment of compressor blading.

Turbulent boundary layers have been investigated in certain of the papers discussed in the previous section. For example, Buyuktur:, Kestin and Maeder (45) examined the behaviour of a tripped flat-plate boundary layer in a strongly favourable pressure gradient. Their measurements were mainly confined to heat transfer coefficients, and no turbulence effects

were apparent for intensities in the range 1% to 4.5%. This, and other early papers on the same topic, are reviewed by Kestin (60). Junkhan and Serovy (58) performed a similar experiment, covering a somewhat wider range of intensities, and obtained a corresponding result. A more detailed investigation has been carried out by Kearney et al (59), again for an accelerated turbulent boundary layer, using hot wires and pitot tubes to obtain velocity profiles. No effect of turbulence intensity on the profiles was observed, nor on distributions of Stanton number, which was also measured. In this case, a prediction method was also employed, using the theory of Spalding and Patankar (32) and including the turbulent kinetic energy equation; this permitted the calculation of turbulent intensity effects on the turbulent boundary layer. Significantly the predictions agreed with the experimental data up to the maximum experimental intensity of about 4%, and there were negligible differences in Stanton number and other parameters. Extension of the predictions to cover 10% freestream turbulence resulted in an increase in Stanton number; however, it was considered that with intensities of this magnitude, a boundary-layer calculation alone was unlikely to be adequate, and the predicted result questionable in the circumstances.

On the above evidence, it would appear that the turbulent boundary layer is largely unaffected by moderate freestream turbulence levels. However, certain experimenters have been led to draw different conclusions, and their work clearly requires detailed consideration in the light of this apparent disparity. The first example is the work of Talmor and Weber(77), who studied a highly accelerated turbulent boundary layer, and noted that reverse transition behaviour was markedly inhibited by an increase in

freestream turbulence; the intensities used ranged from 1.6% to 11%. The experimental technique was unusual in that measurements were taken on a plane surface at a large favourable angle of attack to the airstream, and the reverse transition region was not always regular; in certain tests, it appeared that forward transition was also taking place. Again, heat transfer measurements formed the bulk of the data. In view of the particular configuration selected for the test it may be that the relevance of the results to the general flows considered by previous authors is at least questionable.

A more comprehensive experiment was that of Evans (51), who examined the development of the turbulent boundary layer after transition on a compressor aerofoil model. The effect of freestream turbulence was assessed by the measurement of local skin friction coefficients, for intensities in the range 0.25% to 4%. Evans observed that, at a given location on the blade, turbulent skin friction coefficient fell with rising freestream intensity, but explained that this was the result of the upstream movement of the transition point.

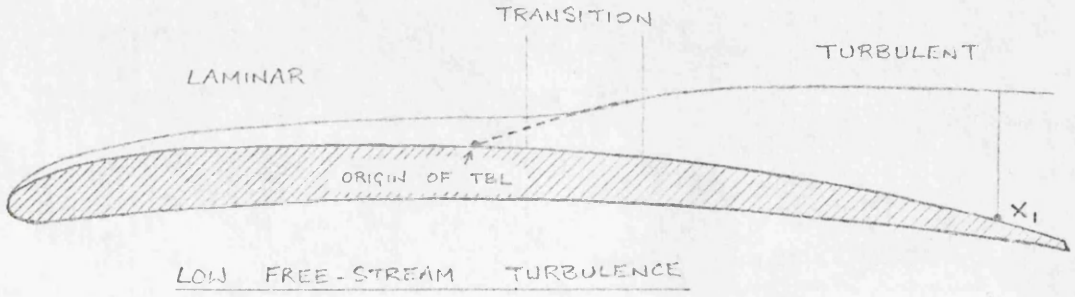

LOW FREE-STREAM TURBULENCE

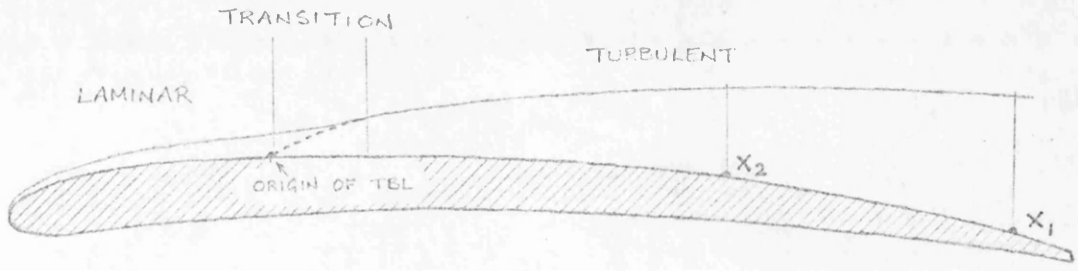

HIGH FREE-STREAM TURBULENCE

This is illustrated in the figure, where it will be seen that for the high turbulence, the turbulent boundary layer at point x_1 has been established for a greater streamwise distance. To allow for this, he compared skin friction coefficients at equal distances from the end of transition (point x_2 for high turbulence), and noted that the observed trend was now reversed: an increase in turbulent intensity brought about an increase in skin friction coefficient (see figure). As in the case of Talmor and Weber (77), it is possible that the result does not in fact contradict the results of other authors previously cited. In this case it can be deduced from Evans data that the boundary layer thickness at the end of transition was not the same for each test, and is a consequence of the movement of the transition point.

The results indicate that the appropriate boundary layer thickness was smaller at the higher freestream turbulence levels, which might be anticipated in view of the comparatively low sensitivity of the purely laminer layer upstream of the transition region. Thus the effective origin of the turbulent boundary layer varied with respect to the end of transition, and was relatively further downstream at the higher turbulence intensities; this is illustrated diagrammatically in the figure.

The indications are that Evans' results may not be at variance with the deductions made by the authors whose work was previously discussed, and it is possible that confirmation could be obtained if the origin of Evans' turbulent boundary layer could be deduced. Unfortunately, calculation (by upstream extrapolation) of the exact origin is not possible for this case, because of the pressure gradient and surface curvature effects; this highlights the clear necessity for further basic flat-plate research at zero pressure gradient.

To sum up, there is no conclusive evidence to show that moderate freestream turbulent intensities have a significant effect upon the development of the turbulent boundary layer. The measurements by Evans (51) of turbulent scale effects suggest that the most effective interaction between boundary layer and freestream occurs at the high wave number region of the energy spectrum. This region is present in both wind tunnel and compressor turbulence. Freestream turbulence in the low wave number range, a feature of compressor flows which is normally absent from wind tunnels, appears to have little effect on the boundary layer.

No results have been found at the present time which would substantiate, without question, the viewpoint that the turbulent boundary layer is markedly affected by freestream turbulence. Such a result would require that this freestream turbulence effectively penetrates the layer and influences the wall region, which is unlikely unless its intensity at least approaches that within the layer itself. A similar opinion has been expressed by Kestin (60). The required conditions may be obtained with freestream intensities in excess of 10%, but this is substantially higher than the accepted range for compressor turbulence. Even the peak value of 8% reported by Schlichting and Das (73) was regarded as being unrepresentatively high, as the compressor inlet did not follow jet engine design practice, and a figure of about 5% would seem to be more typical.

It may be that the relevance of the experimental results obtained from the author's present series of tests is doubtful for special applications in which the freestream turbulent intensity is particularly high, and for such circumstances further investigations are required.

Appendix B - The Effects of Body Forces

Introduction

It was indicated in the main text that the flow process was strongly influenced by buoyancy and other forces. In this Appendix, the effects are studied in more detail, and estimates are made of the effects of these transverse forces on the development of the boundary layers. The estimate is of necessity a qualitative one, as a result of the complexity of the flows and the sparseness of relevant experimental data.

The horizontal flat plate, as used in the experiment and described in Section 2.6.6 of the main text, was chosen in preference to a vertical one , to avoid three dimensional flow with the plate heated. In the curved duct, centripetal forces acted in the horizontal plane, and were at least an order of magnitude greater than those due to gravity. Centripetal forces were the dominant influence when the curved plate was heated, and also had an effect in adiabatic conditions, as will be discussed later.

The Flat Plate

The flat plate experiments were conducted in a configuration where the tendency was for the heated (less dense) air to rise from the surface of the plate; in other words, the buoyancy forces reduced the stability of the boundary layer. (The opposite would be true had the flow been on the underside of the plate. Here, heat transfer at moderate rates would exert a stabilising effect, and discourage any circulatory motion in the boundary layer). Essentially the problem is that of combined free and forced convection, and in practice, it is found that, except at very low velocities, forced convection is the dominant mechanism. For laminar layers, the analytical method of Acrivos (38)

confirms this, but cannot be used for the more complicated turbulent layers.

Recent experimental work by Mori and Uchida (62) was concerned with laminar flow of air between parallel plates, with the lower plate uniformly heated. It was found that a mainstream velocity of 10 ft/s was sufficient to eliminate the longitudinal vortices created by the free convection influences, for a temperature difference of 60 degK. The implication of this result is that the occurence of three-dimensional flow patterns arising from buoyancy forces is unlikely where there is also a considerable forced convection influence. However, transition is a phenomenon which is the result of local instabilities within the laminar boundary layer, and may respond readily to small free convection forces. No direct investigation of the effect of buoyancy on transition has been made, although Nicholl (66) has observed turbulent layers on the heated floor and heated roof of a duct. In the latter case, there was a tendency for the layer to laminarise, and this phenomenon is discussed later in the Appendix. From the very limited experimental data available, estimates have been made of the effects of buoyancy on laminar transition, and these are given in Sections 2.6.8 and 8.4 of the main text.

The Curved Plate

The second experiment involved the use of a curved plate, with boundary layer measurements confined to the convex surface. The figure illustrates a typical velocity distribution for incompletely developed flow in a curved duct. From such a velocity profile, local radial components of acceleration may be calculated, and the corresponding distribution for this profile is also shown in the figure. The effect of these centripetal forces has been described by Townsend (78) in the following manner: "Consider two equal volumes of fluid

initially distant r_1 and r_2 $(r_1 < r_2)$ from the axis (of curvature) and with the velocities of the mean flow at their original positions, U_1 and U_2. Then, if angular momentum is conserved during interchange of their positions, there is an increase in their total kinetic energy of $\Delta E = \frac{1}{2}(U_2^2 r_2^2 - U_1^2 r_1^2)\left(\frac{1}{r_1^2} - \frac{1}{r_2^2}\right)$ which is the minimum possible value from the work done in performing the interchange. If $r_2 > r_1$, ΔE is positive if $U_2^2 r_2^2 > U_1^2 r_1^2$, and the flow is stable to the interchange. If $U_2^2 r_2^2 < U_1^2 r_1^2$, the flow is unstable."

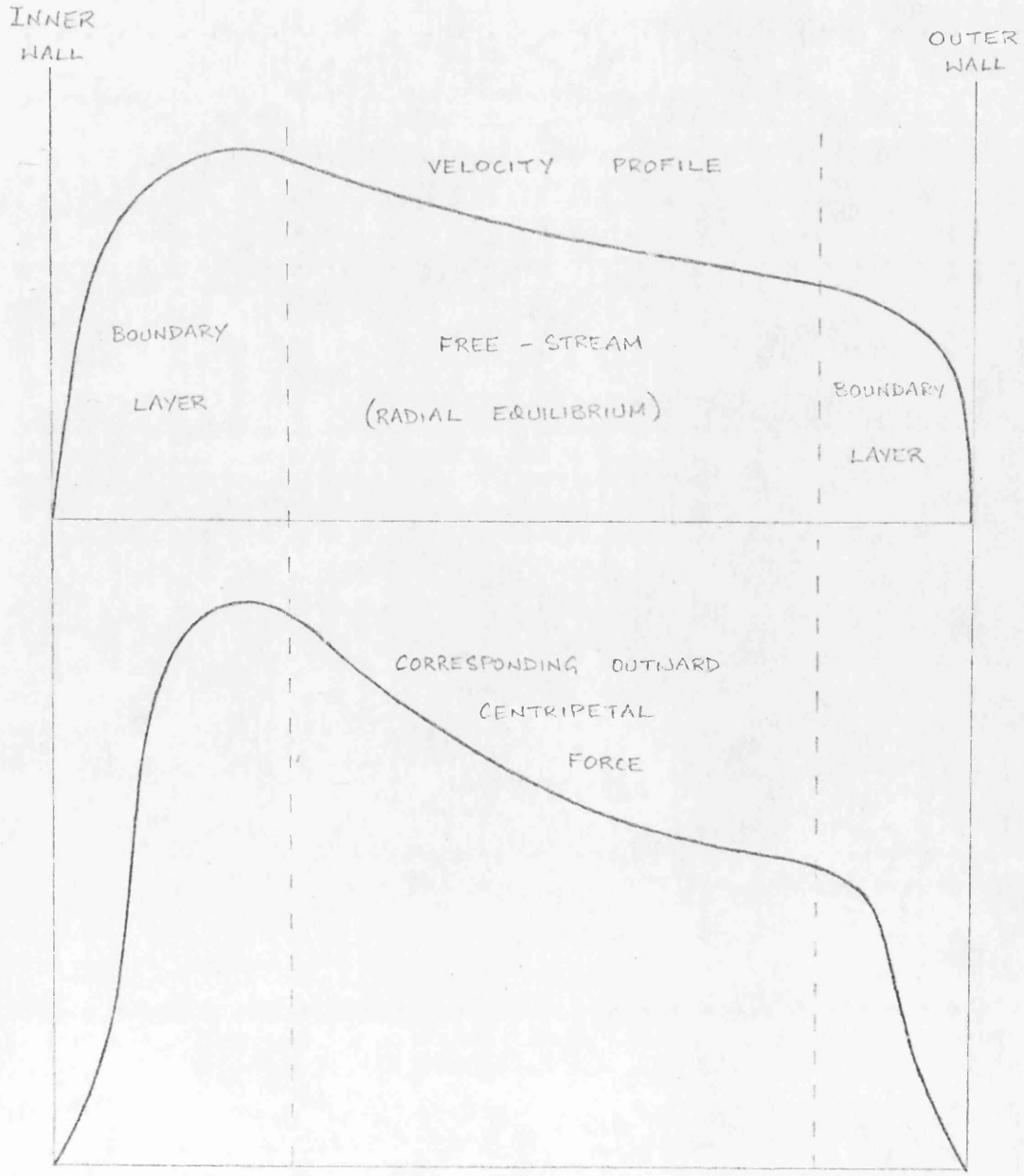

It will be seen from the figure that for the inner wall boundary layer, the product Ur is increasing with distance from the wall, and a stabilising influence is exerted. In a turbulent boundary layer, this may have the effect of inhibiting velocity fluctuations normal to the wall. Conditions near the outer wall are unstable, in that Ur falls with increasing r, and thus the interchange of fluid within the boundary layer is encouraged. In laminar layers, streamwise vortices form, and there is no reason to suppose that a similar pattern is not present in turbulent layers. Thus the flow pattern on the concave surface is likely to be strongly three-dimensional, and not easily amenable to experimental or analytical approaches.

The effects of centripetal forces have been investigated in the flow between concentric cylinders; a comprehensive review of this work has been given by Schlichting (72). The flow characteristics depend on the rotation of both inner and outer cylinders. Specifically, with the inner cylinder at rest and the outer one rotating, stabilising body forces are set up, and transition is delayed considerably; it may be avoided completely if all eccentric motion between the cylinders can be eliminated. Thus it is clear that the centripetal forces inhibit the growth of general turbulence within the laminar boundary layer. For a turbulent layer, it is logical to suppose that very strong stabilising forces would overcome the sources of turbulent energy, and bring about reverse transition.

A different situation is found if the outer cylinder is held at rest and the inner one rotated, since here, the product Ur falls with increased radius. An unstable condition is produced, resulting in the formation of ring vortices for laminar flow. The later experiments of Patel (17), Thomann (34) and Persen (68), none of whom employed concentric cylinders, point to a similar phenomenon in

turbulent boundary layers on concave surfaces.

In the present author's experiments with the curved duct, one would therefore expect strong stabilising forces to act in the boundary layer. Heating would introduce additional forces and again, the effect would be a stabilising one, since the heated (less dense) air would experience a smaller centripetal force per unit volume than the air at ambient temperature. Thus the heated air would tend to remain in close proximity to the plate, and very little circulation would take place. This contrasts with the unstable buoyancy condition on the flat plate. An equally important difference is that in the curved plate flow, the buoyancy forces were the result of the centripetal field, having a magnitude which varied between 30 and 150 times that of the gravitational field. The " free convection" influences within the boundary layer would be correspondingly greater.

Laminarisation

In the presence of powerful stabilising forces, the ability of a turbulent boundary layer to maintain itself must be questioned. In this respect, the current literature on reverse transition is unhelpful; most experimenters have studied the effect of favourable freestream pressure gradients, and quote limiting parameters based on gradient strength (see Section 1.4). However, Nicholl's (66) measurements of turbulent boundary layers under stable buoyancy conditions (although from gravitational force only) are of relevance. With $T_{wall}/T_{\infty} = 1.35$, he noted very rapid turbulent decay. It should be mentioned that his measurements were taken at freestream velocities of the order of 5 ft/s, an order of magnitude below those used by the present author. Nicholl also employed a flat plate at zero pressure gradient, unlike the present case where

there was a severe adverse pressure gradient to promote separation. Thus no direct comparisons of a quantitative nature may be drawn.

In the experiments of Eskinazi and Yeh (50) on fully developed flow in a curved channel, extensive hot-wire measurements were made, and fluctuating components compared in magnitude over a range of streamwise positions. A study of the variation with distance downstream of the radial velocity component $\overline{v^2}$ showed a steady decay near the inner wall and amplification near the outer wall, confirming the anticipated effects of body forces. The changes in $\overline{v^2}$ were transmitted in reduced measure to the other fluctuating components.

As no hot-wire measurements were available for the present author's curved plate boundary layers, the exact conditions within them must be in some doubt. However, a study of the velocity profiles measured between $x = 10$ in. and $x = 20$ in. indicates negligible divergence from the universal turbulent profile, except in the region immediately upstream of the separation point. The kinked profiles in this region are of the form considered typical of turbulent layers. It must therefore be concluded that if laminarisation was in progress, it was not far advanced.

A further point may be worthy of mention. It is well known that a laminar boundary layer separates more readily than a turbulent one. What is not clear is whether a turbulent layer in the process of laminarisation is more sensitive in this respect than one that is fully turbulent, although logic suggests this should be so. If this is the case, then heat transfer from the wall, which produces a stably stratified flow and a further reduction in turbulence in the boundary layer, would reduce the resistance of the layer to those influences which tend to cause separation. Consequently, the

separation point would be likely to move upstream. Experimental evidence on the separation behaviour of laminarising boundary layers required to support this theory is not available, and its collection is likely to present many practical difficulties.

The scope for further work in this field is considerable. There is little experimental data on the combined effects of free and forced convection in the turbulent boundary layer and this needs to be remedied before reliable theoretical approaches can be made. Investigation of centripetal effects, at present largely confined to laminar boundary layers, could be extended into the turbulent regime to examine the possibility of reverse transition. Here, it may be difficult to spearate the influences of curvature and pressure gradient.

Compressor Conditions

For the present author's curved plate experiment, it has been concluded that the boundary layer at separation was at least predominantly turbulent. From this it would appear that the stabilising influences were effectively opposed by the strong adverse pressure gradient. On a compressor aerofoil, the same qualitative conditions apply for the suction surface; the centripetal field is much greater, but so is the freestream velocity.

Studies of suction surface boundary layers on compressor aerofoils (e.g. Evans (51)) in adiabatic flow have indicated that transition takes place around mid-chord (depending on static pressure distribution) after which a typical turbulent layer develops. No signs of subsequent laminarisation have been found, nor are they likely to be, following natural transition in an adverse pressure gradient. The effect of heat transfer from the aerofoil has not been

investigated experimentally, but it seems likely that the extra stability conferred on the suction surface layer will result in delayed transition. However, the dominating influence on the behaviour of the boundary layer is that of the streamwise pressure gradient, and this will be largely unaffected by the heat transfer. Thus the movement of the transition point is likely to be very small.

On the pressure surface of the compressor blade, instability is present in the boundary layer, and it seems likely that Taylor-Görtler vortices will form. These are well-known in laminar layers, and Patel's (17) observations have pointed to their presence in turbulent layers as well. The addition of heat transfer from the wall gives even greater instability, and would be expected to contribute to the strength of the vortices.

Conclusions

It appears from the evidence available that the stabilising influences in convex-surface boundary layers are ineffectual in the presence of significant adverse pressure gradients. On the suction surface of a compressor aerofoil, the point of separation (if present) is determined by the growth of the turbulent boundary layer, and laminarisation is not a significant effect. The conclusion to be drawn from this is that in this respect the results from curved plate experiments, such as the present one, may be applied directly to the suction surfaces of compressor aerofoils, despite the somewhat different flow conditions.

Appendix C - Corrections for Thermocouple Probe

An estimate was made of the heat losses in the thermocouple probe, and the temperature errors resulting from these losses. The analysis was carried out for the thermocouple nearest the plate surface, for the following conditions:-

Mainstream air velocity, 100 ft/s

Air velocity at thermocouple, 50 ft/s

Ambient air temperature, 293 K

Air temperature at thermocouple, 383 K

Plate surface temperature, 433 K

These clearly are rather more extreme conditions than were encountered during the experimental work.

The dimensions of the thermocouple are shown in the figure on this page. The temperature errors are of course dependent on the temperature distribution along the thermocouple wires; however, the design of the instrument makes this very difficult to estimate. As a first approximation, the temperature distribution was calculated for the outer stainless steel sheath, after making the following assumptions:-

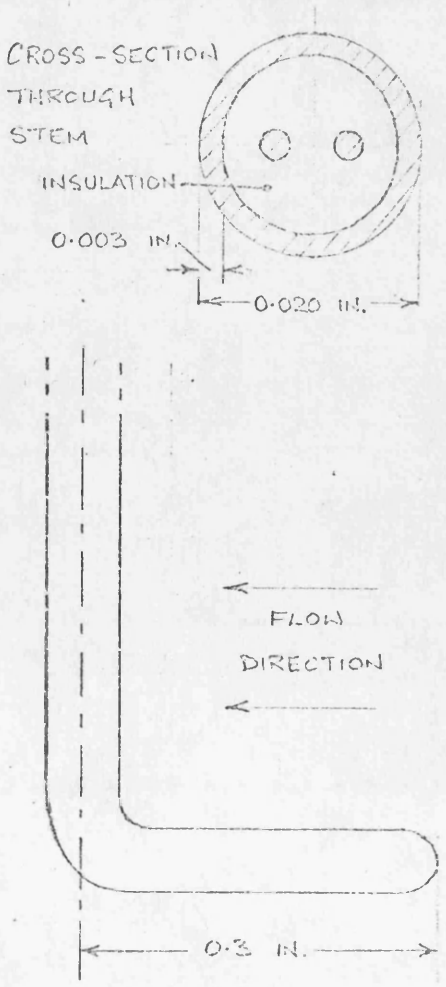

1) that the entire length of sheath parallel to the plate surface was at a uniform temperature;

2) that the effects of the copper tube, which shields the thermocouples from approximately y = 1.5 in. upwards, may be neglected. This is obviously a gross oversimplification, but is probably not seriously in error, for the following reasons. Firstly, poor thermal contact existed between tube and thermocouples, as an intentional feature of the probe design. Secondly, the metal pedestal of the probe was located with one end in contact with the plate surface, and the other attached to the copper tube about 2 in. from its end. Thus conduction up the walls of the tube would be small. Also, of course, for at least one inch of its length normal to the plate surface, the thermocouple would be unshielded, and any conduction which took place would be along the sheath (and, of course, along the wires inside the sheath).

3) that the presence of the probe did not disrupt the airflow to such an extent that the normal calculations for heat transfer coefficients were invalidated.

Radiative heat transfer for the portion of sheath parallel to the plate surface was small, mainly because of the low emissivities of the surfaces involved. It probably amounted to less than 10^{-5} CHU/hr, and could be a gain or a loss to the probe, depending on the exact values of emissivity taken.

Convection rates for this portion of the sheath were comparatively large; thus for a 1 deg C temperature difference, the heat transfer rate was calculated as 3×10^{-3} CHU/hr. However, the crucial factor in the calculation was the balance of conduction and convection rates for the sheath normal to the plate surface.

For the cylindrical sheath with its axis normal to the flow, the heat transfer coefficient was 0.036 CHU/ft^2.hr.deg C. The temperature distribution along the sheath was given by

$$\frac{d^2 T}{dy^2} = - \frac{h P}{kA} (T - T_a)$$

where h is the above heat transfer coefficient,

P is the sheath perimeter ($2\pi \times$ outer radius),

k is the thermal conductivity of stainless steel,

A is the cross-sectional area of the hollow sheath

and T_a is the ambient air temperature.

The solution is of the form

$$(T - T_a) = C_1 e^{my} + C_2 e^{-my}$$

where $m = \sqrt{\frac{h P}{k A}}$

Putting in figures

$$m \doteq \sqrt{\frac{0.036 \times 10^{-2}}{24 \times 10^{-6}}} = \sqrt{15} = 3.88$$

C_1 and C_2 were evaluated from boundary conditions.

The effect of the boundary layer at $y \doteq 0$ was neglected as a first approximation, so that for

$$y \doteq 0, \quad (T - T_a) = 90.$$

For the second boundary condition, it is possible to estimate the point at which the sheath temperature approached the ambient. This estimate could then be checked by comparing the conduction rate at a certain value of y with the total heat loss rate by convection from this value of y up to the above estimated point. However, it is simpler to consider the most extreme case of an infinitely long sheath, for which the solution is greatly simplified. The conductivity rate at $y \doteq 0$ is given by

$$q'' = kA\,(T - T_a)\sqrt{\frac{h\,P}{kA}}$$

where T = sheath temperature,

$$q = 25 \times 10^{-6} \times 90 \times 3.88$$

$$= 8.7 \times 10^{-3} \text{ CHU/hr}$$

The temperature gradient at this point is

$$8.7 \times 10^{-3} \times 10^{6}/25 = 348 \text{ deg C/foot}$$

$$= 29 \text{ deg C/inch}$$

The temperature distribution for the first few inches of sheath is sketched overleaf.

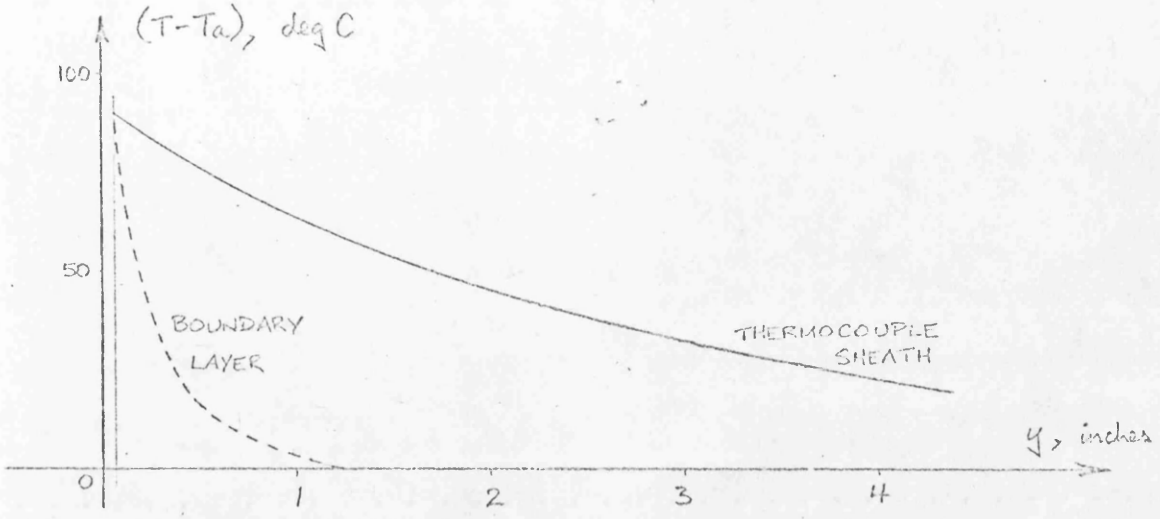

Allowance for the boundary layer temperature distribution (dotted line) would alter the sheath distribution slightly, especially in the region close to y ≒ 0. Further out, it makes little difference.

Thus it is seen that, for the assumptions made, the maximum rate of heat loss from the sheath tip was 8.7×10^{-3} CHU/hr.

To balance this, the sheath tip temperature would be depressed by rather less than 3 deg C.

The above calculations embody many simplifications and assumptions, but nevertheless suggest that the high heat transfer rates near the thermocouple tip maintained its temperature close to that of the local airstream for the experimental conditions. The hot junction and wiring of the thermocouple, which were insulated from the sheath, would be expected to suffer rather smaller temperature losses than the 3 deg C referred to above.

NOMENCLATURE

x	distance along plate surface, in direction of flow
y	distance normal to plate surface
r	radial distance in constant-radius ducts
R	surface radius of curvature
u	velocity in x-direction
$u_* = \sqrt{\frac{\tau_{wall}}{\rho}}$	friction velocity
P	pressure
T	temperature
ρ	density
g	acceleration due to gravity
C_p	specific heat at constant pressure
γ	ratio of specific heats
Pr	Prandtl number
St	Stanton number
q''_{wall}	heat transfer rate at the wall
C_f	skin friction coefficient
τ	shear stress
δ	boundary layer thickness
δ^*	boundary layer displacement thickness
θ	boundary layer momentum thickness
ν	kinematic viscosity
R_{crit}	Reynolds number, based on x, at start of transition
R_{sep}	Reynolds number, based on x, at point of separation
R_{δ^*}	Reynolds number based on δ^*
R_θ	Reynolds number based on θ

$\bar{H} = \delta^*/\theta$, shape factor

H compressible shape factor

$H_1 = (\delta - \delta^*)/\theta$, shape parameter

F Head's entrainment function

K_r radial acceleration parameter

M Mach number

Suffixes

o (except where stated) at stagnation conditions

1 at the tube of the pitot probe nearest the wall

∞ at mainstream conditions

w or wall, at wall conditions

ad adiabatic

p for potential flow

in at entry

BIBLIOGRAPHY I

1.	F.H. Clauser	Turbulent boundary layers in adverse pressure gradients. J.Aero.Sci., Vol. 21, p.91, 1954.
2.	K.R. Czarnecki A.R. Sinclair	An extension of the investigation of the effects of heat transfer on boundary layer transition on a parabolic body of revolution (NACA RM-10) at a Mach number of 1.61. NACA TN 3166, 1954.
3.	A.E. von Doenhoff N. Tetervin	Determination of general relations for the behaviour of turbulent boundary layers. NACA Rep. No. 772, 1943.
4.	J.E. Green	The prediction of the turbulent boundary layer development in compressible flow. J. Fluid Mech. Vol. 31, p.753, 1968.
5.	M.R. Head	Entrainment in the turbulent boundary layer. ARC R & M 3152, 1960.
6.	R.W. Higgins C.C. Pappas	An experimental investigation of the effect of surface heating on boundary layer transition on a flat plate in supersonic flow. NACA TN 2351, 1951
7.	J.H. Horlock	Axial flow compressors. Butterworths Scientific Publications, 1958.
8.	A.R. Howell	Fluid dynamics of axial compressors. Proc. I.Mech.E., Vol. 153, p.441, 1946.
9.	J.K. Jack N.S. Diaconis	Variation of boundary layer transition on two bodies of revolution at a Mach number of 3.12. NACA TN 3562, 1955
10.	H.W. Liepmann G.H. Fila	Investigations of effects of surface temperature and single roughness elements on boundary layer transition. NACA Rep. No. 890, 1947.
11.	N.R.L. Maccallum	The performance of turbojet engines during the "thermal soak" transient. Proc. I.Mech.E., Vol. 184, Part 3G, 1969-70.
12.	N.R.L. Maccallum	Unpublished work: University of Glasgow, 1971.

13. P.M. Moretti, W.M. Kays — Heat transfer to a turbulent boundary layer with varying free-stream velocity and varying surface temperature - an experimental study. Int. J. Heat and Mass Transfer, Vol. 8, p.1187, 1965.

14. B.A. Ntim — Current and future additions to the compressible boundary layer program Q195. Turbine Research Rept. TRR 90071, Rolls-Royce, Ltd. 1971.

15. R.C. Pankhurst, D.W. Holder — Wind-tunnel technique. pp 184-7 Pitman, 1952.

16. V.C. Patel — The effects of curvature on the turbulent boundary layer. ARC R & M 3599, 1969.

17. V.C. Patel — Measurements of secondary flow in the boundary layers of a 180-degree channel. ARC CP 1043, 1969.

18. A.E. Perry, J.B. Bell, P.N. Joubert — Velocity and temperature profiles in adverse pressure gradient turbulent boundary layers. J. Fluid Mech., Vol. 25, p.299, 1966.

19. J.H. Perry — Private communication, based on "V.K.I. short course on boundary layers", December, 1969.

20. J.H. Perry — Compressible boundary layer and wake development. Turbine Research Rept. TRR 90017, Rolls-Royce Ltd., 1968.

21. J.H. Perry — Private communication, 24th August, 1971.

22. W.C. Reynolds, W.M. Kays, S.J. Kline — Heat transfer in the turbulent incompressible boundary layer. NASA Memo. 12-1-58W, 1958.

23. L.F. Richardson — The supply of energy from and to atmospheric eddies. Proc. Roy. Soc. London, A97, 354, 1926.

24. H. Schlichting — Boundary layer theory. 4th edition, pp.380-1. McGraw Hill, 1960.

25. H. Schlichting — Boundary layer theory. 4th edition, Chapter XII, part b. McGraw Hill 1960.

26. H. Schlichting — Boundary layer theory. 4th edition, pp. 37-8. McGraw Hill, 1960.

27. H. Schmidbauer — Turbulent friction layers along convex surfaces. NACA TM 791, 1936.

28. G.B. Schubauer, P.S. Klebanoff — Investigation of separation of the turbulent boundary layer. NACA Rep. No. 1030, 1951.

29. R.M.C. So — Private communication: experimental measurements of the boundary layer on the inner wall of a curved duct. University of Princeton, New Jersey. January 1970.

30. S.L. Sohn — An analysis of the performance of an axial-flow compressor at low Reynolds numbers. J. Aero. Sci. Vol. 23, p.741, 1956.

31. D.B. Spalding, S.W. Chi — The drag of a compressible turbulent boundary layer on a smooth flat plate with and without heat transfer. J. Fluid Mech., Vol. 18, p.117, 1964.

32. D.B. Spalding, S.V. Patankar — Heat and mass transfer in boundary layers. Morgan-Grampian, London, 1967.

33. B.S. Stratford — An experimental flow with zero skin-friction throughout its region of development. J. Fluid Mech., Vol. 5, p.17, 1959.

34. H. Thomann — Heat transfer in a turbulent boundary layer with a pressure gradient normal to the flow. Aero. Res. Inst. of Sweden, FFA-113, 1967.

35. B.J.G. Thompson — A new two-parameter family of mean velocity profiles for incompressible turbulent boundary layers on smooth walls. ARC R & M 3463, 1967.

36. E.H. Warne — Gas turbine fuel and control systems. Proc. I.Mech.E., Vol. 183, Part 3N, 1969.

37. H. Wilcken — Turbulente Grenzschichten an gewölbten Flächen. Ing. Archiv. Vol. 1, p.357, 1930.

38. A. Acrivos — On the combined effect of forced and free convection heat transfer in laminar boundary layer flows. Chem.Eng.Sci., 21, p.343, 1966

39. L. H. Back, R. F. Cuffel, P. F. Massier — Laminarisation of a turbulent boundary layer in nozzle flow - boundary layer and heat transfer measurements with wall cooling. J.Heat Transfer, 92, p.333, 1970

40. L. H.Back, P. F. Massier, R. F. Cuffel — Flow and heat-transfer measurements in subsonic air flow through a contraction section. Int.J. Heat and Mass Transfer, 12, p.1, 1969

41. S. M. Bogdonoff, C. E. Kepler — Separation of a supersonic turbulent boundary layer. J. Aerospace Sci., 22, p.414, 1955

42. P. Bradshaw — The analogy between streamline curvature and buoyancy in turbulent shear flow. J. Fluid Mech., 36, p.177, 1969

43. P. Bradshaw — Private Communication, 12th March, 1969

44. P. Bradshaw, D. H. Ferriss, N. P. Atwell — Calculation of boundary-layer development using the turbulent energy equation. J. Fluid Mech., 28, p.593, 1967

45. A. R. Buyuktur, J. Kestin, P. F. Maeder — Influence of combined pressure gradient and turbulence on the transfer of heat from a plate. Int.J. Heat and Mass Transfer, 7, p. 1175, 1964

46. D. R. Chapman, D. M. Kuehn, H. K. Larson — Investigation of separated flows in supersonic and subsonic streams with emphasis on the effect of transition. NACA Rep. No. 1356, 1958

47. R. E. Chilcott — A review of separated and reattaching flows with heat transfer. Int. J. Heat and Mass Transfer, 10, p.783, 1967

48. G. Chui, S. J. Kline — Investigation of a two-dimensional fully stalled turbulent flow field. Rept. MD-19: AFOSR-67-2047, Stanford University, 1967

49. G. M. Elfstrom — Turbulent separation in hypersonic flow. IC Aero. Rept., 71-16, Imperial College, London, 1971

50. S. Eskinazi, H. Yeh — An investigation on fully developed turbulent flows in a curved channel. J. Aero. Sci., 23, p.23, 1956

51. B. J. Evans — Effects of freestream turbulence on blade performance in a compressor cascade. ARC 33135, 1971

52. G. E. Gadd — An experimental investigation of heat transfer effects on boundary layer separation in supersonic flow. J. Fluid Mech ., 2, p.105, 1957

53. G. E. Gadd — The effects of convex surface curvature on boundary layer separation in supersonic flow. ARC CP289, 1956

54. G. E. Gadd, W. F. Cope, J. L. Attridge — Heat transfer and skin-friction measurements at a Mach number of 2.44 for a turbulent boundary layer on a flat surface and in regions of separated flow. ARC R & M 3148, 1960

55. S. Gray — Stage matching, stall and surge in multi-stage axial flow compressors. Proc.I.Mech.E., 184, Part 3G, 1969-70

56 R. C. Gunness, B. Gebhart — Combined forced and natural convection flow for the wedge geometry. Int.J.Heat and Mass Transfer, 8, p.43, 1965

57. J. O. Hinze — Turbulence, Section 3 - 5, pp. 174 - 204 McGraw-Hill, 1959

58. G. H. Junkhan, G. K. Serovy — Effects of free-stream turbulence and pressure gradient on flat-plate boundary-layer velocity profiles and heat transfer. J. Heat Transfer, 89, p.169, 1967

59. D. W. Kearney et al. — The effect of free-stream turbulence on heat transfer to a strongly accelerated turbulent boundary layer. NASA CR113590, 1970.

60. J. Kestin — The effect of free-stream turbulence on heat transfer rates. Adv. in Heat Transfer, 3, p.1, 1966

61. L. L. Lynes, J. N. Nielsen, F. K. Goodwin — Inhibition of flow separation at high speed. AFFDL - TR - 68 - 119, Air Force Systems Command, Wright-Patterson AFB, Ohio

62. Y. Mori, Y. Uchida — Forced convective heat transfer between horizontal flat plates. Int. J. Heat and Mass Transfer, 9, p.803, 1966

63. Y. Mori, Y. Uchida, T. Ukon — Forced convective heat transfer in a curved channel with a square cross-section. Int. J. Heat and Mass Transfer, 14, p. 1787, 1971

64. M. Morsy
R. S. Silver
Unpublished work
Department of Mechanical Engineering,
University of Glasgow, 1972

65. M. A. B. Narayanan
V. Ramjee
On the criteria for reverse transition in a two-dimensional boundary layer flow.
J. Fluid Mech., 35, p. 225, 1969

66. C.J.H. Nicholl
Some dynamical effects of heat on a turbulent boundary layer.
J. Fluid Mech., 40, p.361, 1970

67. V. C. Patel
M. R. Head
A simplified version of Bradshaw's method for calculating two-dimensional turbulent boundary layers.
Aero. Q., 21, p.243, 1970

68. L. N. Persen
Preliminary analytical explorations of heat transfer from boundary layers containing streamwise vortices.
AD-666438, Cincinnati University, Ohio, 1967

69. A. K. Rastogi
J. H. Whitelaw
A procedure for predicting the influence of longitudinal curvature on boundary layer flows.
BL/TN/A/37, Imperial College, London, 1970

70. V. A. Sandborn
Preliminary experimental investigation of low-speed turbulent boundary layers in adverse pressure gradients.
NACA TN 3031, 1953

71. V. A. Sandborn
C. Y. Liu
On turbulent boundary-layer separation.
J. Fluid Mech., 32, p. 293, 1968

72. H. Schlichting
Boundary Layer Theory.,
6th edition, pp. 500 - 504, McGraw-Hill, 1968

73. H. Schlichting
A. Das
On the influence of turbulence level on the aerodynamic losses of axial turbomachines. Flow research on Blading, ed. L. S. Dzung, Brown Boveri Symposium, 1967

74. M. C. Smith
A. M. Kuethe
Effects of turbulence on laminar skin friction and heat transfer.
Phys. Fluids, 9, p.2337, 1966

75. E. M. Sparrow
J. Minkowycz
Buoyancy effects on horizontal boundary-layer flow and heat transfer.
Int.J. Heat and Mass Transfer, 5, p. 505, 1962

76. Stanford
AFOSR-IFP conference on boundary layer prediction methods, ed. S. J. Kline et al., Stanford University, 1968

77. E. Talmor
N. Weber
Heat transfer from boundary layers undergoing an acceleration induced reverse transition.
A.I.Ch.E. J., 16, p. 446, 1970

78. A. A. Townsend The Structure of Turbulent Shear Flow, p. 294. Cambridge University Press, 1956

LIST OF FIGURES

Figure	Title	Opposite Page
1	Axial-flow compressor blading	4
2	Flow around the compressor drum	4
3	Plan view of the wind tunnel	16
4	The flat plate	17
5	The flat plate installed	17
6	The total head probe	18
7	Laminar velocity profiles at zero streamwise pressure gradient	20
8	Laminar, transition and turbulent velocity profiles	21
9	The effect of heating on the laminar boundary layer	26
10	The effect of heating on the transition boundary layer	26
11	Dynamic pressure ratio distributions for four plate temperatures	22
12	The effect of heating on transition - Test 1	23
13	The effect of heating on transition - Test 2	23
14	The curved duct	30
15	Typical temperature distributions for the curved plate	35
16	location of the separation point: typical dynamic pressure plot	35
17	The effect of heating on laminar separation	37
18	The effect of heating on boundary layer separation	38
19	Velocity profiles at x = 6 in. and 10 in.	39

Figure	Title	Opposite Page
20	Velocity profiles at x = 15 in., 20 in. and 25 in.	39
21	Skin friction coefficients	39
22	Distributions of R_{δ^*} , R_θ and H	39
23	Temperature profiles	40
24	Stanton numbers	40
25	Flow visualisation: titanium dioxide run pattern	41
26	Flow visualisation: tuft behaviour	41
27	Power law velocity profiles	49
28	Power law temperature profiles	50
29	Universal velocity profile	53
30	The effect of a 100 deg C rise in wall temperature on turbulent separation: dependence on flow velocity	60
31	Plate vibration curves	61
32	Variation of intensity of turbulence with flow velocity	61
33	The effect of a 100 deg C rise in wall temperature on turbulent separation: dependence on parameter K_T	65
34	Momentum thickness distributions, from the data of Schubauer and Klebanoff (28)	75
35	Shape factor distributions, from the data of Schubauer and Klebanoff (28)	75
36	Momentum thickness distributions, from the author's data	78
37	Shape factor distributions, from the author's data	79
38	Thompson's (35) $H_1(\bar{H})$ curve family, with added curvature correction	80
39	Experimental and predicted separation points	86